Fakultät für Medizin

Institut für Zellbiologie des Nervensystems

Imaging microtubule dynamics in the healthy and diseased nervous system

Tatjana Isabelle Kleele

Vollständiger Abdruck der von der Fakultät für Medizin der Technischen Universität München zur Erlangung des akademischen Grades eines

Doctor of Philosophy (Ph.D.)

genehmigten Dissertation.

Vorsitzender: Univ.- Prof. Dr. Arthur Konnerth

Betreuer: Univ.-Prof. Dr. Thomas Misgeld

Prüfer der Dissertation:

1. Univ.-Prof. Dr. Helmuth Adelsberger

2. Prof. Christian Lohmann, Ph. D., Netherlands Institute for Neuroscience

3. Univ.-Prof. Dr. Martin Kerschensteiner, Ludwig-Maximilians-Universität München

Die Dissertation wurde am 22.09.2014 bei der Fakultät für Medizin der Technischen Universität München eingereicht und durch die Fakultät für Medizin am 26.11.2014 angenommen.

ACKNOWLEDGEMENTS

To begin, I would like to thank my supervisor Prof. Thomas Misgeld for being a wonderful mentor. Your fascination and passion for science was an inspiration to me. I wish to express my gratitude for all your support, guidance and encouragement - I have learned so much during the time in your lab!

Thanks to Prof. Christian Lohmann and Prof. Helmuth Adelsberger for their support as members of my thesis committee and to Prof. Martin Kerschensteiner- your advice and the valuable discussions were invaluable during the progression of my PhD.

Special thanks to Dr. Leanne Godinho for her support and continued sympathy. Your positive energy and the good spirit you are bringing to the lab are irreplaceable.

At the end of my PhD, I appreciate how many great people I have met along the way. Thank for your help and the great fun we had: Barbara, Bogdan, Cathy, Caro, Felix, Gabi, Grace, Laura, Kristina, Marina, Manuela, Michael, Monika, Moni, Natalia, Petar, Peter, Phil, Sarah, Yvonne and Vlad. And a big thanks also to everyone in the Kerschensteiner and Konnerth lab.

During this journey, I once again realized that I have the most amazing friends you could ever wish for! I am deeply grateful how much you helped me to also overcome hard times and your unwavering faith in me has allowed me to accomplish everything. A thousand thanks to: you: Inge, Rebecca, Katharina, Christina, Elena, Susi, Max, Martl, Anna, Angie, Moritz…
Special thanks to Niko for proofreading my thesis, the adventurous distractions on the weekends and all the happiness!

Thanks to my brother Basti for our cooking sessions, concert visits and for always bringing a smile to my face.

Finally, it only remains to say a huge and heartfelt thank you to my parents, Hans and Ingrid, for supporting my 24 years of education- I think I am finally done now ☺. I would like to express my deep gratitude for your love, patience, support and unwavering belief in me. You have always encouraged me to pursue my dreams and have taught me everything I need in life. I love you!

ABSTRACT

Microtubules are major cytoskeletal components of all eukaryotic cells. In neurons, microtubules play key roles in neuronal polarization, organelle transport and neurite remodeling. Disturbances of microtubule organization can be detected early in neurodegenerative diseases, underscoring their importance in maintaining cellular structure and function and making them interesting structures to study in the context of nervous system health and disease. Microtubule organization is regulated by microtubule associated proteins, including plus end tracking proteins (+TIPs) like end binding protein 3 (EB3), which accumulate at the growing plus end of microtubules and indicate their dynamic remodeling. Microtubule behavior can be studied by fluorescently tagging +TIPs, a technique that has thus far been applied *in vitro* and in non-mammalian model systems. To investigate such remodeling *in vivo* in the mammalian nervous system, the aim of my PhD project was to establish a new imaging approach based on transgenic mice that express YFP-tagged EB3 controlled by neuron-specific *Thy1* promotor elements. High resolution time-lapse microscopy of those mice can be used to assay microtubular dynamics *in vivo* in different compartments of mammalian neurons in the peripheral and central nervous system. Furthermore, this approach allows monitoring the status of the microtubular cytoskeleton in acute and chronic models of axonal injury, under the influence of microtubule-modifying drugs and during developmental pruning. With this novel approach I found that an increase in microtubule dynamics is an early indicator of axon destabilization. In such settings, axons can now be protected by microtubule-stabilizing drugs based on a controlled fashion, by recording drug effects at the site of action. Additionally, an increase in comet density is also found during axon regeneration and developmental reorganization. This suggests that increased microtubule dynamics might be a general indicator of axonal plasticity in health and disease.

ABSTRACT

Mikrotubuli sind röhrenförmige Polymere, die einen der Hauptbestandteile des Zytoskeletts in eukaryotischen Zellen bilden. In Nervenzellen (Neuronen) spielen Mikrotubuli eine besonders wichtige Rolle, da sie nicht nur für die mechanische Stabilisierung der Zelle verantwortlich sind, sondern auch für den intrazellulären Transport, sowie die Etablierung und Aufrechterhaltung der Zellpolarität. Veränderungen am mikrotubulären Zytoskelett treten oftmals bereits in frühen Stadien neurologischer Erkrankungen auf. Dies verdeutlicht die entscheidende Rolle, die Mikrotubuli bei der Aufrechterhaltung der Zellhomöostase spielen und macht sie zu hochinteressanten Strukturen bei der Erforschung der zellulären Vorgängen in Neuronen im gesunden und erkrankten Nervensystem. Die Organisation von Mikrotubuli wird von verschiedenen Proteinen reguliert, einschließlich den sogenannten "*plus end tracking proteins*" (+TIPs), die an das wachsende Ende der Mikrotubuli binden. In der Vergangenheit wurde die Markierung solcher +TIPs, wie beispielsweise des "*end binding protein 3*" (EB3), mit fluoreszierenden Proteinen bereits verwendet, um das dynamische Verhalten des Zytoskeletts zu untersuchen. Allerdings waren solche Experimente bislang nur in Zellkultur und in wirbellosen Modellorganismen möglich.

Da jedoch unklar ist, in wie weit die Ergebnisse derartiger Studien auf Säugetiere übertragen werden können, war das Ziel meiner Doktorarbeit, eine neue Methode zu entwickeln, um die dynamischen Veränderungen von Mikrotubuli in lebenden Säugetieren zu erforschen. Zu diesem Zweck haben wir transgene Mäuse generiert, die spezifisch in Nervenzellen ein mit einem gelb-fluoreszierenden Protein (YFP) markiertes EB3-Protein exprimieren. Mit Hilfe hochauflösender bildgebender Verfahren können diese transgenen Mäuse verwendet werden um den Status des Mikrotubuli-Zytoskeletts in verschiedenen neuronalen Kompartimenten des zentralen und peripheren Nervensystems zu charakterisieren. Darüber hinaus ermöglicht diese Methode erstmals Veränderungen der Mikrotubuli nach akuter oder chronischer Schädigung einer Nervenzelle in Säugetieren zu untersuchen, sowie den Einfluss von

Mikrotubuli-modifizierenden Substanzen zu visualisieren. Die Ergebnisse dieser Arbeit zeigen, dass unmittelbar nach Schädigung oder Destabilisierung von Nervenzellfortsätzen (Axonen) die Anzahl dynamischer Mikrotubuli drastisch ansteigt – ein Effekt der durch die Verabreichung Mikrotubuli-stabilisierender Substanzen verringert werden kann, was wiederum auch degenerierende Axone stabilisiert. Eine erhöhte Anzahl dynamischer Mikrotubuli kann auch während der Regeneration oder Neuentwicklung von Nervenzellen beobachtet werden. Zusammenfassend legen diese Ergebnisse nahe, dass eine gesteigerte Mikrotubuli-Dynamik ein genereller Indikator für neuronale Plastizität, sowohl im gesunden als auch im erkrankten Nervensystem, darstellt.

.

Table of content

1. INTRODUCTION

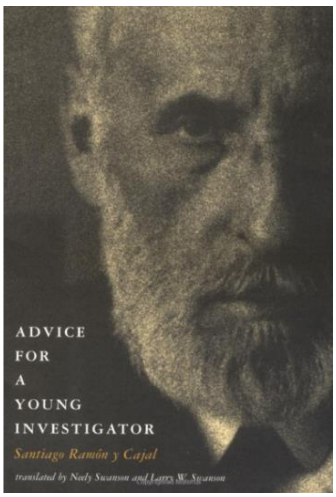

"Any man could, if he were so inclined, be the sculptor of his own brain"

Santiago Ramón y Cajal

Advice for a Young Investigator, 1896

This famous quote by Santiago Ramón y Cajal, who is considered the father of modern neuroscience, implies what is so fascinating and mysterious about the brain (Lopez-Munoz et al., 2006, Ramón y Cajal 1999). On the one hand, our brain can retain memories over decades, but on the other hand it is capable of adapting to new experiences on a time-scale of seconds (Eric R. Kandel 2000). Therefore balancing stability versus plasticity is a major challenge for the nervous system (Song & Brady 2014). In addition, the neurons that form our nervous system are not replaced like most cells in other tissues, but have to function during the entire lifetime of an individual (Spalding et al., 2005). Neurons have a unique morphology with an axonal process that serves to transmit electrical signals and transport cargos over distances of up to one meter in a human (**Fig. 1.1**) (Eric R. Kandel 2000).

Indeed, given this extended morphology, the axon is vulnerable to stress - both acutely after injury, as well as chronically during neurodegenerative diseases. Thus, protection of axons is crucial for neuronal viability and maintenance of neural circuits. The fact that hundred billions of neurons need to sustain their homeostasis to assure stability and plasticity of our nervous system, raises the question about the cellular basis of this homeostatic balance. Here the neuronal cytoskeleton plays a central role, as it on the one hand imparts mechanical stability and ensures homeostasis by mediating resource transport, but on the other hand critically determines the nervous systems ability to remodel by growth and regression.

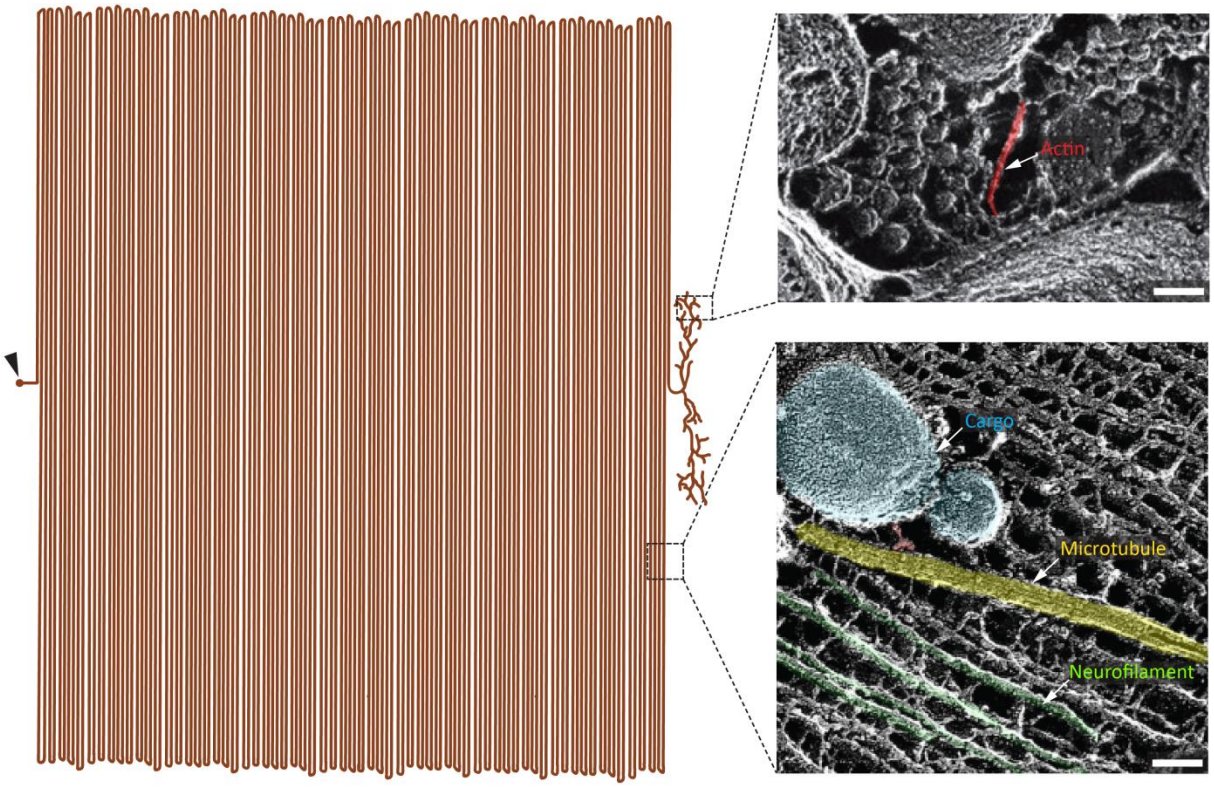

Fig. 1.1 Morphology and ultrastructure of a peripheral motor axon

Motor axons have a rather small cell body (black arrowhead) compared to the long axonal process, that can extend > 1 m (in humans) to innervate the postsynaptic target (cartoon of a motor neuron on the left). Maintaining the overall shape and supplying of the entire neuron with proteins synthetized in the cell body requires a strictly organized cellular scaffold. The cytoskeleton of the cell is composed of actin (upper panel; electron micrograph of a presynaptic terminal with an actin filament pseudo-colored in red), neurofilament and microtubules (lower panel; electron micrograph of a longitudinal axon section; neurofilament in green, microtubules in yellow). Microtubules serve as tracks for fast axonal transport of a variety of cargos (blue), which are attached to microtubules via motor-adaptor protein complexes (red). Scale bars are 50 µm. Electron micrographs modified from Hirokawa 2011, Hirokawa et al., 2010

The neuronal cytoskeleton is composed of three classes of filamentous proteins: microtubules, fibrous actin and neurofilaments (a class of intermediate filaments). Of these, microtubules are not only essential for forming a cellular scaffold that might add structural stability, but are also key structures for intracellular transport, cell migration and polarization (Conde & Caceres 2009, Verhey & Gaertig 2007). However, the microtubule cytoskeleton is not only a static scaffold, as the name would imply, it also needs to be flexible to guarantee plasticity, for example during learning and memory formation. In order to combine mechanical and dynamic requirements, microtubules form a dynamic and tightly regulated network. Not

surprisingly, neuronal microtubules are disrupted in many neurological conditions. Hence, changes in the cytoskeleton are of great interest in translational research, especially since pharmacological stabilization of microtubules has been hailed as a promising therapeutic approach (Baas & Ahmad 2013, Prota et al., 2013). But due to a lack of methods to visualize microtubules *in vivo*, little is known about how microtubule dynamics are regulated in mammalian neurons under physiological and pathological conditions.

The aim of my PhD thesis was to establish a method to image microtubule dynamics *in vivo* in different compartments of the murine nervous system. The approach, which I developed based on a newly-generated transgenic mouse line, now allows measuring microtubule dynamics in PNS and CNS neurons under physiological conditions, during pathology and after exposure to microtubule-modifying drugs. Using this approach, I could show for the first time in a mature mammal that the density of dynamic microtubules increases after injury and in neurodegenerative disease states, even before axons showed morphological indications of re-growth or fragmentation. Thus, increased microtubule dynamics might serve as a general indicator of neurite remodeling in health and disease.

1.1. Microtubules

Microtubules are cytoskeletal polymers found in all eukaryotic cells and are involved in various cellular functions. Microtubules are spatially organized and extremely dynamic structures. First evidence for the existence of microtubules was obtained at the beginning of the 20th century, where thin fibrous structures were described in silver stained preparations of nerve cells. By that time, these structures were named “neurofibrils” and were thought to be involved in the conductance of nerve impulses and later on to be simply artefacts of fixation (Schmitt 1968). Only after studies on marine eggs microtubules were identified as components of the mitotic spindle (Brinkley 1997, Schmidt 1939). In 1951, Inoue and Dan

(Inoué & Dan 1951) could prove that the spindle fibers are composed of labile subunits, which can assemble and disassemble to form a dynamic equilibrium. During the following years, transmission electron microscopy allowed a more detailed description of the composition of microtubules (Brinkley 1997, Fawcett & Porter 1954, Manton & Clarke 1952). Since then, due to technical improvements in microscopy and biochemistry, there was tremendous progress in understanding the structure of microtubules and their function for cell physiology.

1.1.1. Function of microtubules

Being a major part of the cytoskeleton, microtubules are crucial for maintaining cell shape and stability in all eukaryotic cells (Conde & Caceres 2009, Verhey & Gaertig 2007). But their function goes beyond merely serving as an intracellular skeleton. One of the most studied functions of microtubules is the proper segregation of chromosomes during mitosis and meiosis as microtubules are forming the mitotic spindle (Wade, 2009). During cell divisions, microtubules originate from the two centrosomes and extend to the chromosomes at the center of the spindle. The assembly and disassembly of the mitotic spindle is driven by changes in microtubule dynamics (Gouveia & Akhmanova 2010). Therefore, microtubules are an interesting target in cancer therapy, because blocking the mitotic spindle can inhibit cell division of tumor cells (Jordan & Wilson 2004, Prota et al., 2013). Moreover, microtubules are involved in cell migration and motility, as they are the main component of eukaryotic cilia and flagella (Falnikar et al., 2011, Wittmann & Waterman-Storer 2001). Microtubules also interact at many levels with other cytoskeletal elements, particularly with actin filaments (Myers et al., 2006).

In neurons, where cargos need to be transported over long distances, microtubules are of distinct importance. Microtubules serve as tracks for fast intracellular transport of many

different vesicles and organelles (Caviston & Holzbaur 2006, Hirokawa 1998). Motor proteins, like dynein and kinesin, which are coupled to diverse cargoes via adaptor proteins, bind to the microtubule lattice and actively transport cargos along axons and dendrites (Hirokawa et al., 2010). Besides ensuring proper supply with organelles, ion channels and other proteins, microtubules also play important roles in establishing and maintaining a neuron's polarity (Neukirchen & Bradke 2011). During the last years, microtubules were discovered to be also involved in spine dynamics in the brain (Jaworski et al., 2009), which makes them interesting structures to study in the context of learning and memory formation.

1.1.2. Composition of microtubules

Interpreting the influence of the microtubule cytoskeleton in different cellular contexts requires a deeper knowledge of the underlying mechanism of microtubule formation and their molecular composition (**Fig. 1.2**). Microtubules consist of globular α and β monomers, which interact non-covalently to form stable tubulin heterodimers. α-β-tubulin dimers polymerize in a head-to-tail fashion and build a polar filament with two structurally and functionally distinct ends. In most species, 13 protofilaments are combined laterally to a hollow tube with a diameter of 25 nm (Conde & Caceres 2009, Downing & Nogales 1998a, McIntosh 1974). The α-tubulin subunit is orientated towards the predominantly stable minus end whereas β-tubulin is pointing towards the plus end, which is very dynamic and can undergo rapid switches between phases of growth and shrinkage (Conde & Caceres 2009, Desai & Mitchison 1997, Nogales 2000). In many cells, the minus end of a microtubule is anchored at a microtubule organizing structure (MTOC) that provides stability and can trigger microtubule nucleation. In contrast, microtubules in axons and dendrites are not anchored to a MTOC. Instead a third member of the tubulin family – γ-tubulin – is often attached at the minus end to stabilize the microtubule. Moreover, γ-tubulin also serves as template for the assembly of a new

microtubule. In neurons however, new microtubules can also be formed by severing of already existing ones (Conde & Caceres 2009, Wade, 2009, Yau et al., 2014).

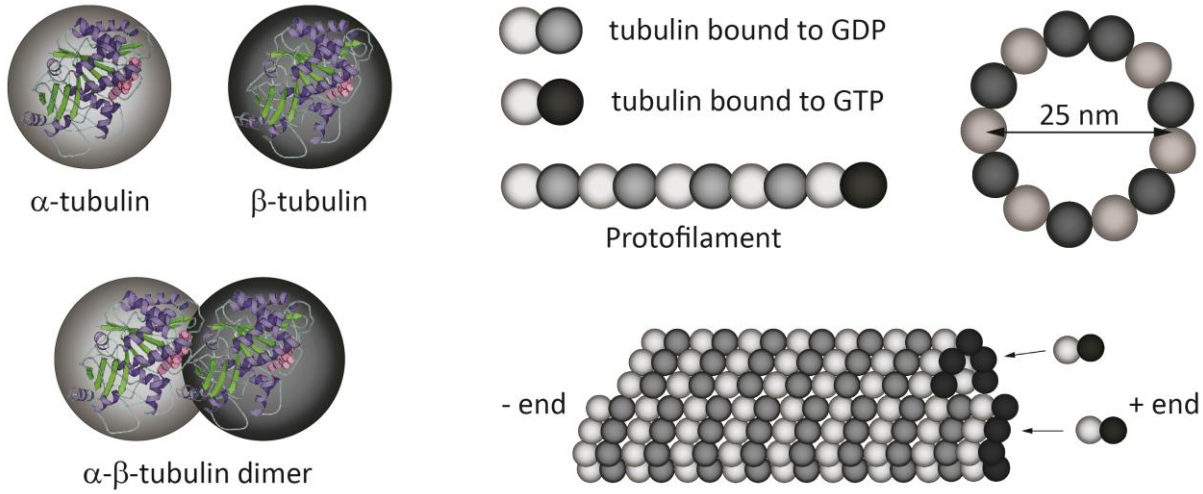

Fig. 1.2 Composition of microtubules

Microtubules are composed of α- and β-tubulin heterodimers, which assemble in head-to-tail orientation to form polarized protofilaments. New α- and β-tubulin dimers are added at the plus (+) end of the microtubule. Newly added dimers contain GTP-β-tubulin, which is hydrolyzed to GDP-tubulin shorty after polymerization. In most species, 13 protofilaments assemble to form a hollow tube with a diameter of 25 nm. Crystal structure modified by a model from Nogales, 2000

During microtubule growth, α-β-tubulin dimers are added at the plus end of the lattice. Free tubulin dimers can bind two guanosine triphosphate (GTP) molecules, one at the non-exchangeable site (N-site) of α-tubulin and one at the exchangeable site (E-site) of β-tubulin (Noda et al., 2012). GTP at the N-site of α-tubulin is never hydrolyzed, whereas GTP bound to β-tubulin can undergo hydrolysis and release inorganic phosphate. If a new α-β-dimer is added during growth of the microtubule, the catalytic domain of the α-subunit contacts the E-site of the previously added β-subunit and becomes ready for GTP hydrolysis. A delay between polymerization and hydrolysis creates a layer of GTP-tubulin at the plus end, a so called "GTP-cap", which stabilizes the microtubule lattice. The GTP cap stabilizes the microtubule lattice and when it is stochastically lost, the protofilaments disassemble and the microtubule undergoes depolymerization. During or soon after polymerization, the tubulin

subunits hydrolyze their GTP cap into GDP, which makes the subunit non-exchangeable (Akhmanova & Steinmetz 2011, Conde & Caceres 2009). Thus, microtubules are mainly composed of GDP-tubulin, except the GTP cap at the plus end. This molecular composition also implies two main characteristics of microtubules: Their dynamic nature and their polarity, both of which are crucial for microtubule function (Downing & Nogales 1998b).

1.1.3. Dynamic instability

Microtubules are highly dynamic structures, which undergo rapid switches between growth, pause and shrinkage – a behavior termed "dynamic instability" (Mitchison & Kirschner 1984) (**Fig. 1.3**). The transition from shrinkage to growth is called "rescue", whereas the change from growth to depolymerization is called "catastrophe" (Noda et al., 2012). Dynamic instability has been observed both *in vitro* and *in vivo* (Conde & Caceres 2009) and cryo-electron microscopy studies in the early 1990s made it possible to visually distinguish growing from shrinking microtubules (Gouveia & Akhmanova 2010). Microtubule catastrophe can be triggered by a single random event, for instance the loss of a protective end structure such as the GTP-cap. This leads to a sudden loss of GDP-tubulin subunits from the plus end resulting in protofilaments that splay apart and form a "fountain-like" structure (Akhmanova & Hoogenraad 2005, Akhmanova & Steinmetz 2008, Conde & Caceres 2009). Rescue events, where shortening microtubules switch to a polymerizing state, are dependent on the concentration of free tubulin *in vitro* (Akhmanova & Hoogenraad 2005, Walker et al., 1988). *In vivo* however, it has been shown that GTP remnants present at older parts of the microtubule lattice can also trigger rescue. During microtubule growth, GTP hydrolysis is not always complete, leaving some tubulin dimers with a GTP conformation along the microtubule lattice. If a microtubule is depolymerizing, these GTP remnants

become exposed and promote microtubule polymerization (Gardner et al., 2013). But dynamic behavior of microtubules is not only intrinsically regulated, for example by the presence of a GTP cap, but is also controlled by multiple other factors, such as post-translational modifications or microtubule associated proteins (MAPs) (Conde & Caceres 2009).

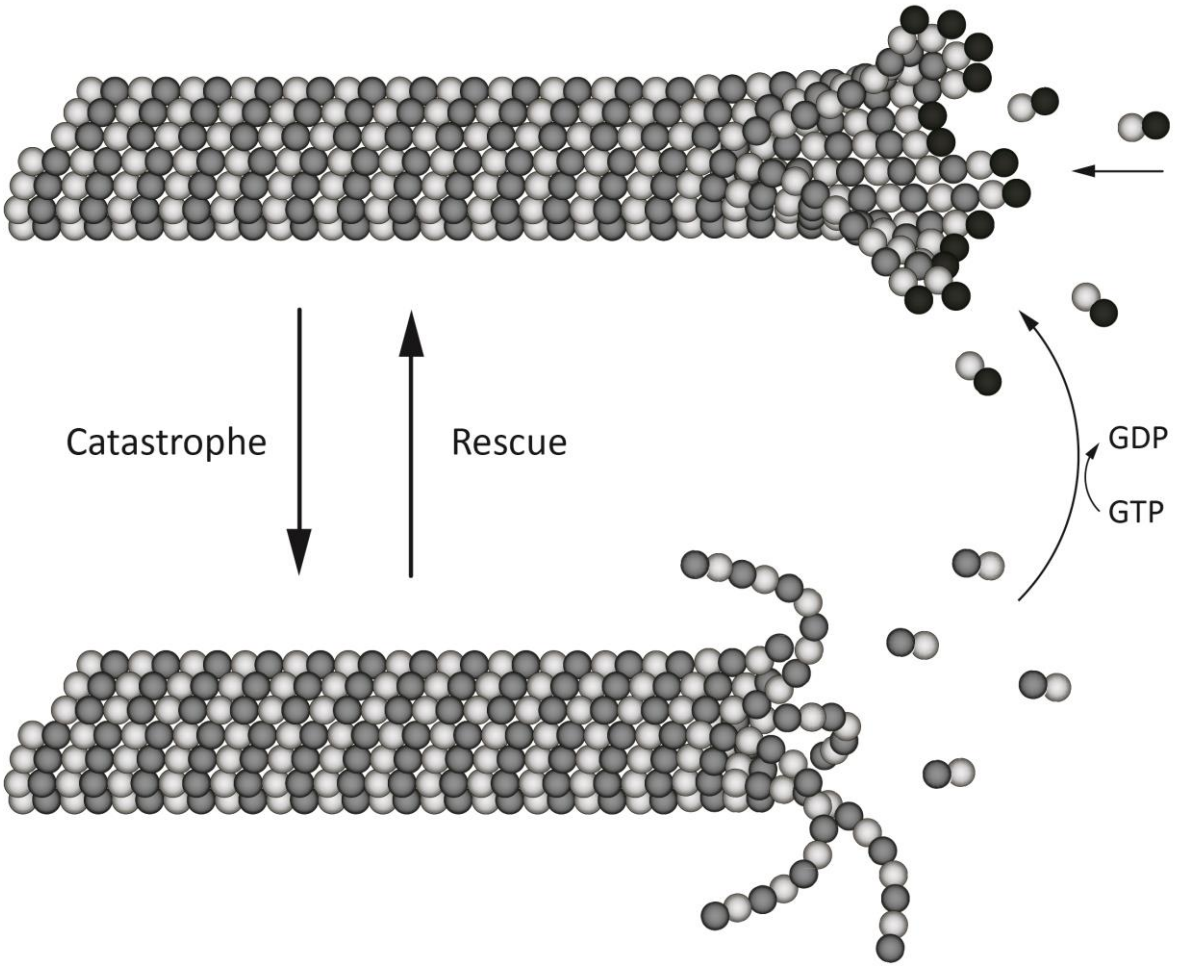

Fig. 1.3 Dynamic instability

Microtubules are highly dynamic structures, which undergo rapid switches from growth to shrinkage ("catastrophe") and the other way round ("rescue"). New tubulin dimers bound to GTP are added to the plus end during growth and subsequently GTP is hydrolyzed to GDP. Therefore microtubules contain mainly GDP-tubulin, except a GTP-cap at the plus end that stabilizes the microtubule lattice. If the GTP-cap is stochastically lost, protofilaments splay apart forming a fountain like structure and the microtubule undergoes depolymerization.

1.2. Microtubule organization in neurons

The fundamental feature of a neuron to receive, process and transmit signals in a specific direction requires a polarized cell morphology. Therefore neurons are compartmentalized into multiple dendrites and one long axon. Many studies have shown that the microtubule cytoskeleton plays a key role in establishing and maintaining neuronal polarity, which is important for directed signal transmission and cargo transport. Neuronal microtubules are nucleated at the centrosome and subsequently released by the action of the microtubule severing protein katanin. The resulting short microtubule polymers are then transported into neurites by molecular motors (Baas et al., 2006, Conde & Caceres 2009). Microtubules in neurons exist as dense bundles along the axial length of axons and dendrites. But individual microtubules do not extend along the entire neurite, but instead many individual microtubule fragments are regularly spaced in longitudinal arrays and cross-linked by microtubule associated proteins (Conde & Caceres 2009).

1.2.1. Microtubule orientation

Microtubules are not only polarized structures themselves, but as a population are also organized in a way that matches their intrinsic polarity with the cell's geometry. Cell polarity can be observed in most eukaryotic cells and serves to establish an internal organization (Li & Gundersen 2008). In many cells the plus end of a microtubule is pointing towards the periphery of the cell (de Forges et al., 2012). This allows cells to establish an asymmetric distribution of cargos and organelles and hence an overall polarity. Such cell polarization has important functions in different cell types, including asymmetric cell division, establishment of epithelial borders or cell migration (de Forges et al., 2012, Stiess & Bradke 2011). In neurons, which are probably the most polarized cells in our body, polarity forms the basis for the establishment of different compartments, which have a distinct molecular composition and

function (**Fig. 1.4**). It enables the neuron to segregate signal reception, integration and propagation in axons and dendrites (Neukirchen & Bradke 2011). A distinct orientation of microtubules in different neuronal compartments is also crucial to establish direction specific cargo transport.

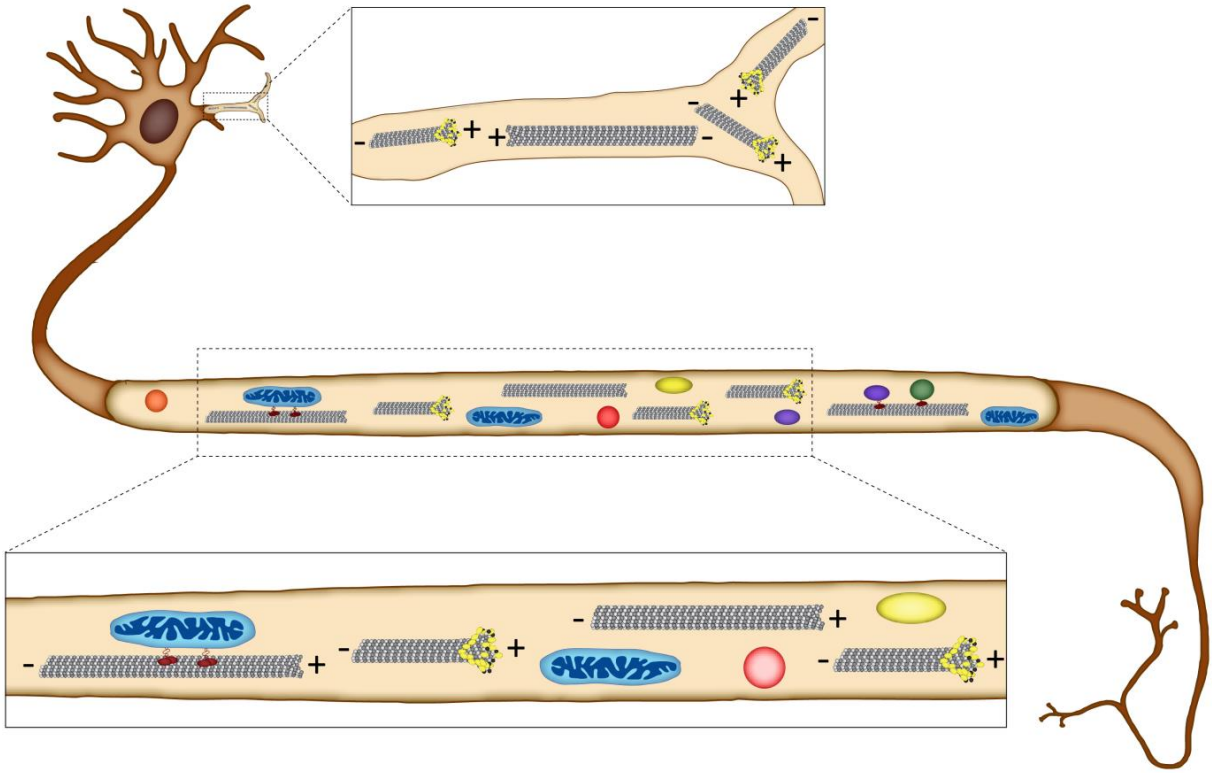

Fig. 1.4 Microtubule orientation in neurons

In axons, microtubules are uniformly orientated, with their plus end pointing outwards towards the periphery ("plus end out orientation)". In contrast, dendritic microtubules show a mixed orientation of microtubules, where the plus end can point towards the cell body or the periphery. In both, axons and dendrites, microtubules serve as tracks for cargo transport. Microtubule can be relatively stable, but a large proportion of microtubules dynamically switch between growth and shrinkage.

Many studies on fixed tissue (Baas et al., 1988, Burton & Paige 1981, Heidemann & McIntosh 1980) or *in vitro* (Stepanova et al., 2003) and in invertebrate model systems (Erez et al., 2007, Stone et al., 2008) have shown that microtubules in axons are longer than in dendrites and relatively uniformly distributed. Around 95% of axonal microtubules are orientated with their plus end pointing outward towards the synapses. In contrast, vertebrate dendrites have a mixed orientation of microtubules (Baas et al., 1988, Stepanova et al., 2003),

while in flies dendrites shown a minus end-out orientation (Rolls et al., 2007, Stone et al., 2008). Remarkably, – in flies – if an axon is injured and undergoes degeneration the dendrite closest to the initial axon repolarizes towards a uniform plus end out orientation and becomes the new axon (Stone et al., 2010). These results demonstrate how critical microtubule orientation is for defining the identity of axons and dendrites.

1.2.2. Microtubule interacting proteins

Microtubules are involved in many fundamental cellular processes and their organization needs to be tightly regulated depending on the intracellular context. As a consequence, a large number of proteins are interacting with microtubules, such as microtubule associated proteins (MAPs), which promote microtubule stabilization or destabilization, microtubule severing proteins or microtubule based motor proteins of the kinesin and dynein superfamilies (**Fig. 1.5**) (Conde & Caceres 2009).

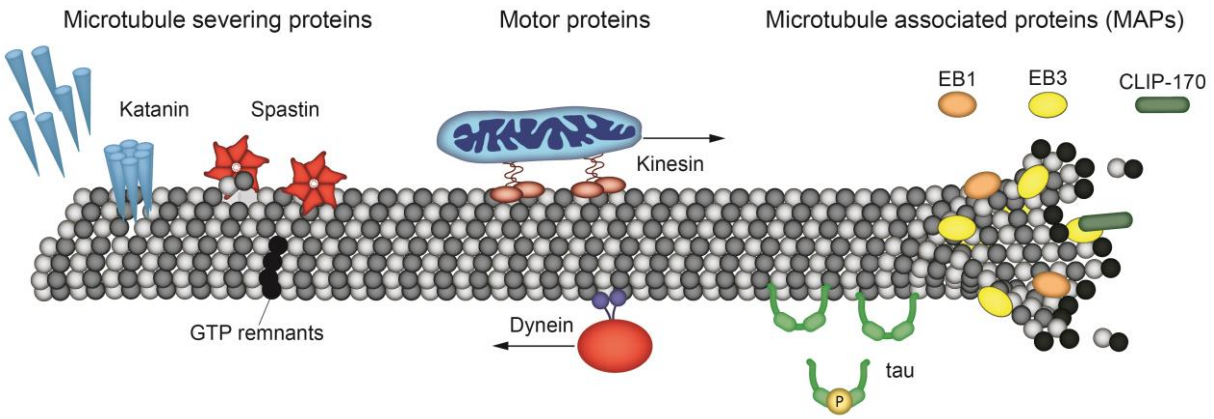

Fig. 1.5 Microtubule interacting proteins

Microtubule dynamics are regulated by a number of microtubule interacting proteins. Microtubule associated proteins (MAPs) bind to the microtubule lattice (e.g. tau) or the growing plus-tip (e.g. EB1, EB3 or CLIP-170). Motor proteins regulate microtubule based anterograde (kinesin) or retrograde (dynein) transport. Microtubule severing proteins (such as spastin and katanin) create internal breakages along the microtubule lattice.

1.2.2.1. Microtubule associated proteins

Microtubule associated proteins (MAPs) can regulate microtubule dynamics temporally and spatially by binding to soluble, non-polymerized tubulin subunits, microtubule tips or the entire microtubule lattice (Akhmanova & Steinmetz 2008). In neurons, two main types of classical MAPs can be found: high molecular weight proteins, including MAP1 and MAP2, and lower-weight tau proteins. Their occurrence can be unique to particular neuronal compartments, for example MAP2 is only found in cell bodies and dendrites, whereas tau is enriched in axons (Conde & Caceres 2009, Wade 2009). Many MAPs bind along the microtubule lattice to increase stability or influence the interaction with motor proteins. The function of MAPs is often regulated by phosphorylation, which tends to induce dissociation of the phosphorylated MAPs from the microtubule. One prominent example is phosphorylation of tau, which can inhibit the function of tau and destabilizes microtubules (Ikegami & Setou 2010, Wade 2009). Hyper-phosphorylation of tau leads to accumulations of tau protein in the cytoplasm of axons and is found in neurodegenerative disease like Alzheimer's or familial tauopathies (Baas & Qiang 2005, Lee et al., 2001). Other MAPs have destabilizing effects on microtubules or can induce depolymerization. Stathmin for example is a tubulin-sequestering protein that binds to free tubulin dimers and promotes GTP hydrolysis (Belmont & Mitchison 1996, de Forges et al., 2012).

A subset of MAPs binds specifically to the plus tip of microtubules and is therefore called plus end tracking proteins (+TIPs; **Fig. 1.6**). +TIPs regulate microtubule dynamics and nucleation as well as interaction with other cellular components, such as cell membranes or the actin cytoskeleton (Bjelic et al., 2012, Conde & Caceres 2009). *In vivo*, +TIPs form comet-like accumulations at the growing but not at the shrinking plus end. Although the mechanism of +TIP localization is not fully understood, many studies favor the so-called "treadmilling" model, where +TIPs remain stationary with respect to the microtubule lattice

(Akhmanova & Hoogenraad 2005, Schuyler and Pellmann, 2001). The plus end specificity of +TIPs could happen either through a preferential binding to a structure of the freshly polymerized microtubule or through copolymerization with new tubulin subunits followed by a removal from older parts of the lattice due to tubulin conformation changes during tube formation (Jaworski et al., 2008). Malfunction of +TIPs lead to various human diseases including some forms of cancer, neurodevelopmental disorders or mental retardation (Jaworski et al., 2008).

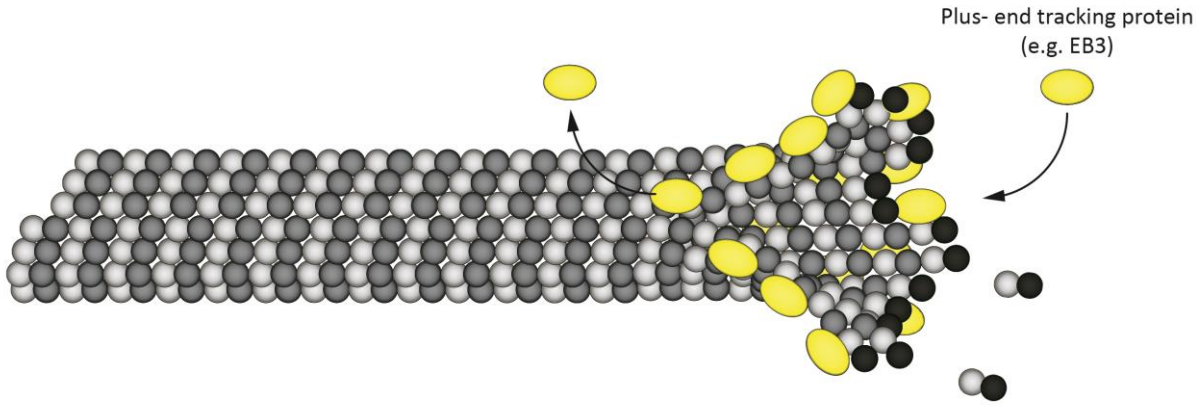

Fig. 1.6 Mechanism of plus end tracking

Plus end interacting proteins (+TIPs), such as EB1, EB3 or CLIP-170, recognize and bind to the growing tip of microtubules, whereas they are removed from older parts of the lattice.

Many different +TIPs have been identified, since the discovery of the first +TIP, the cytoplasmic linker protein CLIP-170 (Perez et al., 1999). All +TIPs share a limited number of evolutionary conserved structural elements (Akhmanova & Steinmetz 2008). According to their structural motifs, they can be grouped into different classes. Amongst these, cytoskeleton-associated Gly-rich proteins (CAP-Gly rich proteins) and end-binding proteins (EBs) are two important and well-studied families of +TIPs.

CAP-Gly rich proteins: +TIPs, which have a cytoskeleton-associated protein Gly-rich domain at their N-terminus, are classified as CAP-Gly rich proteins. Cytoplasmic linker proteins and a large subunit of the dynactin complex, $p150^{glued}$, belong to this +TIP family

(Akhmanova & Steinmetz 2008, Galjart 2010). Although details about the exact function and interaction partners are still unclear, CLIPs seem to be positive regulators of microtubule growth and can also affect the activity of other end binding proteins (Galjart 2010).

End-binding proteins: End-binding (EB) proteins are small dimers, where each monomer contains a highly conserved N-terminal calponin homology (CH) domain and a conserved C-terminal domain, separated by a linker sequence. The N-terminal domain is responsible for the microtubule binding whereas the C-terminal part contains a coiled-coil domain that mediates the dimerization of EB monomers (Akhmanova & Steinmetz 2008, Hayashi & Ikura 2003, Komarova et al., 2009). EB proteins rapidly exchange at the growing plus tip of microtubules, most likely by recognizing a structural element associated with microtubule polymerization (Komarova et al., 2009). Regarding the function of EBs, there are discrepancies between *in vivo* and *in vitro* model systems (Galjart 2010, Jaworski et al., 2008). This makes it difficult to understand the exact function of EBs and the interaction with other proteins. But overall, EBs seems to promote microtubule growth by suppressing catastrophe events. EB proteins are generally considered as the core component of +TIP networks, because they autonomously track growing plus ends independently of other binding partners and interact with almost all other +TIPs (Akhmanova & Steinmetz 2010). Mammalian cells contain three different EB proteins: EB1, EB2 and EB3, which are highly conserved amongst each other (Su & Qi 2001). In neurons, only EB1 and EB3 have so far been found throughout the cytoplasm.

1.2.2.2. Microtubule severing proteins

While most other microtubule regulating proteins interact with the plus end, microtubule severing proteins act along the entire lattice, cutting it into short fragments. In contrast to depolymerization, which happens only at microtubule ends, severing proteins create internal

breaks by an ATP-dependent reaction along the entire microtubule. A variety of studies show that microtubule severing enzymes are involved in many cellular activities, such as promoting microtubule growth, reorganization of the cytoskeleton, cell division or cell migration (Roll-Mecak & McNally 2010, Sharp & Ross 2012). The first microtubule severing protein was identified in Xenopus eggs in 1993 and was named after the Japanese name for sword: katanin (McNally & Vale 1993). During the following year, two other classes of severing enzymes, spastin and fidgetin have been described. All three proteins belong to the family of AAA ATPases (Roll-Mecak & McNally 2010).

Katanin: Katanin consists of a P60 and a P80 subunit and severs microtubules from the centrosome but is also widely distributed throughout neurons. Levels of katanin are increased during axon growth but return to lower levels as soon as the axon has reached its postsynaptic target (Karabay et al., 2004). Further experiments also underline the importance of katanin for neurite development and plasticity. It has for example been shown that inhibition of P60-katanin leads to a dramatic increase in microtubule length and compromises axon elongation during development (Ahmad et al., 1999). This is most likely due to the fact that long microtubules are rather immobile, whereas short microtubules can be transported and are important to promote axon growth. Because microtubule severing can have severe consequences for neuronal physiology, katanin activity has to be tightly controlled in neurons. One negative regulator of katanin is the MAP protein tau, which shields the microtubule lattice from severing. There is also evidence that dysregulation of katanin contributes to tauopathies such as Alzheimer's disease, where tau is hyper-phosphorylated and dissociates from the microtubule lattice (Baas & Qiang 2005, Sharp & Ross 2012).

Spastin: The microtubule severing protein spastin has a length of 616 amico acids and contains two major domains: one microtubule interacting domain at the N-terminus and one AAA domain at the C-terminus, responsible for the ATPase activity of the enzyme (Salinas et

al., 2007). The sequence shows large homology with katanin and the functions of both enzymes are a partly overlapping, namely in regulating axon morphology. Interestingly, many years before spastin was identified as a microtubule severing enzyme, it has been studied in the context of autosomal dominant hereditary spastic paraplegia (AD-HSP). This severe neurological disorder is characterized by a progressive weakening and spasticity of the lower extremities caused by a mutation in the spastin gene (Hazan et al., 1999). Only later studies proposed that spastin interacts directly with microtubules as a severing enzyme indicating that defects in microtubule severing can lead to axon degeneration in the human disease (Evans et al., 2005). Like katanin, spastin depletion leads to a decrease in branch formation and axon length, whereas overexpression enhances branch formation (Yu et al., 2008).

Fidgetin: Fidgetin is another AAA family member that is expressed throughout the nervous system and plays an important role in cell division (Roll-Mecak & McNally 2010, Sharp & Ross 2012). Its exact role still remains unclear, but it has been found that mutations in the fidgetin gene lead to severe developmental defects in mice (Yang et al., 2006), suggesting a potential role in development.

1.2.2.3. Motor proteins

As already pointed out, intracellular transport is one of the major functions of neuronal microtubules. Microtubules serve as tracks for fast axonal transport during which organelles and vesicles are actively trafficked by molecular motor proteins that use ATP to translocate along the cytoskeleton. Transported cargos are attached to motor proteins via adaptor proteins and can have many opposing motors stably attached at the same time (Hendricks et al., 2010). As a consequence, depletion of one motor can have an effect on overall transport, not only on transport in the direction that is mediated by the depleted motor protein (Pilling et al., 2006).

This suggests that directionality of transport is not regulated by a simple connection to the motor protein but rather depends on the activity of opposing motors on the same cargo (Welte 2004). Two major groups of motor proteins are present in neurons:

Kinesins: Kinesins move towards the plus end of microtubules and hence are responsible for anterograde transport in axons. Kinesin family members are composed of two identical heavy chains and two light chains, with both components of the assembled motor existing in several variants. Each heavy chain has a motor domain that contains a microtubule binding region and an ATP binding site. ATP hydrolysis is stimulated in the presence of microtubules and allows kinesins to move toward the plus end at a velocity of ~ 1µm/sec *in vitro* (Gennerich & Vale 2009, Verbrugge et al., 2007, Wade 2009). So far, more than 45 kinesin genes have been identified, which give rise to a large group of structurally similar proteins that have different specificity for certain cargos. Mitochondria for example are mainly transported by KIF1Ba and KIF5 (Hirokawa 2011, Hirokawa et al., 2010). Kinesin motor proteins do not only transport cargos along microtubules, but they can also regulate microtubule dynamics. Several kinesins (e.g. kinesin-8, 13 and 14) facilitate microtubule disassembly or depolymerize microtubules in an ATP-dependent manner, such as KIF2a and 2C. In contrast, other kinesin family members, like KIF17, can promote microtubule stabilization (Gumy et al., 2013, Hirokawa et al., 2010). Mutations in KIF genes have also been shown to give rise to a number of neurodegenerative phenotypes (Reid et al., 2002, Zhao et al., 2001).

Dynein: Dynein mediates retrograde transport as it moves towards the minus end of a microtubule (Hirokawa et al., 2010, Welte 2004). Dynein is a large macromolecular complex composed of one to three copies of a heavy chain and various intermediate and light chains that confer diversity. In contrast to the diversity of kinesin superfamilies, only a single cytoplasmic dynein heavy chain is responsible for cargo transport in axons and dendrites

(Hirokawa et al., 2010). Dyneins move at a speed of > 2 µm/sec again using energy derived from ATP hydrolysis. Similar to kinesin mutations, mutations in dynein subunits can cause severe neurological disorders (Lipka et al., 2013).

1.2.3. Posttranslational modifications

While the basic molecular structure of all microtubules is the same, they can be very different in terms of their stability or dynamic behavior. This is achieved by posttranslational modifications of α- and β- tubulin that can occur along a microtubule (Hammond et al., 2008, Ikegami & Setou 2010, Kapitein & Hoogenraad 2011). The stability of microtubules can vary from being very dynamic with a half-life time of several minutes, to being a stable structure with a half-life time of several hours. Stable microtubules have typically accumulated a greater number of tubulin modifications over time (Hammond et al., 2008, Ikegami & Setou 2010, Westermann & Weber 2003). Posttranslational modifications are evolutionary conserved and influence microtubule function, for example via interaction with microtubule interacting proteins, motor proteins or microtubule severing proteins (Hammond et al., 2008). Tubulin modifications can also increase microtubule stability by reducing the activity of microtubule depolymerases (Peris et al., 2009). The most common microtubule modifications in neurons are detyrosination, acetylation and polyglutamylation, which will be explained in more detail below (Fukushima et al., 2009, Ikegami & Setou 2010, Kapitein & Hoogenraad 2011).

Detyrosination/Tyrosination: During detyrosination, the enzyme tubulin tyrosine carboxypeptidase (TTCP) removes the C-terminal tyrosine residue of α-tubulin. This exposes a glutamic acid residue and hence the modified tubulin is often called Glu-tubulin. Detyrosinated tubulin can be further modified by removal of penultimate glutamate, leaving a

so-called Δ2-tubulin. Free tyrosine can also be reattached to the C-terminal glutamate by the enzyme tubulin-tyrosine ligase (TTL), but Δ2-tubulin is no longer a substrate for TTL (Ikegami & Setou 2010, Kapitein & Hoogenraad 2011, Westermann & Weber 2003). Detyrosination has been associated with microtubule stabilization, as long-lived microtubules show a large degree of detyrosination (Janke & Kneussel 2010). Nevertheless, detyrosination of microtubules does not seem to enhance microtubule stability itself (Khawaja et al., 1988). *In vitro* studies also revealed that detyrosination affects the interaction of microtubules with certain motor proteins. Kinesin-1 for example has a stronger affinity to detyrosinated tubulin (Liao & Gundersen 1998). The creation of a TTL knock-out mouse further showed that detyrosination/tyrosination also regulates CLIP-170 localization via its binding to microtubules (Erck et al., 2005).

Acetylation: Tubulin acetylation occurs mainly at the lysine-40 residue of α-tubulin at the inner side of the microtubule lattice. Although acetylation occurs on stable microtubules, it does not seem to be the cause of microtubule stability itself (Palazzo et al., 2003, Westermann & Weber 2003). Microtubule acetylation is involved in regulation of motor-based traffic and anchoring of molecular motors (Hammond et al., 2008, Reed et al., 2006). Histone deacetylases are enzymes mostly known for catalyzing the deacetylation of histones, but they also act on cytoplasmic proteins, such as α-tubulin (Hammond et al., 2008, Hubbert et al., 2002). HDAC6 and sirtuin 2 (Sirt2) can mediate tubulin deacetlyation (Janke & Bulinski 2011). Recent studies have also identified HDAC5 as an injury-regulated tubulin deacetylase, which is activated after injury by calcium influx and proteins kinsase C activity (Cho et al., 2013). A number of studies show that decreased levels of acetylated α-tubulin are also found in neurodegenerative disease (d'Ydewalle et al., 2011, Gardiner et al., 2007, Hempen & Brion 1996) and that tubulin deacetylation can be inhibited by small molecular drugs, such as scriptaid (Su et al., 2000). Therefore, a pharmacological inhibition of HDAC6 could be a

potential therapeutic approach for certain forms of neurodegeneration (d'Ydewalle et al., 2011).

Polyglutamylation: Polyglutamylation is a post-translational modification, where multiple glutamic acids are added to the to the glutamine residue at the C-terminus of both tubulins. The resulting polyglutamate side chains are of variable length and are involved in regulating protein-protein interactions (Hammond et al., 2008). Polyglutamylation of neuronal tubulin is catalyzed by polyglutamylases, multi-protein complexes whose enzymatic subunit are tubulin tyrosine ligase-like (TTLL) proteins (Janke et al., 2005). Different polyglutamylase enzymes have different specificities, for example a preference for binding α- or β-tubulin or creating short versus long glutamate side chains (van Dijk et al., 2007). Additionally, polyglutamylation of neuronal tubulin is also regulated by deglutamylases, which catalyze the removal of glutamate residues (Audebert et al., 1993). It has been demonstrated that microtubule associated proteins and dyneins preferentially bind to polyglutamylated tubulin (Bonnet et al., 2001) and moreover, this modification regulates the interaction and activity of a number of MAPs and motor proteins (Janke & Kneussel 2010, Westermann & Weber 2003). A group of proteins that is regulated by polyglutamylation are microtubule severing proteins which promote disassembly of microtubules. It was for example shown *in vitro* that long side chains of glutamate can induce spastin dependent microtubule severing (Lacroix et al., 2010).

1.3. Microtubule dynamics in development

As pointed out above, microtubules are key players in establishing morphologically and functionally distinct neuronal compartments. To achieve this complex polarity in the mature state, newly born neurons have to undergo several developmental steps, such as cell

migration, axon formation and the establishment of synaptic connections (Witte et al., 2008). Microtubules do not only maintain the polarity of mature neurons, but are also required to initially establish polarity during neurogenesis and they are capable of converting molecular signals into structural changes during development to generate functional neurons (Li & Gundersen 2008).

1.3.1. Neurogenesis and maturation

In general, mature neurons have a much larger proportion of stable microtubules, compared to developing neurons, where the microtubule network is much more dynamic (Conde & Caceres 2009). At different steps of development, microtubules act as key players to form a mature neuron. First of all, microtubules are already involved in the birth of a neuron, as they form the mitotic spindle for cell division. Also, subsequent neuronal polarization and axon formation is dependent on a rearrangement of the microtubule cytoskeleton. Initially, all neurites have a mixed orientation of microtubules. Subsequently one neurite establishes a plus end out orientation and becomes the axon (Witte et al., 2008). Outgrowth of an axon and innervation of the postsynaptic target also require formation of a growth cone, which follows attraction and repulsion cues to find its destination. Microtubule assembly and disassembly, as well as interaction with the actin cytoskeleton in a growth cone form the basis for growth cone motility (Neukirchen & Bradke 2011). The interplay between cytoskeletal elements is also necessary for axon branching, as well as for synapse formation and maintenance (Goellner & Aberle 2012, Wade 2009). Different enzymes, for example GTPases and Rho kinases, are involved in regulating changes of the cytoskeleton during axon outgrowth and motility (Dent & Gertler 2003, Tahirovic & Bradke 2009). Microtubules are also crucial for the motility of neurons, for instance during lamination of the cortex, where new born neurons need to migrate over significant distances to reach their final destination.

Assembly and disassembly of microtubules creates pushing and pulling forces, which allows the neuron to move to its final location (Kuijpers & Hoogenraad 2011). Disturbances in microtubule dynamics or microtubule associated proteins can lead to developmental disorders, which have severe consequences for the organism. For example mutations in genes that regulate cytoskeletal processes lead to migration abnormalities, which result in developmental diseases such as human lissencephaly ("smooth brain") (Jaglin & Chelly 2009, Moon & Wynshaw-Boris 2013).

1.3.2. Developmental pruning

The establishment of a functional neuronal network during development requires more than neurogenesis and formation of neuronal connections. For fine tuning of the neuronal network, individual axons, synapses or dendrites are selectively removed, without affecting the viability of the remaining neuron (Luo & O'Leary 2005). Some invertebrates also show large scale elimination and reformation of neuronal connections during metamorphosis. The latter involves primarily degeneration, whereas local pruning is mediated by local dismantling and ingestion by surrounding glia cells. Over the last decades, the neuromuscular junction (NMJ) has emerged as an excellent model system to study axon pruning. During embryonic development, motor neurons form connections with a large number of muscle cells, which results in converging poly-innervation of single muscle fibers by many motor axons. During the first weeks of postnatal life, individual axon branches are selectively dismantled, ultimately leaving each muscle fiber with only one innervating input (Lichtman & Colman 2000). The transition from multiple to single axonal innervation is driven by competition between co-innervating inputs during which neuronal activity plays an important role (Balice-Gordon & Lichtman 1994, Buffelli et al., 2003). However, in contrast to axon outgrowth, relatively little is known about cellular and molecular mechanisms underlying developmental

axon pruning. Given the importance of the microtubule cytoskeleton for maintaining cell homeostasis and the fact that alterations in microtubule dynamics often lead to degeneration, it seems likely that microtubule dynamics also play an important role in neurite remodeling. Indeed, investigations on the sequence of cellular events during metamorphosis of Drosophila mushroom bodies identified degradation of microtubules as the earliest sign of axon pruning (Watts et al., 2004). Also during synapse elimination at the mammalian neuromuscular junction, microtubule density is sparser in retracting motor axons than in the axon branch that remains at the postsynaptic target (Bishop et al., 2004). Further studies indicate that interactions of microtubule with the actin cytoskeleton or motor proteins also play an important role in axonal pruning (Luo & O'Leary 2005). However, only a few signaling molecules have so far been identified to regulate microtubule dynamics during neurite pruning. There is substantial evidence that RhoA, a small GTP-binding protein, is involved in a signaling pathway that leads to destabilization of microtubule and finally to axon retraction (Billuart et al., 2001, Luo & O'Leary 2005). Studies on Drosophila mushroom bodies also revealed that inhibition of the negative RhoA regulator p190RhoGAP leads to axon branch retraction (Billuart et al., 2001). In contrast, mice that lack KIF2A, a kinesin superfamily protein that acts as microtubule depolymerase, show a protection of axonal microtubules, which in turn lead to a delay in axon dismantling and potentially to skin hyper-innervation (Maor-Nof & Yaron 2013). Remarkably, deletion of other microtubule severing proteins, like spastin or katanin, does not have any impact on developmental pruning at least in flies (Lee et al., 2009, Stone et al., 2012). This implies that KIF2A acts as regulator of microtubule disassembly and axon removal during development.

Even though relatively little is known about the exact regulators, pathways and cellular processes that underlie axon pruning, developmental changes in neurite morphology are strikingly similar to axonal changes after injury or in disease (Neukomm & Freeman 2014).

Hence it seems likely that signaling pathways involved in developmental axon removal might also lead to destabilization during pathological degeneration and *vice versa*.

1.4. Microtubules in injury and disease

Many years of research on cytoskeletal function and dynamics have revealed that microtubules are key players in many dynamic cellular processes, such as providing stability and cargo supply. Not surprisingly, disturbances of microtubule dynamics have severe effects on the neuronal homeostasis and are often found under pathological conditions. Neurodegeneration is often attended by axonal swellings, axonal transport deficits and accumulation of proteins (Cartelli et al., 2013). These symptoms have been associated with alterations of the cytoskeleton and a large body of literature links microtubule dysfunction to neurodegeneration, both after injury (Chen et al., 2012a, Erez et al., 2007, Erturk et al., 2007) and during neurodegenerative disease (Cartelli et al., 2013, d'Ydewalle et al., 2011, Fanara et al., 2007). This makes microtubules promising targets for pharmacological treatment in pathology, especially because the alterations in the cytoskeleton often occur at early stages of neurodegeneration (Baas & Ahmad 2013, Cartelli et al., 2013).

1.4.1. Neurodegenerative disease

Emerging evidence suggests that mutations in cytoskeletal components or microtubule interacting proteins are associated with a number of neurodegenerative diseases (**Table 1.1**; (Chevalier-Larsen & Holzbaur 2006, Franker & Hoogenraad 2013, McMurray 2000). Tubulin mutations for instance impact neuronal viability as they lead to changes in microtubule dynamics, axon guidance or kinesin interaction (Tischfield et al., 2010). This causes severe neurological symptoms (Niwa et al., 2013), such as deficits in cortical development and

neuronal migration disorders (Jaglin & Chelly 2009, Poirier et al., 2010). Hyper-dynamic microtubules were also shown to be an early feature in an animal model of amyotrophic lateral sclerosis (ALS). ALS is the most common motor neuron disease in adults, where motor axons undergo progressive degeneration leading to muscle atrophy and finally death due to respiration failure (Ringholz et al., 2005). Post-mortem studies on mouse models of familiar amyotrophic lateral sclerosis indicate an increase in destabilized microtubules in motor axons. Treatment of those mice with microtubule modifying agents was sufficient to delay disease symptoms (Fanara et al., 2007).

Disease	Mutant protein	Functional defect	Pathology	Reference
Alzheimer's disease	amyloid precursor protein	mutated amyloid-β leads to hyper-phosphorylation of tau	tau dissociates from microtubules and forms neurofibriallary tangles	O'Brien & Wong 2011, Stokin et al., 2005
Charcot-Marie-Tooth (Type 2)	chaperon (HSPB1)	reduced transport of synaptic vesicles	muscle weakness and atrophy	Chevalier-Larsen & Holzbaur 2006, Zhao et al., 2001
Hereditary spastic paraplegia	SPG4 (spastin) KIF5A	inactivation or down-regulation of spastin severing activity	synaptic growth and neurotransmission defects altered microtubule/ motor interaction	Hazan et al., 1999, Evans et al., 2005, Fassier et al., 2013
Lissencephaly	α-tubulin (TUBA1A) β-tubulin (TUBB2B)	Defects in neuronal migration	cortical abnormalities; malformation of cortical laminiation	Jaglin et al., 2009, 2005, Franker & Hoogenraad 2013
Parkinson's	parkin synuclein	inclusions of a-synuclein, microtubule dysfunction, axonal transport deficits	loss of dopaminergic neurons in the substantia nigra	Cartelli et al., 2010, McMurray 2000
(distal) Spinal muscular atrophy	dynein (DYNC1H1)	transport deficits	motor neuron degeneration; brain abnormalities	Fiorillo et al., 2014, Franker & Hoogenraad 2013
Tauopathies	different tau mutations	accumulations of tau, microtubule and axonal transport deficits	Dementia, movement disorders	Lee et al. 2001

Table 1.1 Mutations in proteins that are linked to microtubule dynamics

Similarly, alterations in microtubule associated proteins can induce changes in microtubule stability and are often found in neurological disorders. Tau protein defects for example are associated with a range of neurodegenerative diseases known as tauopathies (Lee et al., 2001). The most prominent example of tau aggregation can be found in Alzheimer's disease, where

so called neurofibrillary tangles are formed. Mutations in microtubule-associated motor proteins were shown to have a negative impact on axonal transport and can lead to neuronal death (Cairns et al., 2004). There is also growing evidence about microtubules being involved in a number of other neurological diseases, such as Huntington's disease (Li et al., 2000, Trushina et al., 2004; Reddy et al., 2009), Prion diseases (Zhang & Dong 2012) or hereditary spastic paraplegia (Evans et al., 2005, Fassier et al., 2013).

Overall, many studies have linked neurodegenerative diseases to mutations that alter the conformation of microtubules or are accompanied with a dysfunction of the microtubule cytoskeleton (**Table 1.1**). But although defects in the cytoskeleton indeed seem to be a common feature of neurodegeneration, the literature is often controversial on the details of such cytoskeletal disruptions and it is not always clear to what extent findings in animal models of neurological diseases can be transferred to humans.

1.4.2. Injury

Acute damage of nerve cells, such as nerve crush or traumatic brain injury, impacts the cellular homeostasis and can causes axon loss or death of the affected neuron. Axons, which often span long distances to reach their postsynaptic target, are preferentially affected during nerve injury and undergo subsequent degeneration.

After trauma, a series of processes is initiated in the axon ultimately leading to degeneration. Within half an hour after injury, axons undergo sudden fragmentation that extends over 200-300 µm on both, the proximal and the distal, axon ends. This process is called acute axonal degeneration (AAD) and is mediated by mechanisms similar to Wallerian degeneration, which however follows a more delayed time-course (Kerschensteiner et al., 2005). But in contrast to AAD, Wallerian degeneration only affects the distal part of the injured axon, which undergoes fragmentation followed by clearance of the resulting debris by surrounding

glia cells (Beirowski et al., 2009). Wallerian degeneration and other forms of axonal degeneration are not passive events, but rather active, cellular processes. Although little is known about the underlying molecular mechanism, microtubule destabilization is an early phenomenon in the sequence of cellular responses. During AAD, Ca^{2+} influx leads to a condensation of neurofilaments and a fragmentation of microtubules (Knoferle et al., 2010). During Wallerian degeneration microtubule breakdown is the first detectable event after trauma (Zhai et al., 2003). It has become clear that injury triggers a cascade of intracellular events, such as rise in Ca^{2+} levels, destruction of cellular organelles and a widespread breakdown of the cytoskeleton. Furthermore, changes in axonal transport, local protein synthesis or gene expression can be observed after injury (El Bejjani & Hammarlund 2012, Neukomm & Freeman 2014). Recent studies (Park et al., 2013) also found a reduction in cellular NAD and ATP levels, microtubule depolymerization and mitochondrial swelling after sciatic nerve injury. This study also found that axons had a reduction in microtubule number 24 hours after axotomy. Microtubule depolymerization occurs before mitochondrial swelling but both phenomena can be prevented by addition of NAD. Moreover, experiments in flies found a large increase in microtubule dynamics immediately after axon severing. Interestingly, dendrites do not undergo up-regulation of dynamic microtubules after severing. Instead, one of the dendrites switches its mixed microtubule orientation to plus end out orientation and becomes the new axon (Stone et al., 2010). Such results demonstrate that a change in microtubule dynamics is not only a response to axon damage, but also required for regeneration of the nervous system. Studies on Aplysia neurons revealed that axotomy leads to a reorientation of microtubules and the formation of so called “traps” at the cut end. Formation of traps has been described in cultured Aplysia neurons after axotomy, where a Ca^{2+} dependent reorientation of the microtubules leads to an accumulation of vesicles and the formation of a trap (Erez et al., 2007).

Beside the activation of cellular pathways after nerve injury, there is also a mechanical damage to the microtubule cytoskeleton, which causes axon degeneration itself. Dynamic stretch of axons induces a physical damage to the microtubule lattice and leads to a disassembly around the breaking points. Immediately after stretch injury, deformations along the axons occur, but decomposition of microtubules allows a delayed recovery of straight axon morphology. However, as a result axonal transport is blocked, which leads to protein accumulations, axonal swellings and finally degeneration (Tang-Schomer et al., 2010).

At least in the peripheral nervous system, axons are in many cases capable to regenerate, whereas damaged axons in the CNS fail to spontaneously regenerate (Gordon-Weeks & Fournier 2014). In the PNS, the surviving proximal stump of the axon can re-grow to innervate its original postsynaptic targets (Nguyen et al., 2002). During both events- axon degeneration and regeneration- the microtubule cytoskeleton plays a decisive role. After injury of a peripheral axon, the proximal tip forms a growth cone that finds the way back to the original target. In the CNS, instead of a growth cone the proximal tip forms a retraction bulb, which prevents growth (Erturk et al., 2007). It has long been known that microtubule rearrangement is essential for growth cone formation, axon guidance and branching (Dent & Gertler 2003, Sabry et al., 1991). Application of reagents that promote microtubule depolymerization is sufficient to transform growth cones into retraction bulbs. On the other hand, stabilization of the microtubule cytoskeleton enhances regeneration in the CNS, prevents the formation of a retraction bulb and promotes regrowth (Erturk et al., 2007, Sengottuvel et al., 2011). The failure to reestablish a functional microtubule cytoskeleton at the proximal stump seems to be the primary cause of retraction bulb formation in the CNS.

Alterations in microtubule behavior are partly triggered by changes in posttranslational modifications. Ca^{2+} influx for example induces a protein kinase C mediated activation of histone deacetylase 5 (HDAC5), which in turn promotes tubulin deacetylation (Cho & Cavalli 2012). Blocking of Ca^{2+} influx inhibits PKC or HDAC5 activity and tubulin deacetylation,

which leads to a decrease of axon regeneration. Also levels of tyrosinated tubulin were found to be increased after axotomy (Mullins et al., 1994).

Altogether, these findings suggest that a breakdown of the microtubule cytoskeleton is upstream of other cellular events during axon degeneration and reorganization of the cytoskeleton plays a key role in regeneration. Thus, stabilizing the microtubule cytoskeleton could be a promising approach to prevent axon degeneration after injury. Axon damage provokes acute axonal stress, compared to a chronic and more long-term stress during neurological diseases. However the cytoskeletal changes are comparable in both settings and might share the same cellular mechanisms. Microtubule stabilizing agents might therefore not only be interesting therapeutic approaches after injury, but also in other, more chronic neurological conditions (Stanton et al., 2011). Yet, in spite of a broad literature about microtubule alterations in disease, the direct relationship between microtubule dynamics and neuronal pathogenesis is still vague. This is in part due to the limited set of techniques for imaging microtubule dynamics *in vivo* in the mammalian nervous system (Fanara et al., 2007).

1.4.3. Microtubule modifying drugs and therapy

As previously pointed out, a large set of studies shows that the microtubule cytoskeleton is very sensitive to changes in cell physiology and early affected under pathological conditions. As a consequence, alterations in the microtubule cytoskeleton often lead to a breakdown of other cellular processes and ultimately to neurodegeneration. For this reason, pharmacological targeting of microtubules has long been of interest for therapy after injury and in disease. In particular, microtubule stabilizing drugs have proven beneficial effects in different diseases and injury models by preventing degeneration and scar formation as well as promoting axon

growth and regeneration (Cartelli et al., 2013, Erturk et al., 2007, Fanara et al., 2007, Hellal et al., 2011, Sengottuvel et al., 2011).

Taxanes: Paclitaxel (also known under its trade name "Taxol") and its derivatives are probably the best studied microtubule modifying substances and have been tested in various conditions and disease models. Initially paclitaxel was described as an antitumor agent, isolated from the yew tree Taxus brevifolia (Wani et al., 1971). Taxol's stabilizing effects on microtubules remained unknown until 1979, when *in vitro* experiments revealed a promotion of microtubule assembly after paclitaxel treatment (Schiff & Horwitz 1980). Paclitaxel and its equivalents bind to a pocket on the luminal surface of β-tubulin – called the "taxane site"– along the entire lattice. It is suggested that this leads to a conformation change of β-tubulin, which stabilizes lateral interactions of protofilaments and inhibits the effects of GTP-hydrolysis (Baas & Ahmad 2013, Brunden et al., 2014). Microtubule disassembly is suppressed and assembly is favored, which causes an overall stabilization of microtubules, mitotic arrest and apoptosis in dividing cancer cells (Baas & Ahmad 2013). The taxane site is also targeted by tau and hence taxol application can induce a displacement of tau from microtubules (Ballatore et al., 2012). Paclitaxel has been used as chemotherapeutic reagent in oncology for many years now. But because paclitaxel is applied at rather high concentrations for cancer treatment, it often goes along with severe side effects, in particular peripheral neuropathies (Baas & Ahmad 2013, Gornstein & Schwarz 2014). The beneficial effects of microtubule stabilizing drugs on neurons after injury or during disease, if applied at low doses in the nano- or micro-molar range, was first shown in tau transgenic mice. A number of studies show, that paclitaxel has beneficial effects on mice that develop a brainstem and spinal cord tauopathy. After paclitaxel treatment, microtubule density returned to normal levels, axonal transport recovered and motor performance was improved (Brunden et al., 2011, Zhang et al., 2005). Moreover, low doses of paclitaxel have also beneficial effects on mouse

models of hereditary spastic paraplegia (Fassier et al., 2013). Application of paclitaxel after axon trauma can reduce degeneration (Tang-Schomer et al., 2010) and improves regeneration of injured axons (Hellal et al., 2011, Sengottuvel et al., 2011). In contrast, 0.5 µM Paclitaxel was found to enhance axon degeneration and mitochondrial swelling in sciatic nerve explants (Park et al., 2013). These findings point out how different doses of microtubule stabilizing drugs can have opposing effects on the cytoskeleton and cell physiology. While low doses promote polymerization of microtubules and have beneficial effects during axon degeneration and regeneration, high doses lead to a "freezing" or even depolymerization of the microtubule cytoskeleton often followed by cell death, advantageous for cancer therapy. But despite the positive effects of paclitaxel on degeneration and regeneration, there is one disadvantage that makes this drug insufficient for treatment of humans: paclitaxel and its derivatives cannot cross the blood brain barrier (Baas & Ahmad 2013). Hence it has been of great interest throughout the last years to find other components, which have similar characteristics as taxol but are capable of passing the blood brain barrier. As such, several other classes of microtubule stabilizing molecules have been described, mostly natural products, which act in a similar manner and interact in close proximity to the taxane site (Stanton et al., 2011).

Epothilone: Epothilone A and B target the taxane binding site (Bollag et al., 1995) and were initially isolated from soil bacteria as antifungal agents (Reichenbach & Hofle 2008). A few years later, Epothilone D was isolated from myxobacteria and appeared to have even more suitable features for therapy (Kolman 2004). In fact, studies that use Epothilone D treatment in different disease models indicate a potential use for human therapy. Weekly intraperitoneally injection of the Epothilone D analog BMS-241027 in different mouse models of tauopathies were sufficient to increase the total number of microtubules, restore normal microtubule dynamics and axonal transport. Also a decrease in axon dystrophy and neurodegeneration was also observed after Epothilone D treatment (Zhang et al., 2012).

Currently the Epothilone D analog BSM 241027 is in phase 1 clinical trial for patients with mild Alzheimer's disease (Clinical Trials.gov; Identifier: NCT01492374). Other experiments revealed that Epothilone D treatment of mice with MPTP-induced Parkinsonism can rescue microtubule dysfunction and prevent neurodegeneration. Epothilone D treated MPTP mice also show improved axonal transport in dopaminergic neurons and normalization of posttranslational microtubule modifications (Cartelli et al., 2013).

Perloruside A: Perloruside A was isolated from the marine sponge Mycale hentscheli and is a cytotoxic agent with paclitaxel-like activities (West and Nordcote, 2000). It does not interact with the taxane binding site but instead binds to the outer surface of β-tubulin (Huzil et al., 2008). Cultured cortical neurons treated with okadaic acid, a compound that inhibits the outgrowth of neurites by tau hyper-phosphorylation, showed an increase in axonal outgrowth and branching, as well as restored levels of acetylated tubulin after Perloruside A treatment (Das and Miller, 2012).

HDAC inhibitors: Beside microtubule stabilizing agents, there is also increasing interest in drugs that inhibit the activity of histone deacetylases (HDACs). HDACs are enzymes that regulate the acetylation status of different proteins, including tubulin. During the last years, HDAC inhibitors have gained attention as potential therapeutic reagents in cancer treatment but also for neurodegeneration (Kazantsev & Thompson 2008). HDAC 6 inhibitors, like Tubastatin A, can improve neuron viability after central nervous system injury (Rivieccio et al, 2009) and are sufficient to protect cortical neurons against glutathione-depletion induced oxidative stress (Dallavalle et al, 2012). Mouse models for Charcot-Marie-Tooth disease (CMT) or distal hereditary motor neuropathy (HMN) are characterized by a decrease in acetylated tubulin and axonal transport deficits. Inhibition of HDAC6 via Trichostatin A, Tubacin and, most efficiently, with Tubastatin A, was sufficient to restore the number of moving mitochondria and decreased disease symptoms (d'Ydewalle et al., 2011).

There is an increasing list of natural and synthetic microtubule modifying agents. Stabilizing or modulating the microtubule cytoskeleton has proven to be a promising approach in translational research and is moving towards clinical trials. However, it is important to keep in mind that many of these drugs come along with different side effects, for example neuropathies or a disturbance in axon-dendritic compartmentalization (Baas & Ahmad 2013). Furthermore it is still not known if changes in microtubule dynamics are cause or consequence in neurodegeneration, as direct studies of microtubule dynamics in the mammalian nervous system are currently challenging.

1.5. Imaging of microtubules

Due to the fundamental role that the cytoskeleton plays in physiology of developing and mature neurons, studying microtubule dynamics is of great interest in many different research areas. However, this is very challenging, because of the small size of microtubules, their poor accessibility and sensitivity to manipulations of cell homeostasis. Over the last decades, different approaches aimed to investigate microtubule dynamics *in vitro* and in different model organisms.

1.5.1. History of microtubule imaging

Microtubules have been observed for the first time more than a century ago by light microscopy of silver stained nerve preparations, but initially their function remained unclear (Schmitt 1968). Live imaging of dividing sea urchin eggs made it possible to identify microtubules as components of the mitotic spindle (Schmidt 1939). By that time, it was already known, that microtubules are present in all plant and animal cells, but other functions, beside the formation of the mitotic spindle, were still not identified. Experiments on the squid

giant axon implied that microtubules play a role in stabilization, cell motility and intracellular transport (Schmitt 1968). Electron microscopy of rat anterior horn cells for the first time allowed visualization of microtubules in axons and dendrites. It was described, that microtubules have a diameter of 24 nm and extend straight along neurites (Wuerker & Palay 1969). Before time-lapse imaging of cellular structures in neurons became possible, for example by fluorescently tagged molecules, further investigations of the neuronal cytoskeleton focused on polarization and orientation of microtubules. The so called "Hook method", established in the late 1970s, allowed visualization of microtubule polarity *in vitro* in conditions where externally added tubulin assembles onto existing microtubules as laterally attached ribbons. Depending on whether the attached ribbons curve clockwise or counter-clockwise, the polarity of a microtubule in relation to its origin can be determined (Heidemann & McIntosh 1980). With this method, the uniform polarity of axonal microtubules was discovered (Burton & Paige 1981, Heidemann & McIntosh 1980) and a few years later also the non-uniform distribution in dendrites (Baas et al., 1988, Burton 1988). With the help of electron microscopy, even morphological differences between growing and shrinking microtubules could be resolved (Mandelkow et al., 1991, Simon & Salmon 1990).

1.5.2. Fluorescently tagged microtubules

In the 1980s direct visualization of microtubule dynamics in living cells became possible *in vitro* and in single cell assays using fluorescently conjugated microtubules. 5- and 6-carboxy-Xrhodamine-N-hydroxysuccinimide labeled tubulin was used to monitor the dynamic instability of microtubules in living fibroblast lamelli (Sammak & Borisy 1988) and showed that microtubules undergo periods of assembly and disassembly. Furthermore, this method helped to determine different depolymerization rates and growth parameters (Sammak & Borisy 1988, Schulze & Kirschner 1988). In the beginning this approach was limited

because of a low throughput and was not easily applicable to investigations in intact tissue. To improve this, approaches were established based on the expression of tubulin subunits and microtubule associated proteins tagged with fluorescent proteins. Generation of a fusion protein between human CLIP-170 and GFP was the first method that allowed monitoring the dynamic properties of microtubules in HeLa and Vero cells using time-lapse fluorescence microscopy. GFP was attached to the N-terminus of CLIP-170, since this site does not interfere with the function of CLIP-170. Time-lapse recordings of GFP-CLIP170 revealed that this protein binds to the plus end of the microtubule and moves with the growing tip – a behavior that was named "treadmilling" or "plus-end tracking" (Perez et al., 1999). In the following years, a number of studies used fluorescent proteins fused to tubulin (Komarova et al., 2002) and +TIP proteins other than CLIP-170 (Akhmanova et al., 2001, Hoogenraad et al., 2000, Komarova et al., 2005) to further investigate the dynamic behavior of microtubules and the protein interactions at the growing plus tip. However, all live imaging studies were done in non-neuronal cells until in 2003, when Stepanova and colleagues (Stepanova et al., 2003) fused end-binding protein 3 to GFP (EB3-GFP) to investigate microtubule dynamics in cultured Purkinje and hippocampal neurons. This assay allowed studying microtubule behavior in different neuronal compartments and types of neurons. Microtubules appeared as comet like structures with a growth speed of ~0.22 µm/sec and could be followed over an average distance of ~1-2 µm *in vitro*. Application of nocodazole or paclitaxel was found to abolish EB3-GFP comets (Stepanova et al., 2003). Further studies using fluorescently tagged CLIPs or EBs gained deeper insight into microtubule behavior in cultured neurons, during development (Neukirchen & Bradke 2011), after injury (Erez et al., 2007) or in spine plasticity (Jaworski et al., 2009). More recently techniques were developed to image microtubule dynamics also *in vivo*, in Drosophila (Stone et al., 2008) and in zebrafish (Norden et al., 2009), mostly using tagged EB1 or EB3. These studies have proven that fluorescently tagged +TIPs are an efficient and non-toxic approach to investigate microtubule behavior

under various conditions. This allowed important predictions about the role of microtubule dynamics in the mammalian nervous system under physiological and pathological conditions. However, actually testing such predictions *in vivo* was so far not possible, because a method that allows imaging microtubule dynamics in the mammalian nervous system *in vivo* were not established. At the same time, an approach like this would be extremely useful especially for translational research, because studies in mammals might be more transferable to human therapy than investigations in non-vertebrates and most translational disease models are established in mice or rats. To what degree findings from *in vitro* and invertebrate model systems can also hold true in mammals also remains unclear, as non-mammalian neurons differ substantially from mammalian ones, for example in their regeneration behavior (El Bejjani & Hammarlund 2012, Tanaka & Ferretti 2009).

1.6. Experimental aims

The aim of my PhD project was to develop a novel approach that allows imaging microtubule dynamics *in vivo* in the murine nervous system. This included the accomplishment of the following tasks:

1.) Characterization of newly generated *Thy1*:EB3-YFP transgenic mouse lines in terms of expression pattern and level of overexpression. Furthermore I performed histological and functional control experiments, to ensure that overexpression of EB3-YFP does not cause toxicity or abnormal behavior of dynamic microtubules.

2.) To image microtubule dynamics in different compartments of intact mammalian neurites, I established different *ex vivo* and *in vivo* preparations and matched them with suitable forms of high-resolution microscopy (wide-field, confocal and two-photon microscopy) to characterize microtubule dynamics in mature neurites of the peripheral and central nervous system.

3.) After characterizing microtubule dynamics under physiological condition, I investigated how microtubule dynamics are altered after axon injury, during neurodegenerative disease and under the influence of microtubule modifying drugs.

4.) Together with Monika Brill (AG Misgeld, TU Munich) I investigated the role of dynamic microtubules during developmental synapse elimination and performed pharmacological and genetic manipulations of microtubule stability to test the outcome on axonal pruning.

2. MATERIALS AND METHODS

The experimental procedures that were performed during this PhD thesis are to a large degree described in the manuscript *Kleele et al., 2014* published in *Nature Communications*. The descriptions provided here are based on the published text that I wrote.

2.1. Animals

Thy1:EB3-YFP transgenic mice were generated by Dr. Leanne Godinho as described previously (Marinkovic et al., 2011). To label growing microtubule tips, regulatory elements of the *Thy1*-promotor were used to express yellow fluorescent protein (YFP) tagged end-binding protein 3 (EB3) specifically in neurons (Caroni 1997, Feng et al., 2000). An N-terminal in-frame fusion was generated between the coding sequence of YFP and EB3. The EB3 sequence was derived from an EB3-GFP vector (provided by B. Link, Medical College of Wisconsin, USA) that comprises an in-frame cloning of human EB3 cDNA (AA2892, Image clone 714028) into pEGFP-N1 (Clonetech, Palo Alto, CA; (Stepanova et al., 2003)). The EB3-YFP fusion gene was cloned downstream of the *Thy1*-promoter (Marinkovic et al., 2011). *Thy1:*EB3-YFP transgenic mice were generated using standard pronuclear injection procedures in collaboration with Ronald Naumann (Max-Planck Institute, Dresden). Ten founder lines were obtained and characterized for their expression of EB3-YFP in different parts of the nervous system. J045, the lowest expressing line, was used for most experiments, except for cortical imaging, where line J023 was used.

To study mitochondrial transport in *Thy1:*EB3-YFP transgenic mice, animals from the J045 strain were crossed to *MitoMice* (Tg(Thy1-CFP/COX8A)C1Lich/J; (Misgeld et al., 2007), which have CFP-labeled neuronal mitochondria. *ΔNLS-Wld*^{S} transgenic mice ((Beirowski et al., 2009); expressing a "Wallerian degeneration slow" fusion protein carrying two point mutations in a nuclear localization signal; provided by M. Coleman, Babraham Institute,

Cambridge, UK) were crossed to *Thy1*:EB3-YFP mice to study EB3 dynamics during slow Wallerian degeneration. *Thy1*:YFP-16 mice ((Feng et al., 2000); Jackson Laboratory; B6.Cg-Tg(Thy1-YFP)16Jrs/J), expressing cytoplasmic YFP in neurons, were used to investigate axon fragmentation after Paclitaxel treatment. Mice that express cytoplasmic CFP ((Feng et al., 2000); *Thy1*:CFP-5) were crossed to *Thy1*:EB3-YFP mice to study synapse elimination. As an animal model of amyotrophic lateral sclerosis, transgenic mice were used, which overexpress human wild-type or mutated superoxide dismutase 1 (Jackson laboratory; SOD^{WT} (Tg(SOD)2Gur/J), SOD^{G93A} (Tg(SOD-G93A)1Gur/J), SOD^{G85R} (Tg(SOD*G85R)148Dwc/J)). G93A and huSOD transgenic mice were imaged at day P120, G85R animals were used at a "preterminal" disease stage, where they had lost 10% of their peak body weight and were unable to sustain their body weight hanging of a grid for >30 s (Marinkovic et al., 2012).

2.2. Mouse genotyping

Transgenic animals were genotyped by PCR from tail biopsies. Tail snipping and marking of mice using numbered ear marks were done by animal care takers Manuela Budak, Ljiljana Marinkovic and Nebahat Budak. DNA isolation, PCR and gel electrophoresis was performed by Kristina Wullimann, Sarah Bechthold and Peter Krüger. The mouse tails were collected in 1.5 ml tubes and DNA was isolated using a standard protocol:

Lysis of tails			
Reagent	Quantity	Source	PCR program
Gitocher (see **2.13.***)*	15 µl		55°C 5 h
10% Triton	7.5 µl	Roth	
β-Mercaptoethanol	1.5 µl	Sigma-Aldrich, M6250	95°C 5 min
Proteinase K	0.75µl	Sigma-Aldrich, P2308	
H_2O	125.25 µl		4°C ∞
Total	150 µl /Tube		

The mice were genotyped for the expression of fluorescent protein or ΔNLS-Wld^S and SOD mutated proteins. The following primers and protocols (amount for one reaction) were used:

YFP (GFP 379bp)			
Reagent	Quantity	Source	PCR program
Kapa Fast Ready	10 µl	Peqlab, 07-KK5101-03	95°C for 3 min
GFP-F (10pmol/µl)	1 µl	Metabion	95°C 10 sec
GFP-R (10pmol/µl)	1 µl	Metabion	58°C 10 sec 30x
DNA	1 µl		72°C 10 sec
H_2O	7 µl		4°C ∞
Total	20 µl		

GFP-F: 5´-CACATGAAGCAGCACGACTT-3´
GFP-R: 5´-TGCTCAGGTAGTGGTTGTCG-3´

Mito (181bp)			
Reagent	Quantity	Source	PCR program
Kapa Fast Ready	10 µl	Peqlab, 07-KK5101-03	95°C for 3 min
Mito-F (10pmol/µl)	1 µl	Metabion	95°C 10 sec
EYFP-R (10pmol/µl)	1 µl	Metabion	58°C 10 sec 30x
DNA	1 µl		72°C 10 sec
H_2O	7 µl		4°C ∞
Total	20 µl		

Mito-F: 5´-CGC CAA GAT CCA TTC GTT-3´
EYFP-R: 5´-GAA CTT CAG GGT CAG CTT GC-3´

ΔNLS (~300bp)			
Reagent	Quantity	Source	PCR program
Kapa Fast Ready	10 µl	Peqlab, 07-KK5101-03	95°C for 3 min
UFD-F (10pmol/µl)	1 µl	Metabion	95°C 10 sec
D4-R (10pmol/µl)	1 µl	Metabion	58°C 10 sec 30x
DNA	1 µl		72°C 10 sec
H_2O	7 µl		4°C ∞
Total	20 µl		

UFD-F: 5´- ACGACTTGCTGGTGGACAGA -3´
D4-R: 5´- CCAGCTCGAACAGCCTGAG -3´

SOD (235bp)			
Reagent	Quantity	Source	PCR program
Kapa Fast Ready	10 µl	Peqlab, 07-KK5101-03	95°C for 3 min
SOD-F (10pmol/µl)	1 µl	Metabion	95°C 10 sec
SOD-R (10pmol/µl)	1 µl	Metabion	58°C 10 sec 30x
DNA	1 µl		72°C 10 sec
H_2O	7 µl		4°C ∞
Total	20 µl		

SOD-F: 5´- CATCAGCCCTAATCCATCTGA -3´
SOD-R: 5´- CGCGACTAACAATCAAAGTGA -3´

DNA electrophoresis was performed on an agarose gel (Sigma, A9539) in a horizontal gel chamber (DNA Pocket Block-UV; Biozym Diagnostik). To visualize DNA, the agarose gel was prepared (see **2.13.**) and loaded with 15 µl of the PCR reaction mix and 2 µl of 6x loading Buffer (Millipore; 69046-3). Additionally, 8 µl of a 1K ladder (New England Biolabs, N0468L) as applied to the first well. Electrophoresis was driven by application of 90 mV in 1x TAE buffer (Carl Roth, CL86.1). DNA bands were visualized under UV light (312 nm) and documented with Genoplex (VWR).

2.3. Single cell RT-PCR

To determine expression levels of EB3-YFP mRNA, YFP positive and negative Purkinje cells from the same animal (line J045) were isolated to compare wildtype and transgenic levels of EB3 mRNA. Harvesting of Purkinje cells was performed by Jana Hartmann (AG Konnerth, Institute of Neuroscience, TU München) as previously described (Durand et al., 2006). Single cell PCR was done together with Rosa-Maria Karl (AG Konnerth, Institute of Neuroscience, TU München). Reverse transcription was performed as follows: The harvested material was complemented with “Master Mix 1” (1 µl 1% Nonidet P-40 and 1 µl 5 mM random primers p(dN)6, Roche; 1 µl 10 mM of each dNTPs, 1 µl FSB and 1 µl RNasin plus;

Promega), incubated at 70°C and then at 0°C, 5min each. 10 µl of "Master Mix 2" (2 µl FSB, 6.5 µl H2O and 1.5 µl M-MLV reverse transcriptase; Promega) were added and the tubes were incubated for 1-2 h at 37 °C. The resulting cDNA was purified using silica matrix and stored at -80 °C. To compare expression levels in individual cells, 80% of cDNA material of a single Purkinje cell was used. Rapid-cycle PCR reactions were done in 20 µl reactions in glass capillaries according to the manufacturer's instructions using the LightCycler FastStart DNA Master SYBR Green I kit (Roche). The amount of primer used per reaction was 10 pmol and a $MgCl_2$ concentration of 3 mM was used. Rapid cycle RT-PCR was performed on the LightCycler (Roche) and analyzed with the LightCycler analysis software (version 3.5.3) in the log-linear phase using the so called "fit point" method (Durand et al., 2006).

2.4. Cell culture

Preparation of cultured adult DRG neurons and embryonic hippocampal neurons, subsequent transfection with EB3-mCherry and EB3-GFP and time-lapse imaging was performed by Sina Stern and Frank Bradke (DZNE, Bonn) as previously described (Enes et al., 2010).

2.5. Tissue preparation, immunohistochemistry and confocal microscopy

For tissue analysis, mice were transcardially perfused with 4% paraformaldehyde (see **2.14**) diluted in 0.01 M phosphate buffered saline (1x PBS) and post-fixed for 24 h in 4% PFA. Following dissection, the tissue of interest was either prepared for cryosectioning and incubated in 30% w/v sucrose (Carl Roth, 4661.1) in 1x PBS or for vibratome sections in 1x PBS. Sections (30 µm for cryostat, 100 µm for vibratome) were stained with Neurotrace 594 (Molecular Probes, diluted 1:500 in 1x PBS) to label cell bodies and nuclei. Sections were mounted in Vectashield (Biozol, H-1000) and image stacks were recorded using a FV1000

confocal microscope (Olympus) equipped with x20/0.8 N.A. and x60/1.42 N.A. oil-immersion objectives. Images were processed using ImageJ/Fiji and Adobe Photoshop.

Triangularis sterni muscles were fixed in methanol (-20 °C) for 10 min and then for 1 h in 4% PFA, stained with Alexa594-conjugated α-bungarotoxin (Invitrogen, B-13423; 50 mg/µl diluted 1:50 in 1xPBS) and Alexa647-conjugated phalloidin (Invitrogen, A22287; 200 units/ml methanol, diluted 1:50 in 1xPBS) to visualize acetylcholine receptors at the neuromuscular junction or muscle fibers, respectively. Samples were analyzed by confocal microscopy for parameters of neuromuscular health. Some triangularis sterni muscles were stained with tubulin antibodies (Alexa555-conjugated mouse anti-β-tubulin, BD Pharmingen 560339; mouse anti-glu-α-tubulin, Synaptic Systems 302011) using standard protocols.

2.6. Electron microscopy

For ultrastructural analysis, transgenic animals and wild-type litter mates were perfused transcardially with 2.5% glutaraldehyde (Electron Microscopy Science, 16316) and 2% paraformaldehyde (Electron Microscopy Science, 15710; in 0.1 M PBS. Further sample processing and electron microscopy was done by Emily Weigand and Derron Bishop (Indiana University School of Medicine, Muncie, USA) according to protocols described previously (Bishop et al., 2011).

2.7. Imaging microtubule dynamics in different preparations

2.7.1. *Ex vivo* imaging of a triangularis sterni explant

For preparation of a triangularis sterni explant, mice were lethally anesthetized with isoflurane (Abbot) and the anterior thoracic wall (with triangularis sterni muscle and its innervating intercostal nerves attached) was isolated by cutting the ribs close to the vertebral

column. The explant was pinned down on a Sylgard-coated 3.5 cm plastic Petri dish using minutien pins (Fine Science Tools). After excision, explants were kept in 95% O_2/ 5% CO_2-bubbled Ringer's solution (125 mM NaCl, 2.5 mM KCl, 1.25 mM NaH_2PO_4, 26 mM $NaHCO_3$, 2 mM $CaCl_2$, 1 mM $MgCl_2$, 20 mM glucose). During imaging, explants were warmed to 33-36° C (in this range, comet density varied by less than 20%) at a heated stage with a slow and steady flow of warmed and oxygenated Ringer's solution (Kerschensteiner et al., 2008). "Proximal" are recording sites in the intercostal nerve proper; "distal" are sites beyond the entry point of axons into the muscle.

Time-lapse imaging of microtubule dynamics in motor axons was done at an Olympus BX51WI microscope equipped with ×20/0.5 N.A. and ×100/1.0 N.A. water-immersion dipping cone objectives, an automated filter wheel (Sutter) and a cooled CCD camera (Retiga EXi; Qimaging). All devices are controlled by µManager (Edelstein et al., 2010). Neutral density and infrared-blocking filters in the light path were used to prevent photo-toxicity and photo-bleaching. To follow EB3-YFP comets, an ET F46-003 filter was used and 200 images per movie were acquired at 0.5 Hz (2 Hz for analysis of comet track parameters) using an exposure time of 500 ms.

2.7.2. *Ex vivo* imaging of acute cerebellar slices

To study microtubule dynamics in Purkinje cell dendrites, acute cerebellar slices of *Thy1:*EB3-YFP transgenic mice were prepared. Mice were lethally anesthetized with CO_2 and the cerebellum was rapidly removed and placed into oxygenated Ringer's solution at 0-2°C. Slices (300 µm thick) were cut using a vibratome slicer (Leica). After cutting, slices were kept at 34 °C for 1 h and then imaged for up to 4 h at 33-36 °C in oxygenated Ringer's solution. Slices were imaged on an FV1000 confocal microscope (Olympus) using ×20/0.5

N.A. and ×100/1.0 N.A. water-immersion dipping cone objectives. Slice preparation and imaging was done together with Petar Marinkovic.

2.7.3. *In vivo* imaging of the sciatic nerve

For *in vivo* imaging, the sciatic nerve was exposed in anesthetized mice (1.5% ketamine, 0.1% vol/vol xylazine intraperitoneally) as described previously (Misgeld et al., 2007) and imaged at an Olympus BX51WI wide-field microscope, using the parameters described before. Animals were euthanized at the end of the experiment by cervical dislocation in deep anesthesia.

2.7.4. *In vivo* imaging in the spinal cord

In vivo imaging of the lumbar spinal cord was performed together with Philip Williams, carried out as previously described (Nikic et al., 2011, Romanelli et al., 2013). Briefly, mice were anaesthetized by an intraperitoneal injection of ketamine-xylazine (ketamine 87 mg/kg, xylazine 13 mg/kg). Anesthesia was reapplied as needed (60-120 min). To access the dorsal surface of the lumbar spinal cord, a laminectomy was performed. Compact spinal cord clamps (Narishige; (Davalos et al., 2008)) were attached at the vertebral column to minimize movement during high-resolution imaging. For this, symmetrical incisions were made lateral to the spinal column, one pair along the vertebral level rostral, and another pair two segments caudal to the laminectomy site for insertion of the spinal cord clamps. To avoid unsteady breathing mice were intubated following a tracheotomy. To allow for the formation of a liquid reservoir (regularly filled with pre-warmed mouse artificial cerebrospinal fluid; aCSF: 148.2 NaCl, 3.0 KCl, 1.4 $CaCl_2$, 0.8 $MgCl_2$, 0.8 Na_2HPO_4, 0.2 NaH_2PO_4 in mM) and access with a water dipping-cone objective (x25/1.05), an agarose well (2% agarose in aCSF) was built

around the surgery site. Time-lapse recordings were acquired using an Olympus FVMPE-RS two-photon system equipped with a femto-second pulsed Ti:Sapphire laser (Mai Tai HP, Newport/Spectra-Physics). The laser was tuned to 930 nm for excitation of YFP. Detectors consisted of gallium arsenide phosphide (GaAsP) photomultiplier tubes. All light was first filtered through a 690 nm short pass dichroic mirror and a 495-540 nm barrier filter in front of the GaAsP detectors was used for imaging YFP.

2.7.5. *In vivo* imaging of the somatosensory cortex

Cranial window implantation was performed by Petar Marinkovic at the laboratory of Jochen Herms (Center for Neuropathology and Prion Research, LMU München) as previously described (Fuhrmann et al., 2007, Holtmaat et al., 2009).

Imaging was performed 21 days after surgery to allow mice to recover and to wait for wound healing under the cranial window. For time-lapse imaging of the somatosensory cortex, animals were anesthetized as described above and placed into a metal holder. Movies were acquired using the Olympus FVMPE-RS system as described for spinal cord imaging.

2.8. Imaging mitochondrial transport

Transport of mitochondria was measured in EB3-YFP positive and negative littermates of *Thy1*:EB3-YFP transgenic mice crossed to *Thy1*-Mito-CFP mice in intercostal nerves of the triangularis sterni explant (Kerschensteiner et al., 2008). Mitochondria were imaged at an Olympus BX51WI microscope using an ET F46-001 filter for cyan fluorescent protein. Images were acquired at 0.5 Hz using 300 ms exposure time. I determined the number of anterogradely and retrogradely transported mitochondria (“transport flux”) as the number of fluorescent mitochondria per minute that crossed a vertical line placed across the axon.

2.9. Microtubule modifying drugs

Paclitaxel (Invitrogen, P3456) treatment was done in triangularis sterni preparations. Different concentrations of Paclitaxel were diluted in DMSO (Sigma-Aldrich, D8418) and applied to the bath (solvent, 0.2% DMSO). Subsequently, time-lapse recordings were obtained up to three hours after drug application.

For Nocodazole (5 µM, Sigma, M1404) treatment, the drug was dissolved in DMSO and applied to the Ringer's solution in the bath (1% DMSO, Sigma, D2650).

Epothilone B (Selleckchem, S1364) treatment was used in young mice from postnatal day 4 to 12 to modulate synapse elimination. For this, 2.6 µM Epothilone B (0.5 mg/ml stock solution) diluted in 1ml PEG or pure PEG as control and 20-30 µl were injected into the nuchal fold of four day old mice.

2.10. Axotomy

To image alterations in microtubule dynamics after acute axon cut, laser microsurgery (Galbraith & Terasaki 2003) was done at motor axons of the triangularis sterni explant with an FV1000MPE two-photon microscope (Olympus). A femtosecond pulsed Ti:Sapphire laser (Mai Tai HP, Newport/Spectra-Physics) tuned to 710 nm was placed on the axon for 3-5 s at 100% power using a ×60/1.0 N.A. water objective. The explants were rapidly transferred to a wide-field setup and imaged as described above.

For analysis of degenerating and regenerating axons one of the intercostal nerves, that innervates the triangularis sterni muscle, was transected. For this, mice were anesthetized with ketamine-xylazine (as described above) and immobilized on a heated plate. A longitudinal incision was made with a surgical blade and the 3rd intercostal nerve was exposed and cut close to the bone-cartilage transition (Angaut-Petit & Faille 1987). After surgical closure of the wound the mice were placed in a heated recovery chamber. After the desired interval,

triangularis sterni explants were prepared as described previously (Kerschensteiner et al., 2008).

2.11. Image processing and analysis

Comet parameters: Images were analysed using the open-source software ImageJ/Fiji (http://fiji.sc) and the obtained movies were auto-aligned using the "StackReg" algorithm (Thevenaz et al., 1998). Dynamic microtubules were analysed with an MTrack-plugin (developed by E.Meijering, Biomedical Imaging Group, Erasmus Medical Center, Rotterdam). EB3-YFP comets were tracked manually, if they appeared on at least 3 consecutive frames. Polar plots were generated with IGOR software (WaveMetrics). The following parameters were measured: Orientation (angle of comet deviation measured from the local neurite orientation set to 0°); density of dynamic microtubules (average number of moving comets in 200 frames in a random > 50 μm^2 axon area expressed as comets/μm^2) and average speed of EB3 comets (total displacement divided by observation time).

Neuromuscular junction analysis: Confocal stacks of fixed and stained triangularis sterni explants from EB3-YFP positive and negative litter-mates were analyzed as follows: Neuromuscular junction size was determined by measurements area of a bungarotoxin staining on confocal stacks, after the images were converted into binary images using the "Otsu" auto-threshold algorithm in ImageJ/Fiji. Muscle fiber areas were measured on rotated confocal projections as the circumference of individual fibers revealed by phalloidin 647 staining.

Tubulin modifications: For quantifying the ratio of detyrosinated versus total tubulin, antibody staining was performed and confocal images were analysed in ImageJ/Fiji. A region of interest (ROI) was placed within a single plane of the stack inside the axon. Both channels were background-subtracted and their ratio was determined for a single optical section.

Electron micrographs: Electron micrographs were analysed using ImageJ/Fiji. Microtubule length and orientation were measured on lateral axon sections of 25 µm. An orientation angle of 0° was considered parallel to the axial direction of the axon. Microtubule density was counted on cross-sections of random axons ranging between ~4-50 μm^2.

Image representation: Confocal image stacks were processed using ImageJ/Fiji software to generate maximum intensity projections, which was further processed in Adobe Photoshop. Imaging channels were combined after pseudo-coloring using the "*screen*" function in Photoshop and gamma was adjusted non-linearly in some images to show low-intensity objects. For overview images of expression patterns, multiple stitched frames were montaged in Photoshop. For representation of time-lapse sequences showing microtubule dynamics, a maximum-intensity projection of wide-field or scanning microscopy images from a 20 sec time interval were generated. Subsequently, the maximum projection was processed in Photoshop and arrows were placed to visualize anterograde (green) and retrograde (blue) comets, that appeared in this 20 sec movie sequence.

Movie representation: Time-lapse images were processed in Fiji using StackReg plugin for auto-alignment (Thevenaz et al., 1998). Movies from spinal cord and cortical imaging were denoised using the Matlab based Candle algorithm (Coupe et al., 2012).

2.12. Statistics

Statistics were performed using Microsoft Excel and GraphPad PRISM software. Statistical significance was determined using two-tailed t-tests or ANOVA where appropriate. P-values < 0.05 were considered to be significant and indicated by "*"; P-values < 0.01 were indicated by "**" and < 0.001 by "***". Graphs show mean ± s.e.m.

2.13. Buffers and solutions

Gitocher Buffer			
Reagent	Quantity	Concentration	Source
Tris	15 µl	1.43 mol/l	Roth, 4855.1
$(NH_4)_2SO_4$	5 ml	1.66 mol/l	Sigma-Aldrich, M3148
$MgCl_2$	5 ml	0.65 mol/l	
Gelatine	0.05 g		Roth, 4275.3
H_2O	15 ml		
Total	50 ml		

10x Ringer's solution			
Reagent	Quantity	Concentration	Source
$NaHCO_3$	21.84 g	260 mM	Sigma-Aldrich, S6297
$NaH_2PO_4*H_2O$	1.72 g	12.5 mM	Riedel de Hän; #04270
KCl	1.86 g	25 mM	
NaCl	73.05 g	1.2 mM	
H_2O	up to 1 l		
Total	1 l		

1x Ringer's solution			
Reagent	Quantity	Concentration	Source
1M $CaCl_2$	2 ml	2 mM	Sigma-Aldrich, C1016
1M $MgCl_2$	1 ml	1 mM	
H_2O	900 ml		
10x Ringer's solution	100 ml	20 mM	
Glucose	3.6 g		Sigma-Aldrich, 16301
Total	1 l		

1x Ringer's solution is prepared on the day of the experiment ($CaCl_2$ and $MgCl_2$ are prepared monthly). Glucose was added just before the experiment and the solution was bubbled with carbogen gas (95% O_2 and 5% CO_2) at least 30 min before use.

10x Phosphate Buffered Saline (PBS)			
Reagent	Quantity	Concentration	Source
NaH_2PO_4	2.56 g	18.6 mM	Riedel de Hän, 04270
Na_2HPO_4	11.94 g	84.1 mM	Sigma-Aldrich, S3264
NaCl	102.2	1750 mM	G9023S3014
Total	1 l		

Adjust pH to 7.4. For all experiments 1x PBS was used.

Agarose gel		
Reagent	Quantity	Source
1x TAE buffer	50 ml	
Agarose	0.5 g	Seakem, 50004
Gel Red nucleic acid stain	5 µl	VWR International,730-2957
Total	50 ml	

30x Sucrose			
Reagent	Quantity	Concentration	Source
Sucrose	30 g	876.42 mM	Carl Roth, 4661.1
H_2O	up to 100 ml		
Total	100 ml		

4% Paraformaldehyde (PFA)		
Reagent	Quantity	Source
PFA	40 g	Sigma-Aldrich, P6148
NaOH	125 µl	Roth, KK71.1
H_2O	800 ml	
10x PBS	100 ml	
Total	1 l	

Mix PFA, NaOH and H_2O on a heating plate at 50-60°C until the solution is getting clear. Add PBS and adjust the pH to 7.2 - 7.5. Solution has to be filtered and stored at -20°C.

Blocking solution		
Reagent	Quantity	Source
Goat serum	10 ml	Sigma-Aldrich, G9023
Bovine serum albumin	1 g	Sigma-Aldrich, A3912
Triton-X	0.5 ml	Sigma-Aldrich, T9284
20% NaN3	50 µl	Riedel de Hän; #13412
1x PBS	up to 100 ml	
Total	100 ml	

Ketamine-xylazine		
Reagent	Quantity	Source
Ketamine hydrochloride	300 mg	Sigma-Aldrich, K2753
Xylazine	20 mg	Sigma-Aldrich, X1251
H_2O	up to 20 ml	
Total	20 ml	

3. RESULTS

To study cytoskeletal rearrangements in intact mammalian neurites, the aim of this PhD project was to establish a new imaging approach based on transgenic mice that express yellow-fluorescent protein (YFP) tagged end binding protein 3 (EB3). This allows measuring microtubule dynamics *in vivo* and *ex vivo* in PNS and CNS neurites under physiological conditions, after exposure to microtubule-modifying drugs and under pathological conditions. I would like to emphasize that sections 3.1- 3.4 are for many parts modified from my first author publication *"An assay to image neuronal microtubule dynamics in mice"* (Kleele et al., 2014). Section 3.5 is modified from a manuscript that is currently under preparation for submission, where I am co-first author (Brill, Kleele et al., *in preparation*).

3.1. Characterization of *Thy1*:EB3-YFP transgenic mice

We generated transgenic mice, which express YFP tagged EB3 under the control of *Thy1* regulatory elements to visualize microtubule dynamics in neurons. As these transgenic mice overexpress a biologically active fusion protein, which could cause non-physiological interference and the *Thy1* promoter used here is known to show highly variable expression in different transgenic founders (Feng et al., 2000), it was important to first characterize the new transgenic lines in terms of expression pattern, health and suitability for time-lapse imaging.

3.1.1. Line screen

After cloning of the construct (Leanne Godinho, TU Munich) and pronuclear injection (Ronald Naumann, MPI Dresden) ten founder lines were obtained. Neuron-specific *Thy1* promoter elements have been used in the past to generate a broad range of versatile reporter mice for cellular and subcellular *in vivo* imaging (Caroni 1997, Feng et al., 2000, Misgeld et

al., 2007). From previous studies it is also known that individual lines generated from the identical *Thy1* transgene can exhibit very different expression patterns, because the transgene inserts randomly into the genome (Feng et al., 2000). Also the different founder lines that we obtained varied in their expression pattern and the level of expression. Of ten PCR positive founder lines, one founder died, two lines did not have a detectable EB3-YFP signal but seven lines were expressing EB3-YFP sufficiently for further characterization.

Line	Spinal cord		Retina			Cortex	Cerebellum			Hippocampus				Expression level
	MN	DRG	RG	AC	BC		GC	MF	PC	DG	CA1	CA2	CA3	
J043	+	+/-	+	+/-	-	+	+	+	+/-	+	+	+	+	Dim
J045	+	+	+	+	-	+	+	+	+/-	+	+	+	+	Dim
J426	+	+	+	+/-	-	+	+/-	+	+/-	+	+	+	+	Dim
J044	na	na	na	na	na	na	na	na	na	na	na	na	na	Dim
J023	+	+	+/-	+/-	-	L2/3, 5	+	+	-	+	+	+	-	Bright
J030	+	+	+	+/-	+/-	L5	+	+/-	-	+	+	+	-	Very bright
J032	+	+	+/-	+/-	-	+	+	+	-	+	+	+	-	Very bright

Table 3.1 Expression of EB3-YFP in different transgenic mouse lines
+: expression in most cells; +/-: subset expression in < 80% of cells; -: no expression; na: not analyzed
AC: amacrine cells; BC: bipolar cells; CA: cornu ammonis; DG: dentate gyrus; DRG: dorsal root ganglion; GC: granule cells; L: cortical layer; MF: mossy fibers; MN: motor neurons; PC: Purkinje cells; RG: retinal ganglion cells; Lines marked in green were maintained and used for further experiments

These seven mouse lines had YFP fluorescence in a broad spectrum of neurons in the central and peripheral nervous system, but varied in brightness and expression pattern (**Table 3.1**). To test, which mouse line is most suitable for *in vivo* time-lapse imaging, I first investigated, in which transgenic line fluorescently tagged EB3 appears in a punctate pattern and shows comet-like movement. It has been shown *in vitro* in the past that the comet-like pattern is characteristic for a low level of transgene expression, where the transgene does not cause any obvious changes in microtubule behavior (Komarova et al., 2005, Stepanova et al., 2003). In contrast it has also been demonstrated *in vitro*, that massive overexpression of EB3 leads to binding to the entire microtubule lattice (Komarova et al., 2005). I therefore performed high

resolution time-lapse imaging of peripheral axons in the triangularis sterni explant (**Fig. 3.1.**) and identified transgenic lines, which have a dim fluorescent signal and can therefore be assumed to be low expressing lines (J043, J045, J426), as well a mouse lines with a moderate expression level (J044, J023). In both groups of lines, the transgenic fusion protein revealed the tips of microtubules as a dynamic, comet-like pattern against a faint background of cytoplasmic labeling. In contrast in mouse lines, which had a very bright labeling (J030 and J032), EB3-YFP could be observed all along individual microtubules and lacked a comet-like pattern. These mice also developed pathological swellings in some axons of the spinal cord.

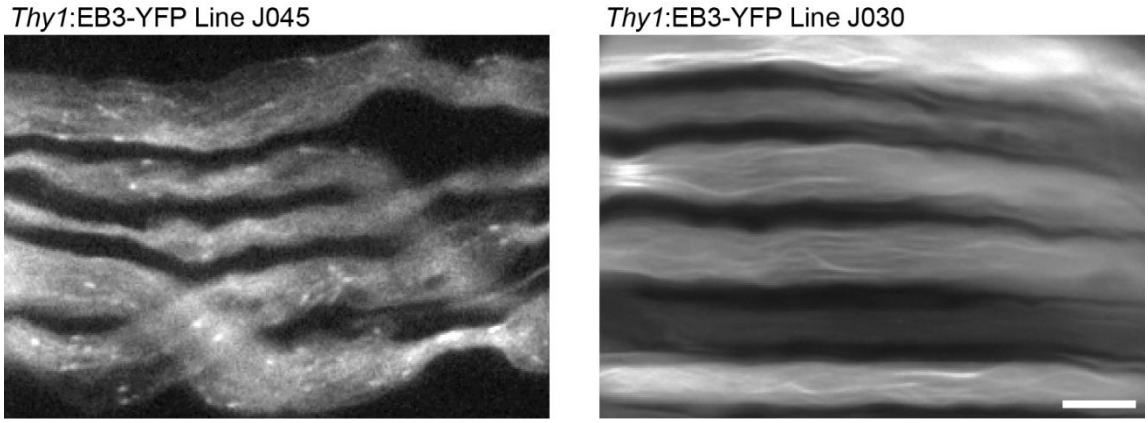

Fig. 3.1 Time lapse imaging of a Triangularis sterni explant
Time-lapse imaging of a low expressing *Thy1*:EB3-YFP transgenic mouse line (J045; left) shows a punctate pattern of comets with a faint cytoplasmic background. In a high expressing mouse line (J030; right), EB3-YFP binds along the entire length of the microtubules. Note that images were individually adjusted to span the entire brightness range. Scale bar is 5µm.

Therefore, I chose two mouse lines (J045 and J023.) with a low expression level for further experiments and prepared a detailed characterization of their expression pattern throughout the central and peripheral nervous system (**Fig. 3.2**). Both lines show a broad spectrum of labeled neurons including cortical and hippocampal neurons, Purkinje cells, retinal cells and motor neurons.

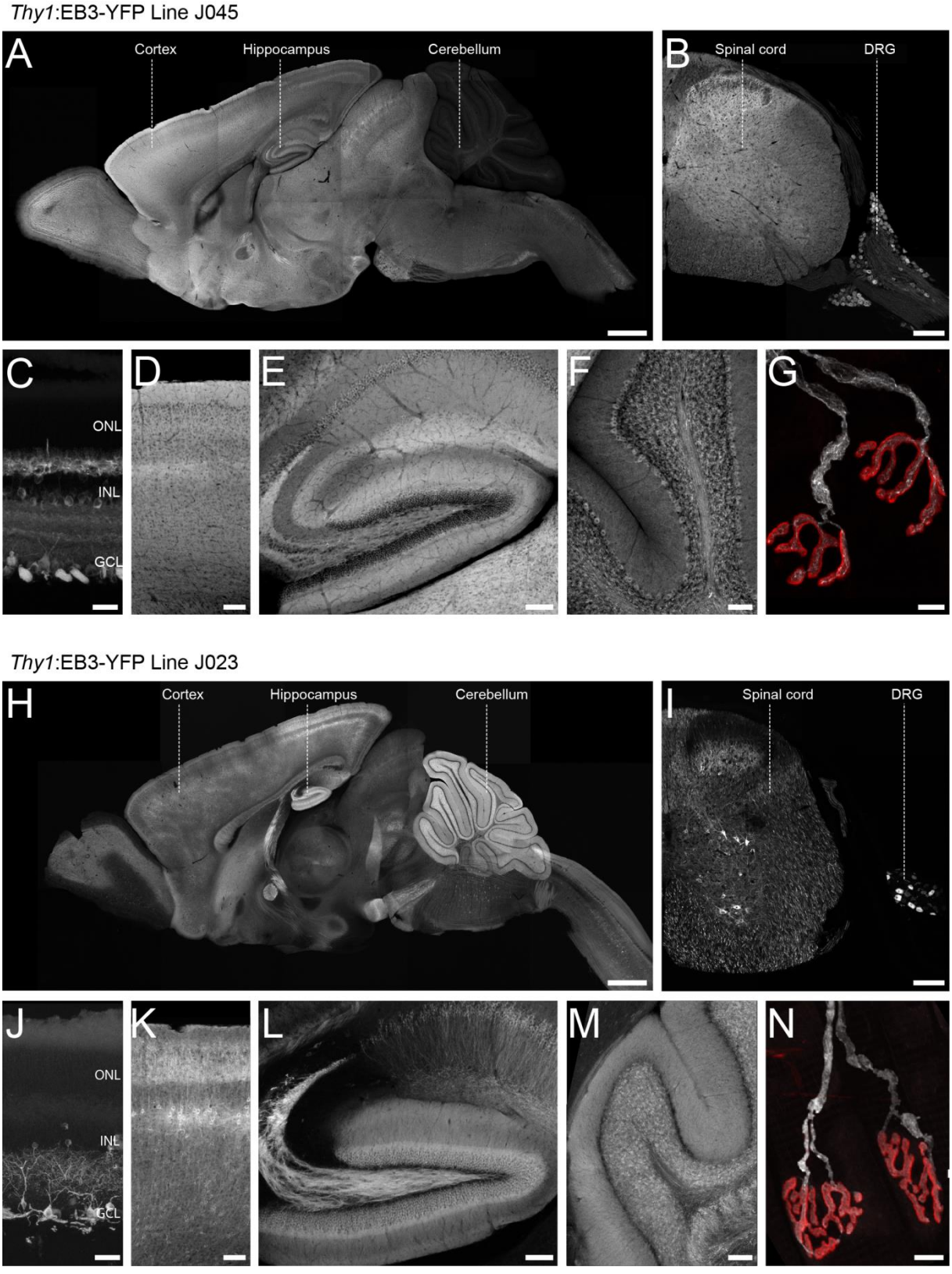

Fig. 3.2 Expression pattern in two *Thy1*:EB3-YFP transgenic mouse lines

EB3-YFP is expressed in transgenic lines J045 (**A**-**G**) and J023 (**H**-**N**) in the CNS (**A**, **H**: sagittal brain section; **B**, **I**: horizontal spinal cord section; **C**, **J**: retina; **D**, **K**: cortex; **E**, **L**: hippocampus; **F**, **M**: cerebellum) and the PNS (**G**, **N**: neuromuscular junctions, postsynaptic receptors stained with bungarotoxin (**red**). Note expression in dorsal root ganglia in **B**, **I**). Scale bar in **A**, **H** 1 mm; in **B**, **I** 200 µm; in **C**, **J** 100 µm; in **D**, **E**, **F**, **K**, **L** and **M** 50 µm and in **G**, **N** 5 µm. From Kleele et al., 2014.

3.1.2. Exclusion of toxicity

Thy1:EB3-YFP transgenic mouse lines (J045 and J023) that were later on used to perform time-lapse imaging of microtubule dynamics were characterized in greater detail, to exclude morphological or functional abnormalities, caused by EB3-YFP overexpression. First of all, the transgene did not cause any obvious changes in behavior, life-time or fertility. Also neuromuscular morphology, posttranslational tubulin modifications, ultrastructure and axonal transport was unaffected compared to EB3-YFP negative litter-mates, described below in more detail. Overall, expression of the transgene seems to be largely non-toxic and inert in low expressing *Thy1*:EB3 animals.

3.1.2.1. Neuromuscular junction parameters

To ensure, that overexpressing EB3-YFP does not influence neuronal morphology, different parameters of the neuromuscular junction (NMJ) were measured in heterozygote transgenic animals and compared to EB3-YFP negative litter mates (**Fig. 3.3**), as neuromuscular junctions respond sensitively to many pathologies and motor axons tend to express relatively high levels of *Thy1*-driven transgenes. Quantification was done for the two transgenic lines that were later used for further experiments (J045 and J023). Phalloidin staining of the triangularis sterni muscle confirmed that both transgenic lines have normal muscle fiber morphology and there is no abnormality in muscle fiber diameter (**Fig. 3.3 A-E**). Also the postsynaptic membrane area, which were visualized with bungarotoxin staining, were of the same size and have the same postsynaptic receptor density compared to negative litter mates. Hence, *Thy1*:EB3-YFP mice do not seem to have any obvious abnormalities in the neuromuscular system. This is of particular importance as I performed many of the following studies at the neuromuscular junction of the triangularis sterni muscle.

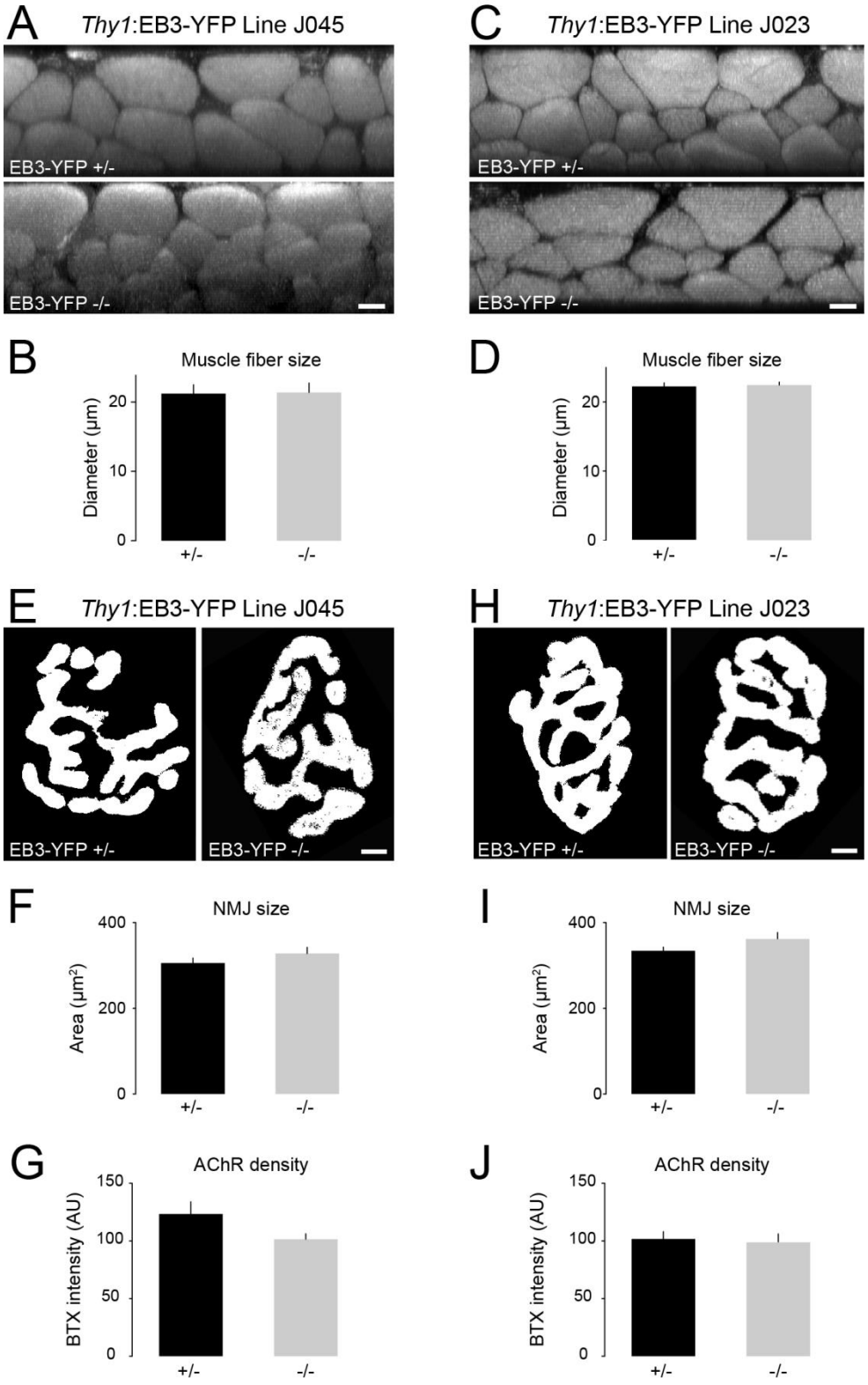

Fig. 3.3 No abnormalities were found at the neuromuscular junction of *Thy1*:EB3 transgenic mice

(**A-D**) *Thy1*:EB3-YFP animals (+/-) from lines J045 and J023 have normal muscle fiber morphology (**A, C**) and diameter (**B, D**) compared to wildtype animals (-/-). (**E-J**) Postsynaptic areas (**E-I**) and postsynaptic receptor densites (**G, J**) were not altered in transgenic animals. All parameters were compared to non-transgenic litter mates (-/-). n >240 muscle fibers or n >50 synapses from 3 animals per genotype. Scale bar is 10µm in **A** und **C** and 5 µm in **E** and **H**.

3.1.2.2. Tubulin modifications

Microtubules accumulate different posttranslational modifications along their lattice, which regulate microtubule behavior and stability. Therefore it is important to control that overexpressed EB3-YFP does not affect tubulin modifications and as a result alters microtubule behavior. Detyrosinated tubulin (Glu-tubulin) is an indicator for microtubule stability, as only freshly polymerized tubulin dimers are tyrosinated, and can be analyzed using specific antibody staining. Double-immunostaining of fixed triangularis sterni muscles revealed that the ratio of all neuronal tubulin (β-tubulin III) to detyrosinated tubulin is the same between transgenic animals and non-transgenic litter-mates, which indicates that posttranslational modifications are not altered in transgenic mice (**Fig. 3.4**)

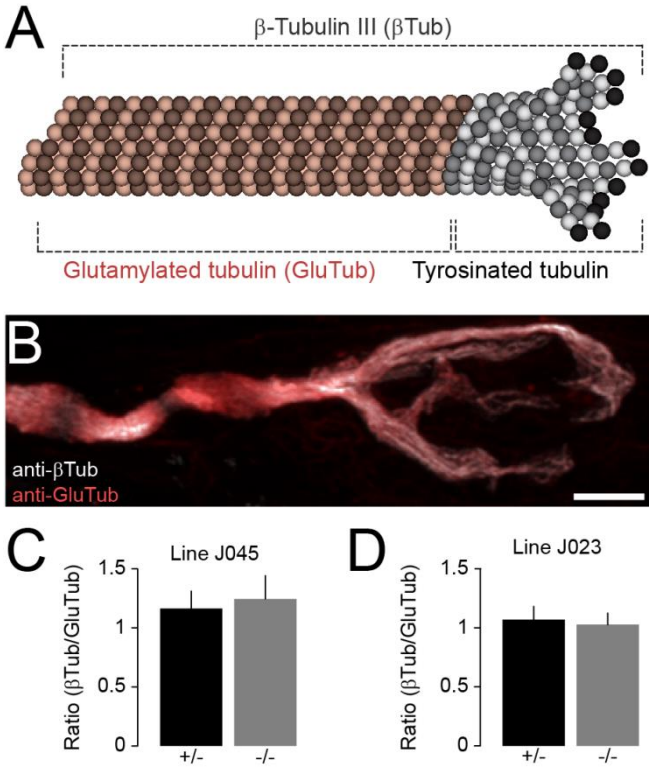

Fig. 3.4 Overexpression of EB3-YFP does not change tubulin modifications

(**A**) β-Tubulin exists in two modifications throughout the lattice: The polymerizing tip contains tyrosinated tubulin, which is subsequently detyrosinated leaving glutamylated tubulin at the older parts of the microtubule lattice. (**B**) Double immunostaining (example from line J045) allows measuring the ratio of all neuronal tubulin (βTub) to detyrosinated tubulin (GluTub). (**C-D**) Comparison of the tubulin ratio in transgenic animals from lines J045 (**C**) and J023 (**D**) and non-transgenic litter mates shows no difference. n >40 axons from 3 mice per genotype. Scale bar in **B** is 5µm.

3.1.2.3. Ultrastructure

To guarantee, that also the ultrastructure of neurons in *Thy1*:EB3-YFP transgenic mice is unaffected by expression of the transgene, samples from the triangularis sterni explant of

transgenic mice and non-transgenic litter-mates were prepared for electron microscopy, which was performed by Emily Weigand and Derron Bishop (Indiana School of Medicine, Muncie, USA). Electron micrographs of those samples did not show any detectable abnormality in axons from *Thy1*:EB3-YFP transgenic mice (**Fig. 3.5**). Microtubule density (**Fig. 3.5 E**) and orientation in relation to the axon length axis (polar plot in **Fig. 3.5 F**) are unchanged compared to the control group. Also other cellular organelles and structures, such as mitochondria or neurofilaments, do not obviously differ between transgenic and non-transgenic animals.

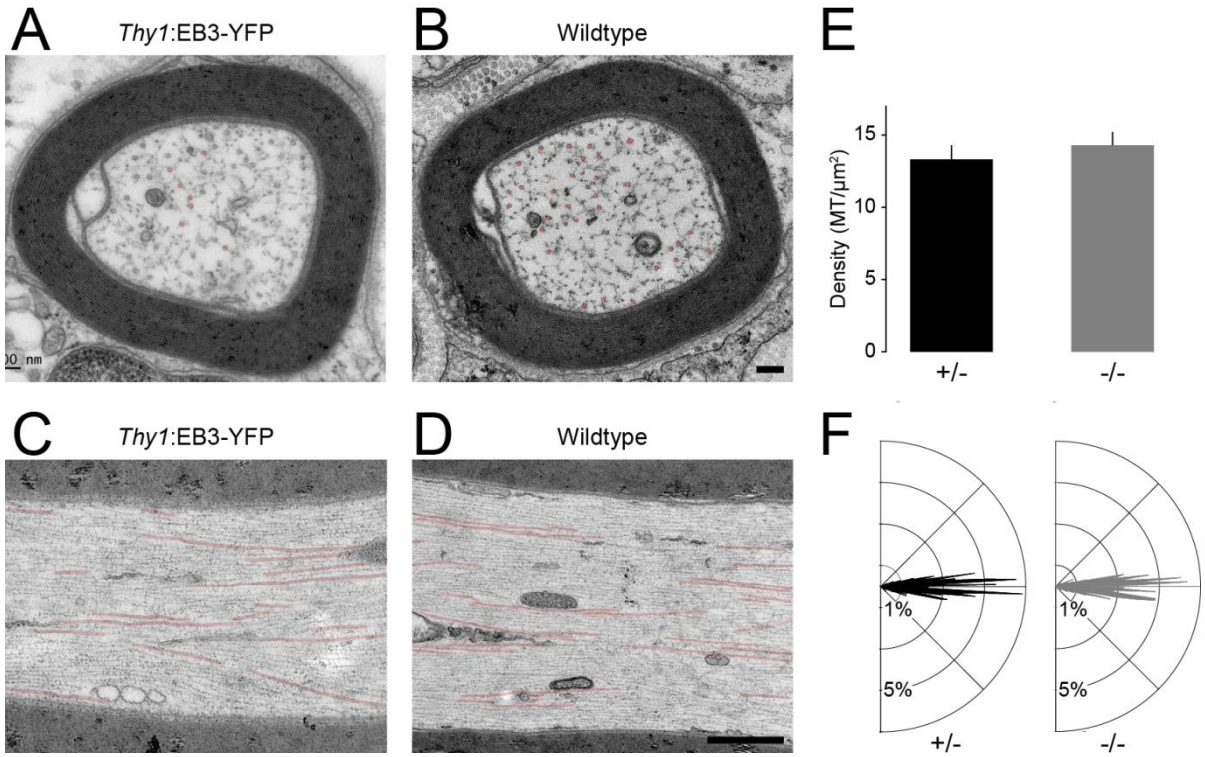

Fig. 3.5 Ultrastructure of PNS axons in *Thy1*:EB3-YFP mice

(**A-D**) Electron micrographs of perpendicular (**A, B**) and longitudinal (**C, D**) section of axons in intramuscular fascicles of *Thy1*:EB3-YFP mice (line J045). The ultrastructure of axons from transgenic animals (+/-) (**A, C**) and non-transgenic litter-mates (-/-) (**B, D**) are indistinguishable. (**E, F**) Quantification of microtubule density (**E**) and orientation in relation to the axon axis (**F**, polar plot) also shows no difference between the two groups. Microtubules are pseudo-colored in red; n ≥3 axons from 2 mice. Scale bar in **B** is 0.1 µm (also for **A**) and in **D** 0.5 µm (also for **C**). Electron micrographs obtained by Emily Weigand and Derron Bishop, Indiana School of Medicine. Modified from Kleele et al., 2014.

3.1.2.4. Axonal transport of mitochondria

Microtubules are forming the tracks for fast axonal transport and therefore are crucial for the distribution of cargos and organelles throughout the neuron. Exclude the possibility that EB3-YFP overexpression alters microtubule based transport, *Thy1*:EB3-YFP transgenic mice were crossed to *Thy1*:Mito-CFP mice (Misgeld et al., 2007), which have CFP-labeled neuronal mitochondria. I found that anterograde and retrograde transport of mitochondria was unaltered in intercostal nerves of *Thy1*:EB3-YFP transgenic mice, suggesting that there is no axonal transport deficit in EB3 transgenic mice (**Fig. 3.6**). Altogether, none of the morphological or functional comparisons between *Thy1*:EB3-YFP transgenic animals and non-transgenic littermates showed any alteration or abnormality due to overexpression of EB3-YFP in the low expressing mouse lines, which were used for the following experiments

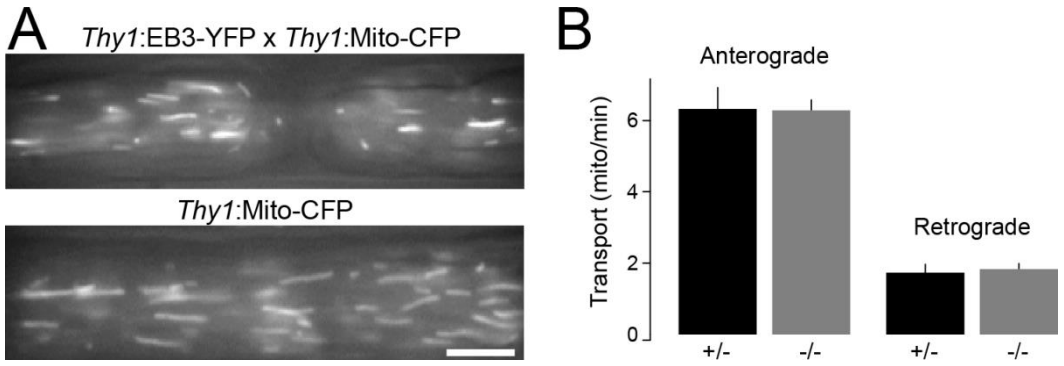

Fig. 3.6 Mitochondrial transport in *Thy1*:EB3-YFP transgenic mice

(**A**) Average intensity projection of a 10 frames time series from intercostal nerves of *Thy1*:Mito-CFP transgenic mice that were crossed to *Thy1*:EB3-YFP mice and positive (above) or negative (below) for EB3-YFP. (**B**) Quantification of mitochondrial transport in anterograde and retrograde direction in intercostal nerves of *Thy1*:Mito-CFP mice that were positive (+/-) or negative (-/-) for the EB3-YFP transgene (line J045). n = 27 axons from 3 mice. Scale bar in **A** 5 µm

3.1.3. Expression levels of EB3-YFP

Despite the fact, that *Thy1*:EB3-YFP transgenic mice do not show any pathological phenotype, we still found it important to estimate the level of EB3-YFP overexpression compared to the amounts of endogenous EB3. However, it comparing endogenous and

transgenic EB3 levels on a proteins level is difficult, because the expression is limited to a subset of neurons and therefore global approaches, for example western blots, are useless as they do not provide single cell resolution. Therefore we decided to instead determine mRNA levels of transgene positive and negative cells. For this, together with Jana Hartmann and Rosa-Maria Karl (AG Arthur Konnerth, Institute of Neuroscience, TU Munich) I performed quantitative real-time PCR on individual Purkinje cells that were harvested from acute cerebellar slices, to measure the level of EB3 mRNA (**Fig. 3.7**; (Hartmann et al., 2004)). As transgenic line J045 has only a subset of Purkinje cells labeled, EB3-YFP negative cells could be used as an internal control by comparing the amount of EB3 mRNA between EB3-YFP positive and negative Purkinje cells in the same slice. In heterozygous animals we detected a ~3-fold increase in mRNA levels in YFP-positive cells compared to YFP-negative Purkinje cells (ΔCp = 1.57, n = 26 vs. 11 cells/ 3 animals). These results confirm the assumption that the level of EB3-YFP overexpression is low in the transgenic line that we in accordance with the absence of any detrimental effects that we could detect.

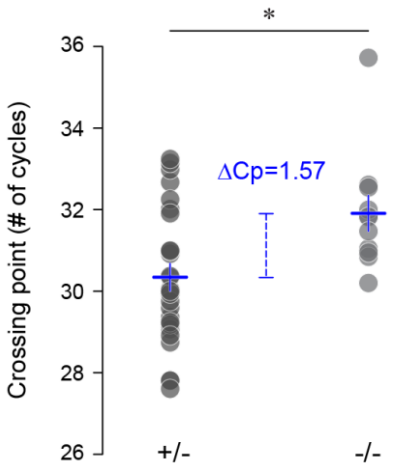

Fig. 3.7 Single cell RT-PCR on EB3-YFP positive and negative Purkinje cells

EB3-YFP positive Purkinje cells (+/-) from *Thy*1:EB3-YFP transgenic mice show a 1.57 difference in the crossing point during RT-PCR, which means a ~3-fold increase in mRNA levels, compared to EB3-YFP negative Purkinje cells (-/-) from the same animal. n = 26 vs. 11 cells from 3 mice. Data obtained in collaboration with Jana Hartmann and Rosa-Maria Karl, Institute of Neurosciences, TUM.

3.1.4. EB3-YFP labeling in cultured neurons

Most of studies using fluorescently tagged end binding proteins were so far performed *in vitro*, where this is a widely used and well-characterized method to study microtubule

dynamics (Perez et al., 1999, Stepanova et al., 2003). Therefore we wanted to compare our new approach with a classical transfection assay.

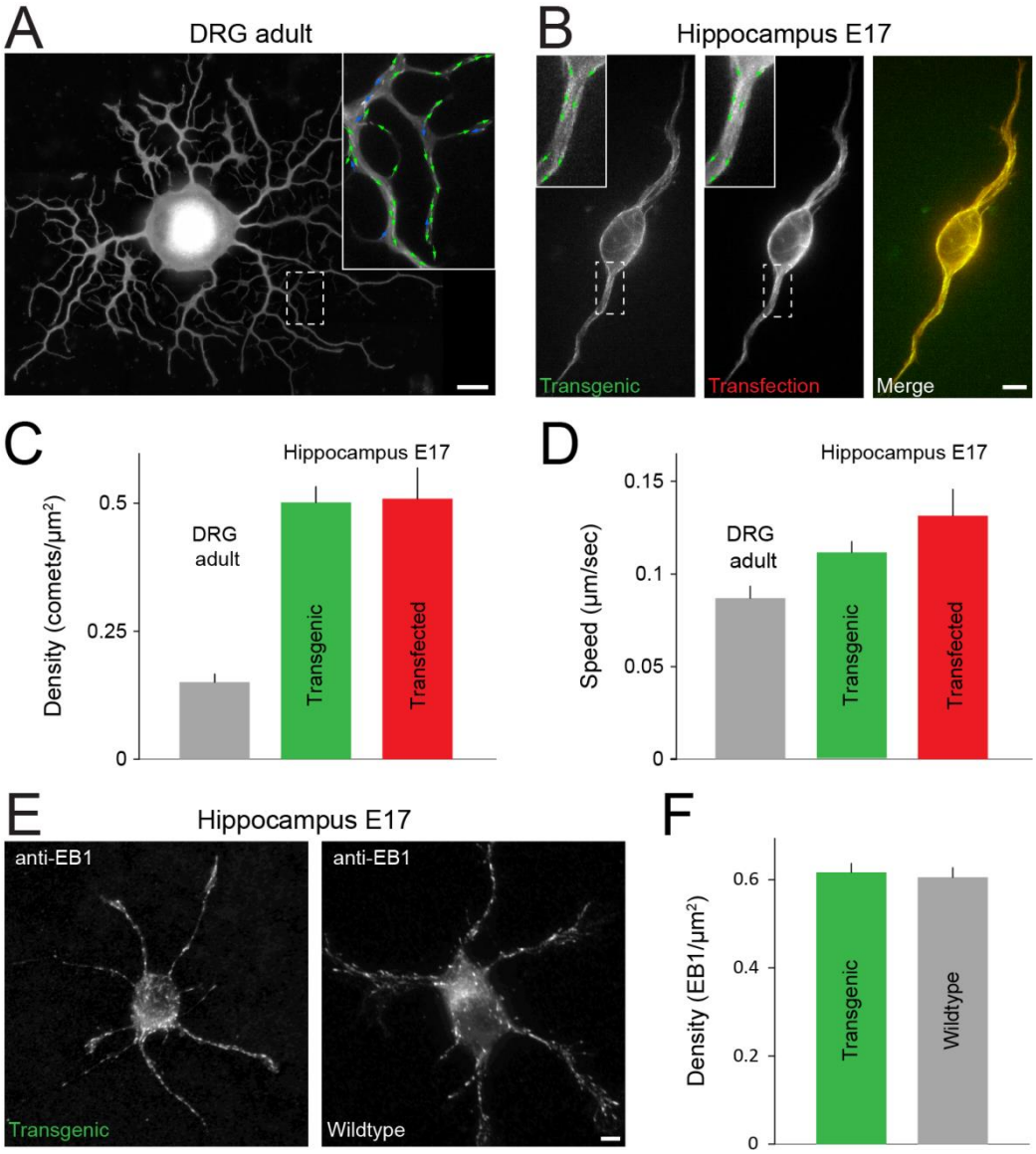

Fig. 3.8 Comparison of endogenous, transfection- and transgene-based EB labeling in neurons

(**A**) Adult DRG neuron from *Thy1*:EB3-YFP transgenic mice. Inset shows a higher magnification of DRG neurites with EB3 comets represented as maximum projection of 20s time-lapse recording, where each comet is represented by a color-coded arrow (anterograde, **green**; retrograde, **blue**) (**B**) E17 hippocampal neurons show a 100% co-localization (insets) of the EB3-YFP transgene and transfected EB3-mCherry comets. (**C, D**) Quantification of density and speed from adult DRG and E17 hippocampal neurons cultured from *Thy1*:EB3-YFP mice and EB3-mCherry transfected wildtype hippocampal neurons. Transgenic and transfected hippocampal neurons do no differ significantly in density (**C**) or speed (**D**; n = 7 neurites from 3 cells for each group). (**E, F**) Immuno-staining of EB1 in *Thy1*:EB3-YFP transgenic and wildtype E17 hippocampal neurons show a similar pattern and density of speckled staining (**E**). Quantification of EB1 speckle density shows no significant difference between those two groups (**F**; n = 32 neurites from 9 cells for each group). Scale bar in **A** 20µm and in **B, E** 5µm. Data obtained in collaboration with Sina Stern and Frank Bradke, DZNE Bonn. Modified from Kleele et al., 2014.

For this, Sina Stern (AG Frank Bradke, DZNE Bonn) isolated adult DRG and embryonic hippocampal neurons from *Thy1*:EB3-YFP mice (line J045) and transfected them with EB3-mCherry (**Fig. 3.8**). Time-lapse recordings demonstrated that the characteristics of transgene-based labeling matched those seen in classical transfection-based assays (Stepanova et al., 2003). The transgene-based labeling co-localized with labeling derived from the EB3-mCherry transfected construct (**Fig. 3.8 B**) and showed the same dynamic behavior (**Fig. 3.8 C, D**). In addition to general toxicity, EB3 overexpression could affect the interaction with other plus-end binding proteins, such as EB1 or CLIP proteins. To exclude this possibility, cultured E17 hippocampal neurons were fixed and stained for end binding protein 1 (EB1; **Fig. 3.8 E**). Densities of endogenous accumulations of EB1 were not affected by the presence of EB3-YFP (**Fig. 3.8 F**).

3.2. Microtubule dynamics in different cell types and neuronal compartments

To explore the potential of our new assay to investigate changes in the cytoskeleton of intact mammalian neurons, I used different *ex vivo* and *in vivo* preparations of the PNS and CNS to characterized microtubule dynamics in different neuronal compartments and cell types under physiological conditions.

3.2.1. Peripheral motor axons *ex vivo*

High resolution imaging of peripheral intercostal nerves of a triangularis sterni explant revealed the typical comet-like pattern of EB3-labeling (**Fig. 3.9**). Time-lapse recordings show that EB3-YFP comets appear suddenly, propagate for a distance of a few microns and disappear (speed: 0.112 ± 0.003 μm/s in distal axons *ex vivo*; n = 32/8). Determining the density of EB3 comets provides a direct measure of the local dynamics of the microtubule cytoskeleton and varies in different neuronal compartments (**Fig. 3.9 B**; 0.065 ± 0.002

comets/µm^2 axonal area in distal motor axons, n = 32 axons/ 8 animals; 0.025 ± 0.001/µm^2 in proximal intercostal axons, n = 27/6; 0.118 ± 0.007/µm^2 in synaptic terminal, n = 13/4). The orientation of dynamic microtubules in motor axons is rather uniform with the vast majority (95 ± 1% in distal intercostal axons; n= 32/8) having a "plus-end out" polarity (**Fig. 3.9 D**), as it was previously reported for other model systems (Stepanova et al., 2003, Stone et al., 2008).

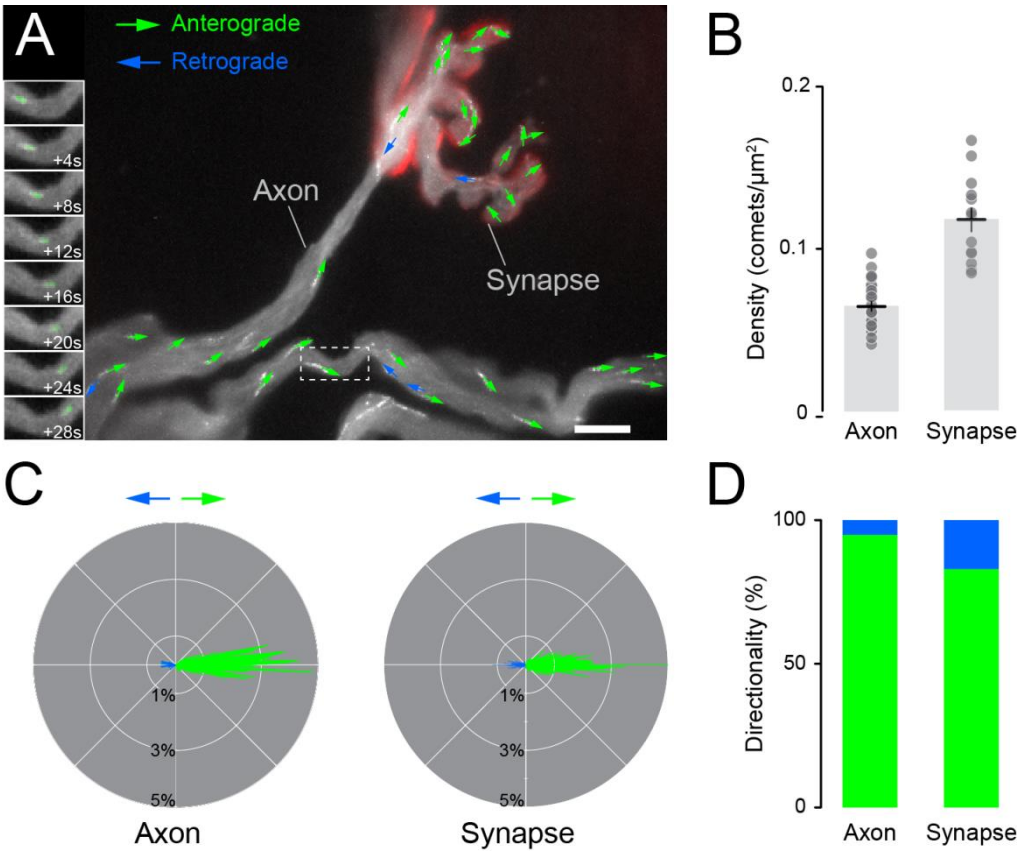

Fig. 3.9 Imaging microtubule dynamics in peripheral motor axons of *Thy1*:EB3-YFP mice

(**A**) Neuromuscular junction (postsynaptic receptors labeled with fluorescently-tagged bungarotoxin, **red**) and terminal motor axons in a triangularis sterni explant. The **main panel** shows microtubule dynamics in axon and synapse with EB3 comets represented as maximum projection of 20s within a time-lapse recording, where each comet is represented by a color-coded arrow (anterograde, **green**; retrograde, **blue**). **Inset** shows 8 frames cropped (dashed box in **main panel**) from a time-lapse sequence of this area highlighting an anterograde directed EB3 comet (pseudo-colored in **green**). (**B**) Comet density in axonal and synaptic compartments (n ≥ 10 axons and synapses from ≥ 3 mice). (**D**) Polar plots (i.e. frequency histograms with angular orientation shown in a circle) of comet directionality in relation to neurite orientation (anterograde to right) in axons and synaptic terminals (n ≥ 13 motor axons from ≥ 3 mice). (**E**) Frequency of comet orientations color-binned for anterograde and retrograde orientations. Scale bar in **A** is 5 µm. Modified from Kleele et al., 2014.

In neuromuscular presynaptic terminals the orientation of microtubules is similar to axonal microtubules, albeit the orientation in relation to the length axis is less stringent (**Fig. 3.9 C**,

"plus-end out" orientation: 83 ± 3%; n = 13/4). While the speed in mature axons was found to be lower than reported *in vitro* and in invertebrates (e.g. 0.22 µm/s in hippocampal cultures (Stepanova et al., 2003) other EB3-YFP comet characteristics, such as orientation and length, seem to be largely conserved across models.

In vitro studies have shown that microtubule growth can be divided into phases of growth, pause and reset (Applegate et al., 2011). For such detailed analysis of individual microtubule tracks the imaging frequency of 0.5 Hz, which I normally used was not sufficient, but rather 2 Hz proved necessary (**Fig. 3.10**).

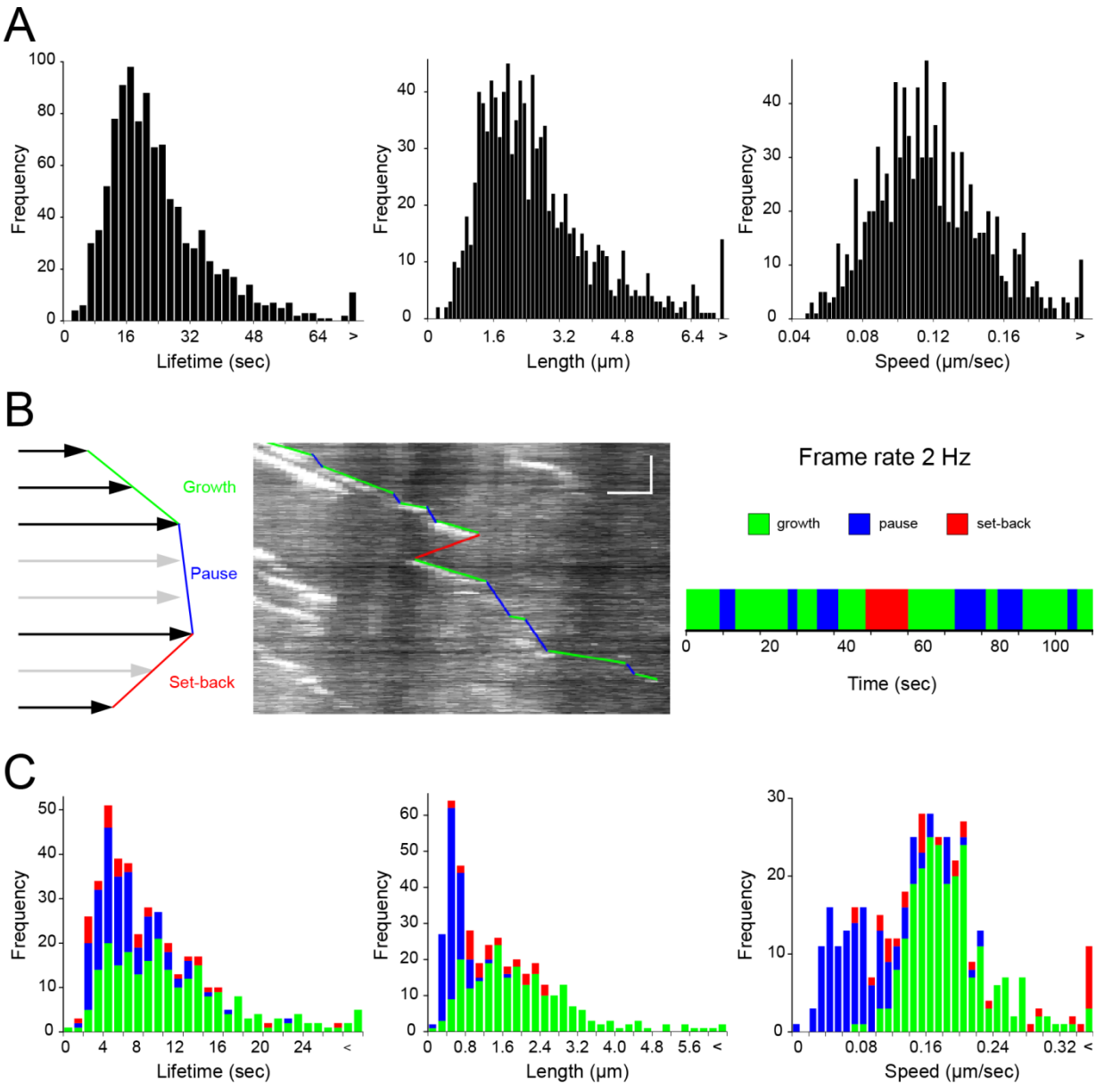

Fig. 3.10 High-frequency analysis of microtubule tracks

(**A**) Histograms showing the distribution of lifetime, length and speed of the dynamic microtubules in distal motor axons of the triangularis explant, which were also used to generate plots in **Fig. 3.9**. (**B**) Analysis of track characteristics derived from 2 Hz imaging in intercostal axons of *Thy1*:EB3-YFP triangularis explants. Schematic of movement behaviors (**left**), kymograph of an axon segment with classified track segments indicated for one comet (**middle**), analysis as "event classification" along the time axis (**right**). (**C**) Frequency distribution of track segments color coded for respective behavior (n = 69 tracks from 2 animals). Scale bars in **B** 2 µm, horizontal bar; 10 sec, vertical bar. Modified from Kleele et al., 2014.

At this frequency, an individual microtubule track can be subdivided into multiple phases of growth, pause and set-backs (**Fig. 3.10 B**). Set-back of a microtubule track is most likely intermediate depolymerization, but can in some instances also be a newly polymerizing microtubule that is growing along the same path. Based on such recordings, histograms showing the distribution of lifetime, length and speed of microtubules (**Fig. 3.10 A**) can be complied (**Fig. 3.10 C**), which might be sensitive indicators of the microtubule actions of drugs or gene products in future investigations. However, because high frequency imaging leads to faster photo-bleaching, I performed the subsequent experiments at 0.5 Hz, which is sufficient to analyze changes in microtubule density and orientation, which are the primary read-outs of interest in the context of axon remodeling and degeneration.

3.2.2. Purkinje cell dendrites *ex vivo*

In contrast to axons, dendrites of cultured or invertebrate neurons were previously reported to have a mixed orientation of microtubules (Baas et al., 1988, Stepanova et al., 2003) or even a minus-end out polarization in flies (Stone et al., 2008). To test if this also holds true in mammalian dendrites, acute cerebellar slices of transgenic mice, which express EB3-YFP in a subset of Purkinje cells, were prepared and imaged on a confocal scanning microscope (**Fig. 3.11**).

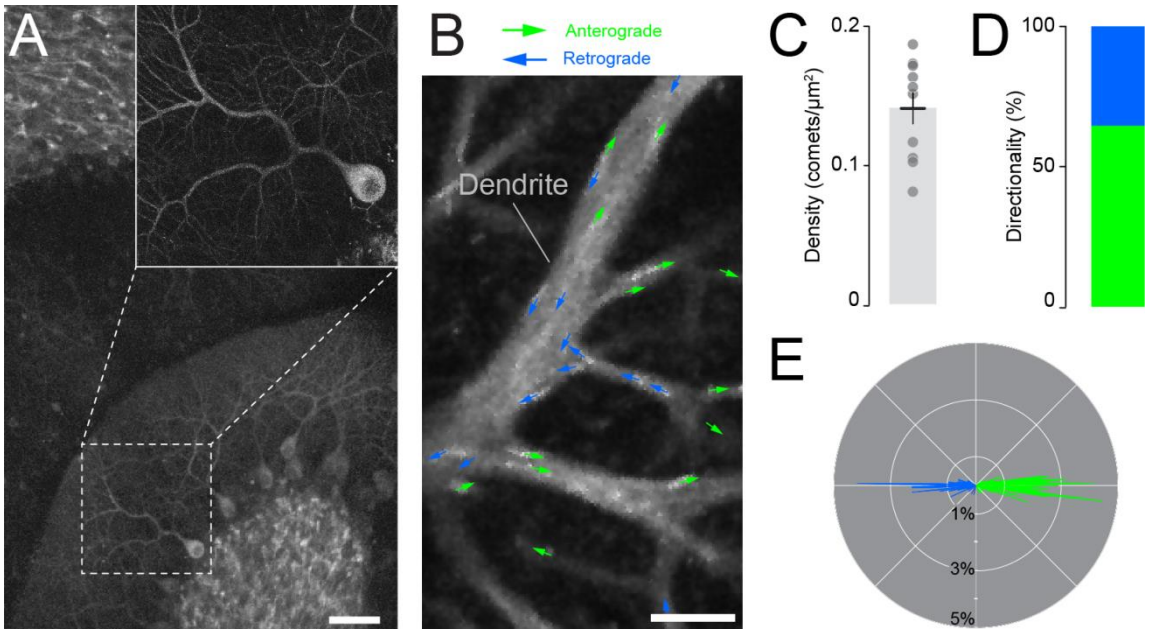

Fig. 3.11 Microtubule dynamics in Purkinje cell dendrites of *Thy1*:EB3-YFP mice

(**A**) Acute cerebellar slices of *Thy1*:EB3-YFP transgenic mice (line J045), which express EB3-YFP in a subset of Purkinje cells (**Inset**). (**B**) Microtubule dynamics in dendrites of a Purkinje cell in an acute cerebellar slice (represented as previously). (**C**) Comet density is also higher compared to motor axons (n = 10 dendrites from 3 mice). (**D**) Quantification of comet directionality reveals a more frequent occurrence of retrograde directed comets.(**E**) Polar plot shows the comet directionality in relation to neurite orientation (anterograde to right) in Purkinje cell dendrites (n = 10 dendrites from 3 mice). Scale bar in **A** 50 µm and in **B** 5 µm. Recordings performed in collaboration with Petar Marincovic. Modified from Kleele et al., 2014.

Microtubule dynamics in proximal Purkinje cell dendrites in acute cerebellar slices show a very dense (0.141 ± 0.011/µm^2; n = 10/3) pattern of comets of mixed orientation ("plus-end out" orientation: 65 ± 4%; **Fig. 3.11**) and hence is in line with previous reports about microtubule orientation in dendrites (Stepanova et al., 2003, Stone et al., 2008).

3.2.3. Sciatic nerve *in vivo*

A major ambition of this project was to establish *in vivo* imaging of microtubule dynamics in different parts of the nervous system. This in the beginning seemed challenging due to the small size of microtubules, the faintness of the EB3-YFP fluorescent signal and the presence of movement artefacts. However, wide-field microscopy proved sufficient to allow time-lapse imaging of microtubule dynamics in peripheral axons of the sciatic nerve in anesthetized

Thy1:EB3-YFP mice (Misgeld et al., 2007). Quantification of the recordings in the sciatic nerves revealed a similar comet pattern compared to motor axons of the triangularis sterni *ex vivo* (**Fig. 3.12**; 0.042 ± 0.005/µm^2, measured at mid-thigh level, an intermediate proximal-distal position in the sciatic nerve, n = 15/3). Also directionality of microtubules shows the typical plus-end out orientation in axons of the sciatic nerves and also other parameters of microtubule growth are comparable to *ex vivo* preparations.

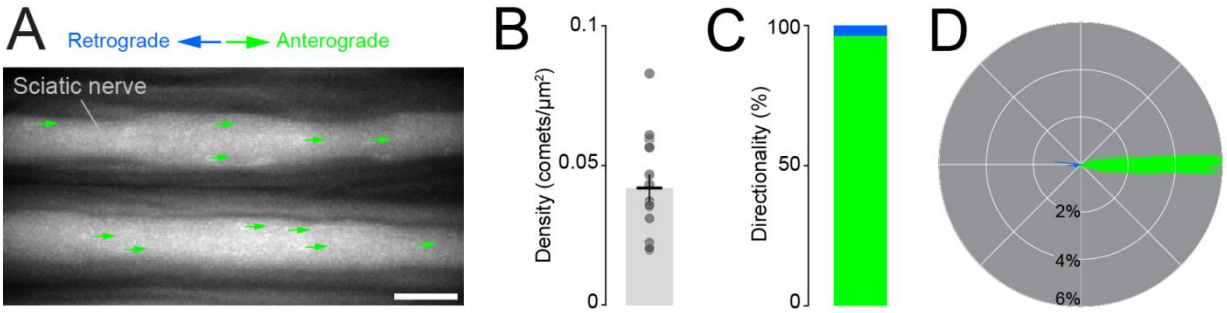

Fig. 3.12 *In vivo* imaging of microtubule dynamics in the sciatic nerve
(**A**) Microtubule dynamics in the sciatic nerve of an anesthetized *Thy1*:EB3-YFP mouse (represented as previously). (**B-D**) Quantification of microtubule dynamics in sciatic nerve (n = 15 axons from 3 mice) showing comet density (**B**), orientation (**C**) and directionality in relation to the neurite axis represented in a polar plot (**D**). Scale bar in **A** 5µm. Modified from Kleele et al., 2014.

3.2.4. Central motor axons of the spinal cord *in vivo*

Despite the successful *in vivo* recordings of microtubule dynamics in the sciatic nerve, wide-field or confocal microscopy was not sufficient for *in vivo* imaging in the central nervous system. Nevertheless, this would be an important technological progress by allowing studies of microtubule dynamics in the spinal cord or brain under physiological or pathological conditions. Therefore, I devised together with Philip Williams (TU Munich) a two-photon imaging assay to measure microtubule dynamics in individual spinal axons of live anesthetized mice (**Fig. 3.13**). The *in vivo* density of dynamic microtubules in the spinal cord (0.033 ± 0.002/µm2; n= 15/3) was in a similar range to what we measured in explanted intercostal nerves and in the sciatic nerve *in vivo*. Also microtubule orientation ("plus-end

out": 93±1; n=15/3) and comet speed (0.147 ± 0.004 µm/sec; n=15/3) were comparable to previous measurements.

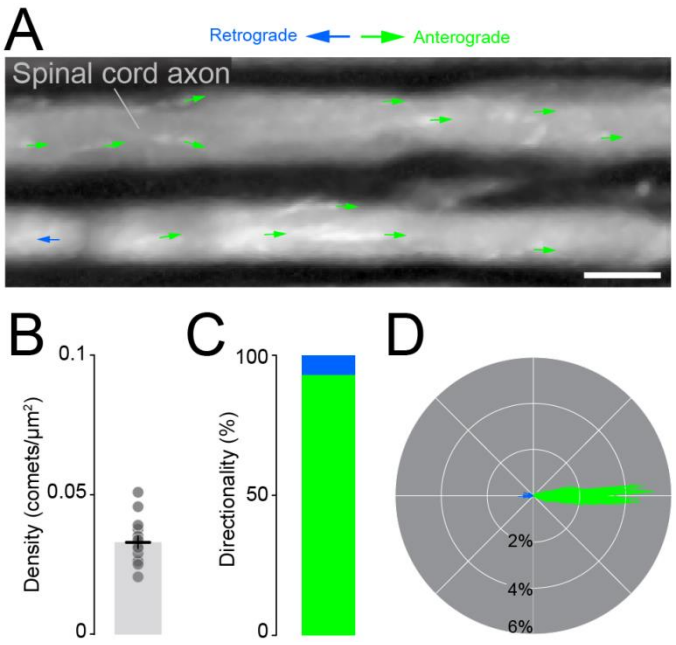

Fig. 3.13 Microtubule dynamics in axons of the spinal cord *in vivo*

(**A**) *In vivo* imaging of microtubule dynamics in axons of the lumbar spinal cord of *Thy1*:EB3-YFP transgenic mice (represented as previously). (**B-D**) Quantification of microtubule dynamics in central motor axons of the spinal cord (n = 15 axons from 3 mice) showing comet density (**B**), orientation (**C**) and directionality in relation to the axon axis represented in a polar plot (**D**). Scale bar in **A** 5µm. Data obtained in collaboration with Phil Williams. Modified from Kleele et al., 2014.

3.2.5. Chronic imaging of cortical neurites *in vivo*

To image microtubule dynamics *in vivo* in the brain, our collaboration partner Petar Marinkovic (from Jochen Herms' lab, LMU Munich) implanted chronic cranial windows onto the somatosensory cortex (Fuhrmann et al., 2007, Holtmaat et al., 2009). For these experiments, we used *Thy1*:EB3-YFP transgenic mice from line J023, which has a subset of neurons from Layer 2/3 and 5 labeled. Three to four weeks after surgery, I performed high-resolution two-photon imaging on those mice under anesthesia (**Fig. 3.14**). Despite movement artifacts and reduced signal-to-noise levels in the time-lapse recordings compared to other sites of imaging, density (0.222 ± 0.017/µm2; n= 18/5), speed (0.101 ± 0.004 µm/sec; n= 18/5) and predominant orientation (73±4; n= 18/5) of dynamic microtubules in individual cortical neurites could be analyzed. Most of the imaged neurites are likely dendritic processes,

as confirmed by injection of an adeno-associated virus expressing cytoplasmic CFP, which reveals the presence of spine-like protrusions (**Fig. 3.14 B**). This *in vivo* imaging paradigm also allowed longitudinal assessment of microtubule behavior over periods of 7 days (**Fig. 3.14 C**). Under physiological conditions, the parameters of dynamic microtubules do not change significantly over time (**Fig. 3.14 D-F**), confirming that this assay provides a robust base-line for future *in vivo* assessment of microtubule changes in plasticity paradigms.

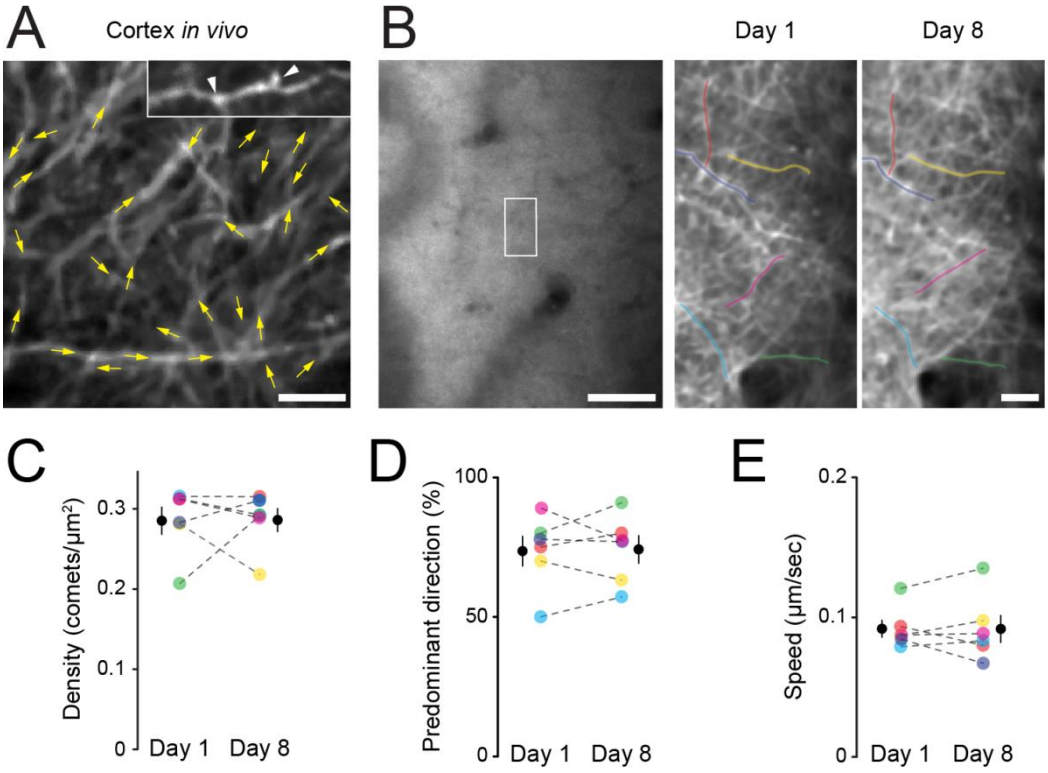

Fig. 3.14 Chronic *in vivo* imaging through a cranial window

(**A**) Neurites of the somatosensory cortex of *Thy1*:EB3-YFP transgenic mice imaged through a cranial window *in vivo*. Comets are color coded in yellow, because the anterograde and retrograde direction cannot always be defined in this preparation. (**B**) Injection of an adeno-associated virus expressing cytoplasmic CFP allows visualizing spine-like protrusions, suggesting that most of the imaged neurites are dendrites. (**C**) Repetitive imaging of the same neurites in the somatosensory cortex *in vivo* over one week. A larger overview of the cranial window (**left**) allows identification of the same six neurites on day 1 and 8 (boxed on the **left**; neurites pseudo-colored on the **right**). (**D-F**) Density, predominant direction and speed measured in the same six neurites (identified by color and linked by dashed line; black data symbol shows mean ± s.e.m.) as shown in **B** on day 1 and day 8. Scale bar in **A** and **B** (higher magnification panels) 5 µm in **B** (overview) 50 µm. Data obtained in collaboration with Petar Marinkovic. Modified from Kleele et al., 2014.

Together, the *ex vivo* and *in vivo* experiments show, that axons show a lower density of stringently-oriented dynamic microtubules compared to dendrites, where densities are higher

and orientations more variable (**Table 3.2**). Moreover, along axons there appears to be a proximal-to-distal gradient of increasing density but lower orientation stringency of comets.

Compartment	**Density** (comets/µm^2)	**Orientation** (% anterograde)	**Speed** (µm/sec)
Axon proximal (intercostal *ex vivo*)	0.025 ± 0.001	98 ± 0	0.151 ± 0.003
Axon distal (intercostal *ex vivo*)	0.065 ± 0.002	95 ± 1	0.112 ± 0.003
Synapse (NMJ *ex vivo*)	0.118 ± 0.007	83 ± 3	0.102 ± 0.002
Dendrite (Purkinje cell *ex vivo*)	0.141 ± 0.011	65 ± 4	0.139 ± 0.006
Axon (sciatic nerve *in vivo*)	0.042 ± 0.005	96 ± 1	0.148 ± 0.006
Axon (spinal cord *in vivo*)	0.033 ± 0.002	93 ± 1	0.147 ± 0.004
Axon & Dendrites (cortex *in vivo*)	0.203 ± 0.023	77 ± 5	0.106 ± 0.005
DRG neurite (*in vitro*)	0.151 ± 0.016	78 ± 7	0.087 ± 0.006
Hippocampal neurite (in vitro)	0.502 ± 0.030	93 ± 1	0.111 ± 0.006

Table 3.2 Quantification of microtubule dynamics in different neuronal compartments
mean ± s.e.m.; n > 10 neurites/ 3 mice for all measurements

Finally, most parameters of microtubule dynamics appear insensitive to acute isolation in *ex vivo* preparations, stable over time and comparable between PNS and CNS. As the ease of recording, and the stability and quality of measurements are superior in *ex vivo* nerve-muscle explants compared to the *in vivo* setting, I used the triangularis sterni explant for subsequent studies on changes to microtubule dynamics under drug treatment and pathological conditions.

3.3. Microtubule modifying drugs

Microtubules have been shown to play central roles in dynamic processes. Hence disease-related microtubule alterations are of great interest in translational research (Baas & Ahmad 2013, Jordan & Wilson 2004). But targeting microtubules pharmacologically often comes at the risk of severe side-effects and can have very different effects on the cytoskeleton depending on the dosage (Stanton et al., 2011). For example, high doses of microtubule-stabilizing drugs, such as paclitaxel, are used as cytostatic agents in oncology, but their

application is limited by the risk of inducing toxic neuropathies (Jordan & Wilson 2004). Paradoxically, at low-doses, paclitaxel and related drugs are also considered as potential therapeutic agents to promote axon survival, as microtubule stabilization can protect axons after trauma (Hellal et al., 2011) and against degeneration (d'Ydewalle et al., 2011, Fanara et al., 2007). Given the double-edged effect of microtubule stabilizing drugs, it is important to establish precise dosing schemes and to understand the cell biological effects of those substances on the microtubule cytoskeleton. Therefore I tested whether our new assay allows direct monitoring of the effects of microtubule-modifying drugs on the cytoskeleton.

3.3.1. Microtubule stabilizing drugs

Paclitaxel (better known under one of its brand names, Taxol) is probably the best known microtubule modifying drug and is already used in cancer therapy. But as just pointed out, defining the exact therapeutic window and limiting side-effects is crucial for application in humans. To explore, whether our approach can provide a direct readout of the effect that microtubule-stabilizing drugs have on dynamic microtubules, I performed time-lapse recordings of *Thy1*:EB3-YFP intercostal axons treated with different concentrations of paclitaxel (**Fig. 3.15**). Bath application of high Paclitaxel doses led to loss of EB3 comets, suggesting "freezing" of microtubule dynamics (**Fig. 3.15 A and B**). In contrast, at low Paclitaxel doses (≤ 1.5 µM) EB3 comets were partially preserved for at least 3 hours (**Fig. 3.15 B**). The dose-response curve of Paclitaxel treatment (EC_{50} at 60 minutes ≈ 2 µM; **Fig. 3.15 C**) allows identifying a concentration that modulates but not abrogates microtubule dynamics, which suggests that microtubules are only slightly stabilized. This could represent a therapeutic concentration, which promotes axonal regeneration but avoids neurotoxicity.

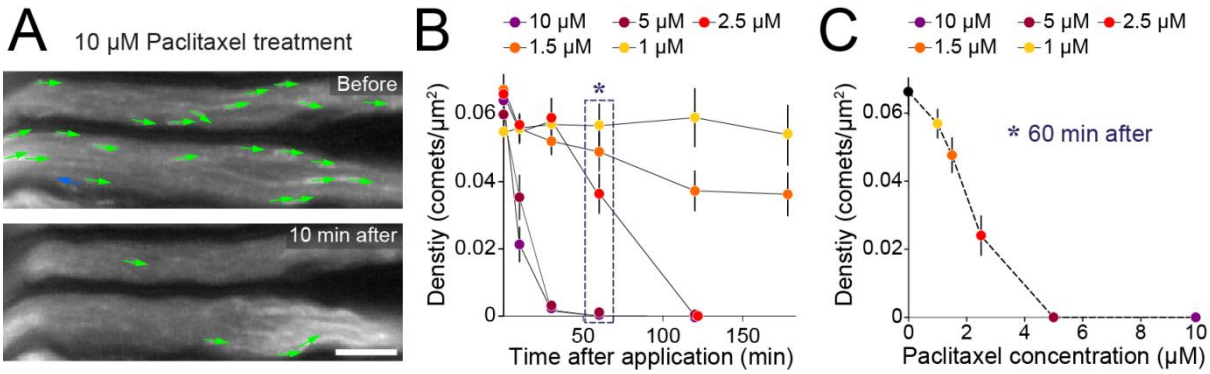

Fig. 3.15 Microtubule dynamics after exposure to the microtubule stabilizing drug Paclitaxel

(**A**) Bath application of 10 µM Paclitaxel leads to a loss of EB3 comets in motor axons of a triangularis explant after 10 min (represented as previously). (**B**) Quantification shows that Paclitaxel application leads to a dose-dependent loss of comets over time (n ≥ 11 axons from 3 mice for each group). (**C**) Corresponding dose response curve measured 60 min after Paclitaxel application. Control values at 0 µM are measured after application of DMSO (the solvent used to deliver Paclitaxel) only. Scale bar in **A** 5 µm. Modified from Kleele et al., 2014.

3.3.2. Paclitaxel block of acute axonal degeneration

To investigate whether such *in situ* dosing would allow predictions about axon preservation or loss after drug treatment, different Paclitaxel doses where tested for their effect on acute axonal degeneration (AAD). AAD is a form of axonal dieback that occurs within half an hour after trauma and leads to a sudden fragmentation of distal and proximal axons ends over 200-300 µm (Kerschensteiner et al., 2005). It has been described that AAD is caused by an influx of calcium, which in turn leads to a fragmentation of microtubules (Knoferle et al., 2010). Therefore, pharmacological stabilization of microtubules with low dosage of Paclitaxel could have a beneficial outcome on AAD after trauma, as suggested previously for spinal injury (Erturk et al., 2007). Indeed, when motor axons were treated with 1.5 µM Paclitaxel before laser cut the extent of fragmentation was significantly reduced (**Fig. 3.16**). In contrast, high paclitaxel doses (10 µM) exacerbated axonal die-back (**Fig. 3.16 B**). These results confirm that a slight stabilization can protection of axons, but the beneficial effect depends critically on the drug dosage.

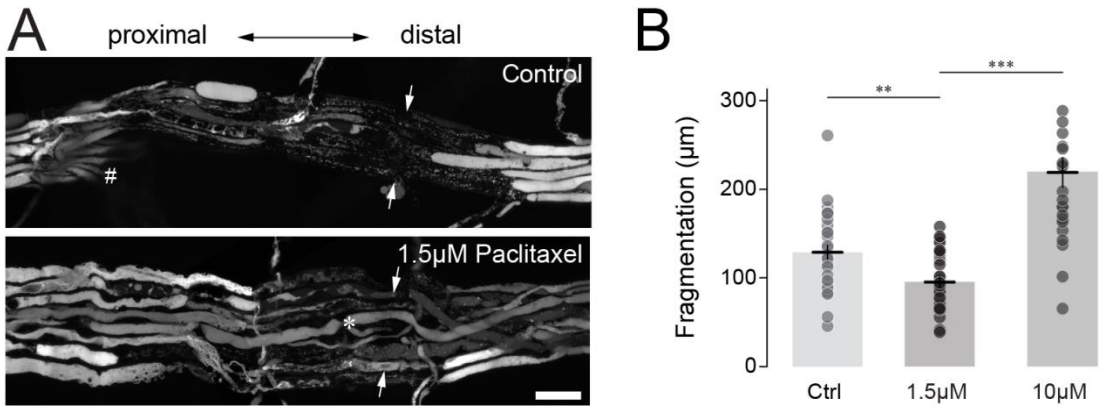

Fig. 3.16 Low-doses of Paclitaxel protect against acute axonal degeneration (AAD) after injury

(**A**) Confocal micrographs of axon fascicles in motor axons of *Thy1*:YFP-16 mice (cytoplasmic labeling in all motor axons), 1 h after multiple axons were severed by two-photon microsurgery (arrows) in untreated (top) and Paclitaxel-pretreated (1.5 µM for 1.5 h before and for 1 h after axotomy; bottom) triangularis sterni explants. Note die-back marked by trails of axon fragments. Some axons were not severed because they lay too deep (asterisk); other axons leave the nerve in a fascicle (pound symbol); both were not included in the analysis. (**B**) Measurement of the AAD-mediated die-back distance in untreated control axons and 1.5 µM or 10 µM Paclitaxel-treated axons (n = 24 axons from 3 mice per group). Scale bar in **A** 20 µm. ***, P<0.001; **, P<0.01. Modified from Kleele et al., 2014.

3.3.3. Microtubule depolymerizing drugs

Next, I wanted to test the influence of the inverse pharmacological manipulation, namely microtubule depolymerizing drugs. Therefore, I applied 5 µM Nocodazole (Samson et al., 1979) to a triangularis sterni explant of *Thy*1:EB3-YFP mice crossed to *Thy1*:Mito-CFP mice. This allows measuring the influence of Nocodazole on both, microtubule dynamics and axonal transport (**Fig. 3.17**). Application of 5µM Nocodazole leads to an immediate abrogation of comets suggesting swift depolymerization of the microtubule cytoskeleton (**Fig. 3.17 A**). Surprisingly, axonal transport of mitochondria was not reduced within the imaging period of one hour, but mitochondria changed their morphology into a more rounded shape, which is usually an indicator for organelle pathology (Nikic et al., 2011). However, because

we decided to focus on microtubule-stabilizing drugs as the translationally more relevant class of pharmaceuticals, I did not acquire a complete dataset on Nocodazole's action.

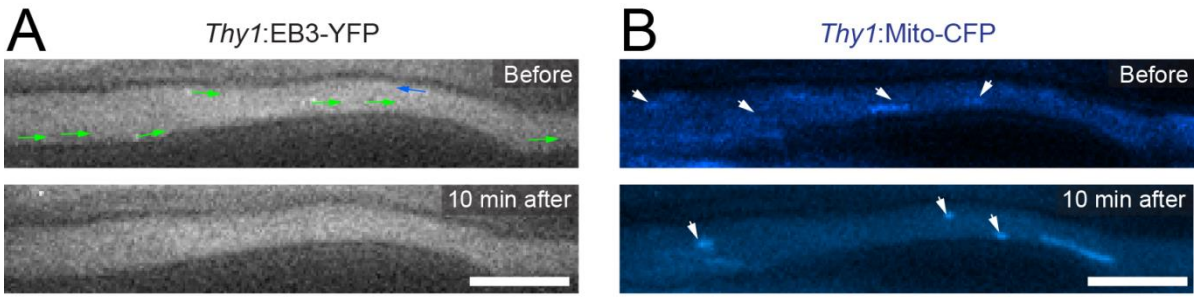

Fig. 3.17 Microtubule dynamics after exposure to Nocodazole

(**A**) EB3 comets in motor axons of *Thy1*:EB3-YFP x *Thy1*:Mito-CFP mice disappear within 10 minutes after bath application of the microtubule depolymerizing drug Nocodazole (represented as previously). (**B**) Mitochondrial transport in the same axon is not abolished (*not shown),* but mitochondria have a rounded morphology after nocodazole treatment (arrowheads). Scale bar in **A** and **B** is 5µm.

Overall, these experiments show that *Thy1:*EB3-YFP mice can be used to test the effect of different microtubule modifying drugs and to define suitable concentrations for treatment, for instance after axon trauma.

3.4. Microtubule dynamics under pathological conditions

In the past, different studies have shown that the microtubule cytoskeleton is very sensitive to changes in cell physiology (Chen et al., 2012a, Chevalier-Larsen & Holzbaur 2006, Mattson 1999). Alterations in microtubule dynamics are often found early after injury or in early stages of neurological diseases. Moreover, a change in microtubule dynamics also leads to various other cellular disturbances, as microtubules are key regulators of other cellular processes. Hence detecting early microtubule alterations during disease modelling can be informative as to whether loss of microtubule integrity could contribute to subsequent events in the cellular physiology of degenerating neurons.

3.4.1. Acute axonal injury

Previous studies in invertebrates have suggested that axotomy has profound acute and chronic effects on microtubule dynamics (Chen et al., 2012a, Erez et al., 2007, Stone et al., 2010). But whether this also holds true in fully mature mammalian axons remains unclear, as non-mammalian axons differ substantially from their mammalian counterparts in their behavior after injury (El Bejjani & Hammarlund 2012). Therefore, I examined the effect of axon trauma on the microtubule cytoskeleton, both acutely after injury and during the subsequent process of axon degeneration and regeneration.

3.4.1.1. Two photon laser dissection

First, I performed two-photon laser transection of peripheral motor axons in the triangularis sterni explant to examine the immediate effect on microtubule dynamics after injury **(Figure 3.18)**. Instantly (<5 min) after transection, injured motor axons showed a >4 fold increase in microtubule density at the proximal stump compared to non-severed axons (at 0-10 μm from the axon-end: $0.283 \pm 0.032/\mu m^2$ axonal area; n = 9/7; **Figure 3.18 A and B**). However, this increase was a rather local phenomenon, as comet density remained normal 60-70 μm proximal to the injury site ($0.053 \pm 0.053/\mu m^2$ axonal area; n = 7/5; **Figure 3.18 B**). The polarity of comets in the area proximal to the cut was largely unaltered, with the majority of comets moving anterogradely, although individual comets at the severed end had a more disorganized orientation than usual. While these results confirm acute injury-induced changes in microtubule dynamics that were also reported in invertebrates (Stone et al., 2010), I did not observe the formation of "traps", where microtubules in a severed axon tip are directed in opposing directions, as described in axotomized Aplysia neurons *ex vivo* (Erez et al., 2007).

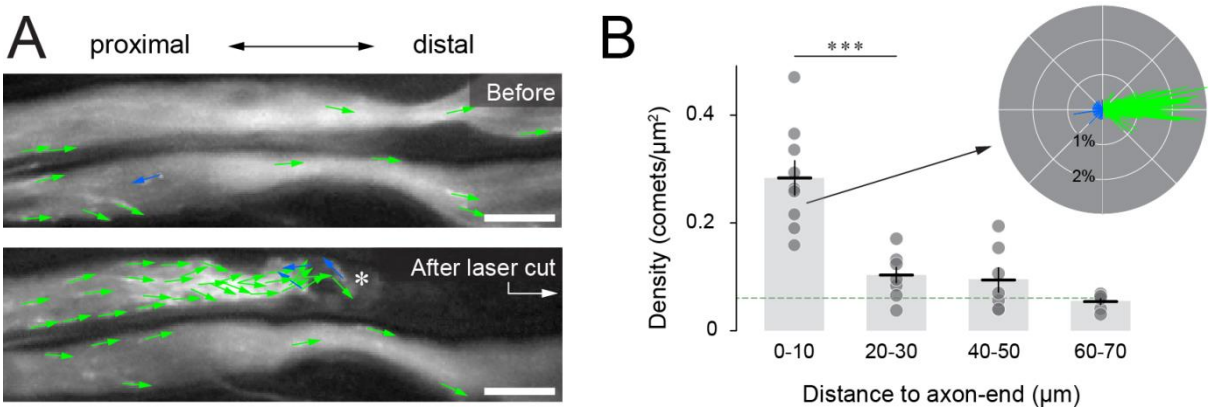

Fig. 3.18 Microtubule dynamics after acute injury

(**A**) Acute axotomy by two-photon laser (axotomy site outside of the frame to the right) induces a rapid increase in comet density at the proximal axon-end (asterisk). The lower axon is also cut, but microtubule dynamics are unchanged, because the cut > 60 µm outside of the frame to the right (arrow; represented as previously). (**B**) Quantification of microtubule dynamics after laser cut shows that this effect is confined to within less than 60 µm from the axon-end (dashed green line indicates control values of uncut axons; n ≥ 7 neurites from ≥ 5 mice for each group). Polar plot of the 0-10 µm segment (inset in **B**) shows that comet orientation is largely unaltered (n = 4 axons from 4 mice). Scale bar in **A** 5 µm. ***, P<0.001. Modified from Kleele et al., 2014.

3.4.1.2. Intercostal nerve axotomy

The local restriction of up-regulated microtubule dynamics after injury raised the question, whether there is also a more global change in the microtubule cytoskeleton at later stages of the injury response, for which there is precedent in fly neurites (Stone et al., 2010). Such a delayed response could for example be the result of a second messenger pathway activated after trauma. To test this, I transected intercostal nerves *in vivo* and then imaged microtubule dynamics distal and proximal to the lesion at time-points between 3 hours and 2 days (**Fig. 3.19**). Indeed, a global increase in comet density started 6 hours after injury and reached a >3-fold increase within two days (at ~1 mm from the lesion, 6 hours after cut: 0.033 ± 0.003 vs. 0.023 ± 0.002/µm2 in uncut contralateral control nerves; 2 days after cut: 0.087 ± 0.006 vs. 0.022 ± 0.001/µm2; n ≥ 9/2). Surprisingly, comet density also increased transiently in the distal nerve stump 6 hours after injury (at ~1 mm from the lesion, 0.117 ± 0.023 vs. 0.054 ±

0.006/µm^2 in uncut contralateral control nerves) but decreased before Wallerian fragmentation set in (0.040 ± 0.011).

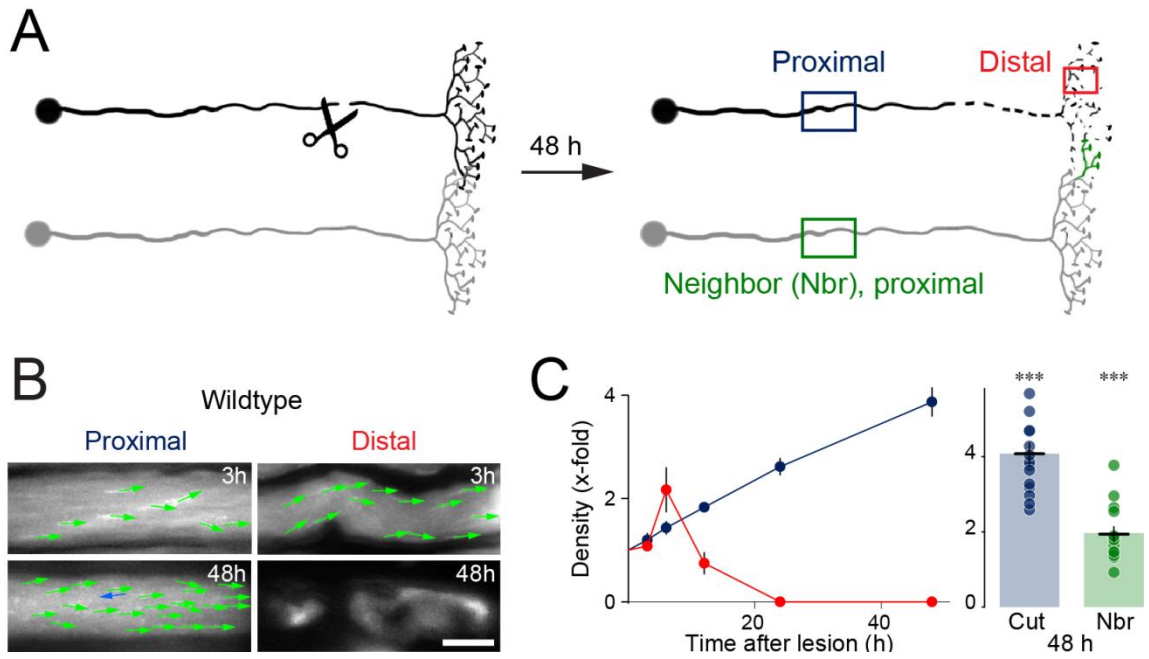

Fig. 3.19 Microtubule dynamics after chronic injury

(**A**) A global change in comet density is found after nerve cut (schematic of experiment and measurement sites). The "neighbor" is an uncut adjacent nerve that can sprout into the denervated territory (green sprout symbol on the right). (**B**) Proximal of the cut (~ 1 mm away) comet density steadily increases, while distally an initial spike in dynamics is followed by a decline before fragmentation (represented as previously). (**C**) Corresponding quantification of comet density after axotomy. Right graph shows that axons that are not cut, but receive a growth stimulus ("Nbr"), also show increased microtubule dynamics after 48 h (n ≥ 10 neurites from ≥ 3 mice for each condition; bar showing "cut, 48h" is a re-plot from time-course on left; horizontal line and data symbols show mean + or ± s.e.m., respectively; In panel **C** some error bars are hidden by the data symbol). Scale bar in **B** is 5 µm. Modified from Kleele et al., 2014.

While the immediate increase in microtubule dynamics seems to be a feature of injured or degenerating axons, the delayed up-regulation in the proximal stump could also be a regeneration signal. After transection, peripheral motor axons form growing tips to re-innervate their original targets (Nguyen et al., 2002). Therefore, I measured microtubule dynamics 9 days after axotomy, where motor axons already have formed growth cones. Indeed, also growing axons tips show a significant increase in microtubule dynamics (9 days after cut: 0.195 ± 0.020; n = 15/3; **Fig. 3.20**).

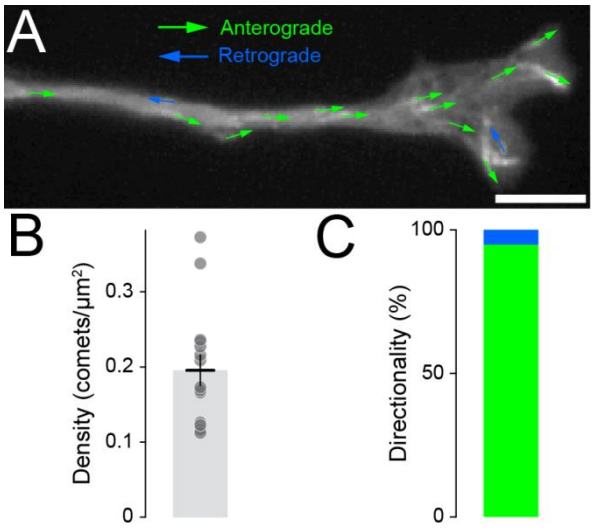

Fig. 3.20 Microtubule dynamics in regenerating axon tips

(**A**) Time-lapse series of microtubule dynamics in a growth cone of a regenerating motor axon in the triangularis sterni 9 days after intercostal nerve axotomy (EB3 comets represented as in previous figures). (**B**) Comet density in distal parts of regenerating axons 9-10 days after axotomy (**C**) Directionality of comets in regenerating axons 9-10 days after axotomy (n = 15 axons from 3 mice). Scale bar in **A** is 5 µm.

So, on the one hand, increased microtubule dynamics seem to be a tag of destabilized or degenerating axons. On the other hand, the delayed and constant increase in microtubule dynamics in the proximal part correlates with regenerative growth, rather than with degeneration. This raised the question whether microtubule remodeling is also found in axons that receive growth-promoting stimuli, but were themselves never injured. As the triangularis muscle is inter-segmental and receives input from several intercostal nerves (Kerschensteiner et al., 2005), transection of one intercostal nerve can induce expansion of motor units in neighboring nerves, as their axons re-innervate vacated neuromuscular junction sites (**Fig. 3.19 A**). Indeed, when I measured microtubule dynamics in neighboring, non-transected intercostal axons, I found a two-fold increase in density of dynamic microtubules (2 days after cut: 0.042 ± 0.004; n = 15/3 vs. contralateral side: 0.020 ± 0.001; n = 10/3; **Fig. 3.19 C, right**). These results suggest that an increase in dynamic microtubules could serve as a general marker of ongoing or imminent remodeling of axonal arbors.

3.4.1.3. Intercostal nerve axotomy in ΔNLS transgenic mice

While the increase in EB3 density in the proximal axon stump of a transected axon is both, a sign of destabilization, but also remodeling of axon branches, the distal increase in comet

density is more likely to be part of the Wallerian degeneration program (Coleman & Freeman 2010). To test if this distal increase is linked to Wallerian degeneration, even though it precedes fragmentation by several hours, *Thy1*:EB3-YFP mice were crossed with *Thy1*:ΔNLS-Wld^S mice (gift of Michael Coleman, Babraham Institute, Cambridge, UK), which express a predominantly axonal and therefore particularly potent version (deleted nuclear localization signal; ΔNLS) of the slow Wallerian degeneration (Wld^S) protein (Beirowski et al., 2009). In ΔNLS-Wld^S mice, the distal stump of cut axons remains intact for up to two weeks (**Fig. 3.21 A**). After axotomy, the distal stump of ΔNLS-Wld^S positive axons had an unaltered density of dynamic microtubules at all time-points examined after injury (up to 3 days; **Fig. 3.21 B** and **C**).

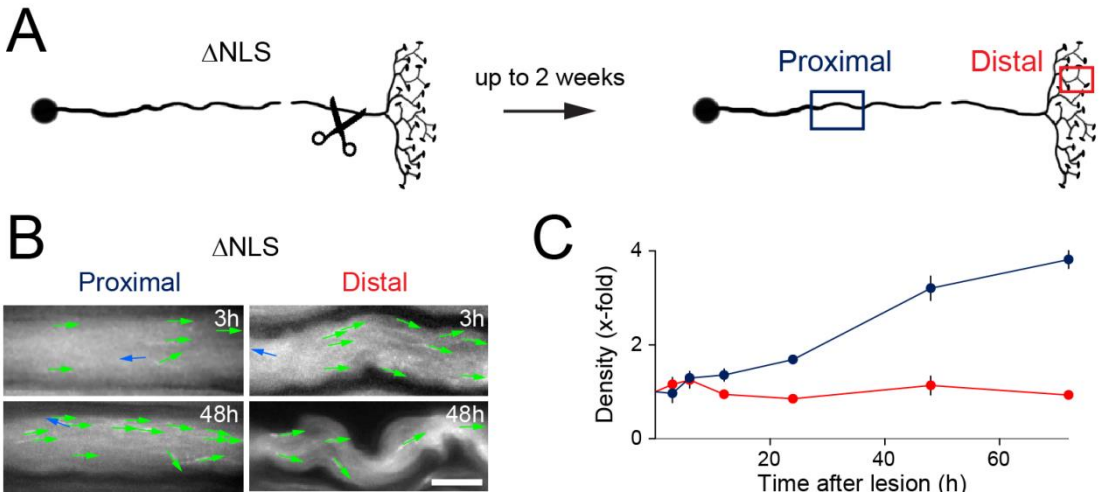

Fig. 3.21 Microtubule dynamics in ΔNLS-WldS transgenic animals after axotomy

(**A**) *Thy*1:EB3-YFP mice were crossed with ΔNLS-Wld^S mice, expressing a potent version of the slow Wallerian degeneration (Wld^S) protein. In ΔNLS-Wld^S mice, the distal stump of cut axons remains intact for up to two weeks. (**B**, **C**) Time-lapse series (**B**) and corresponding quantification (**C**) shows that changes in microtubule dynamics in the distal axotomized stump are abolished in ΔNLS-Wld^S mice. The proximal changes are delayed but still present (n= 15 neurites from 3 mice for each group). In panel **C** some error bars are hidden by the data symbol. Scale bar in B is 5 µm. Modified from Kleele et al., 2014.

Interestingly, the proximal response to axotomy was similar to the wild-type situation, but the increase in comet density was delayed (**Fig. 3.21 B and C**). This could for example be due to a delayed growth stimulus, as it has been shown that the persistence of the distal axon stump

can delay regeneration (Coleman & Freeman 2010). Overall these findings imply that the proximal and distal increases in comet densities are mechanistically distinct and that changes in microtubule dynamics in the distal stump are immediately linked to the Wallerian degeneration program. In disconnected axon segments, increased microtubule dynamics can serve as an indicator of destabilized axons that are destined to degenerate.

3.4.2. Neurodegenerative disease models

The drastic and instant increase in microtubule dynamics in traumatic forms of axon degeneration in *Thy*1:EB3-YFP mice raised the question whether similar changes can be found in chronic neurodegenerative diseases. To test this, Thy1:EB3-YFP transgenic mice were used to study changes in microtubule dynamics in mouse models of two different neurodegenerative diseases.

3.4.2.1. Animal model of amyotrophic lateral sclerosis

First, I tested how microtubule dynamics are altered in animal models of familial amyotrophic lateral sclerosis (ALS), a severe motor neuron disease in humans, which leads to a die-back of motor axons, muscle atrophy and death within a few years after onset of disease in humans. For this, *Thy1*:EB3-YFP mice were crossed to mice that overexpress mutant forms of human superoxide dismutase 1 (SOD mice). SOD mutant mice are a widely used model of ALS. Experiments were performed together with Petar Marinkovic, who previously studied the role of mitochondrial transport in different animal models of ALS. We used two different strains of SOD mice (for description of mutants, see (Marinkovic et al., 2012)), which have either a very rapid ($SOD1^{G93A}$) or a more protracted ($SOD1^{G85R}$) disease course. As control, we used transgenic mice that overexpress a non-mutated form of the human SOD protein

(huSOD). Time-lapse imaging of microtubule dynamics in those mice revealed an increase in density of dynamic microtubules in otherwise intact looking intercostal axons (**Fig. 3.22**). In contrast, 4-month old huSOD mice had normal microtubule dynamics. Interestingly, the effect was more prominent in the proximal parts of the motor axon and less severe in distal parts, even though the disease is characterized by a distal die-back of axons.

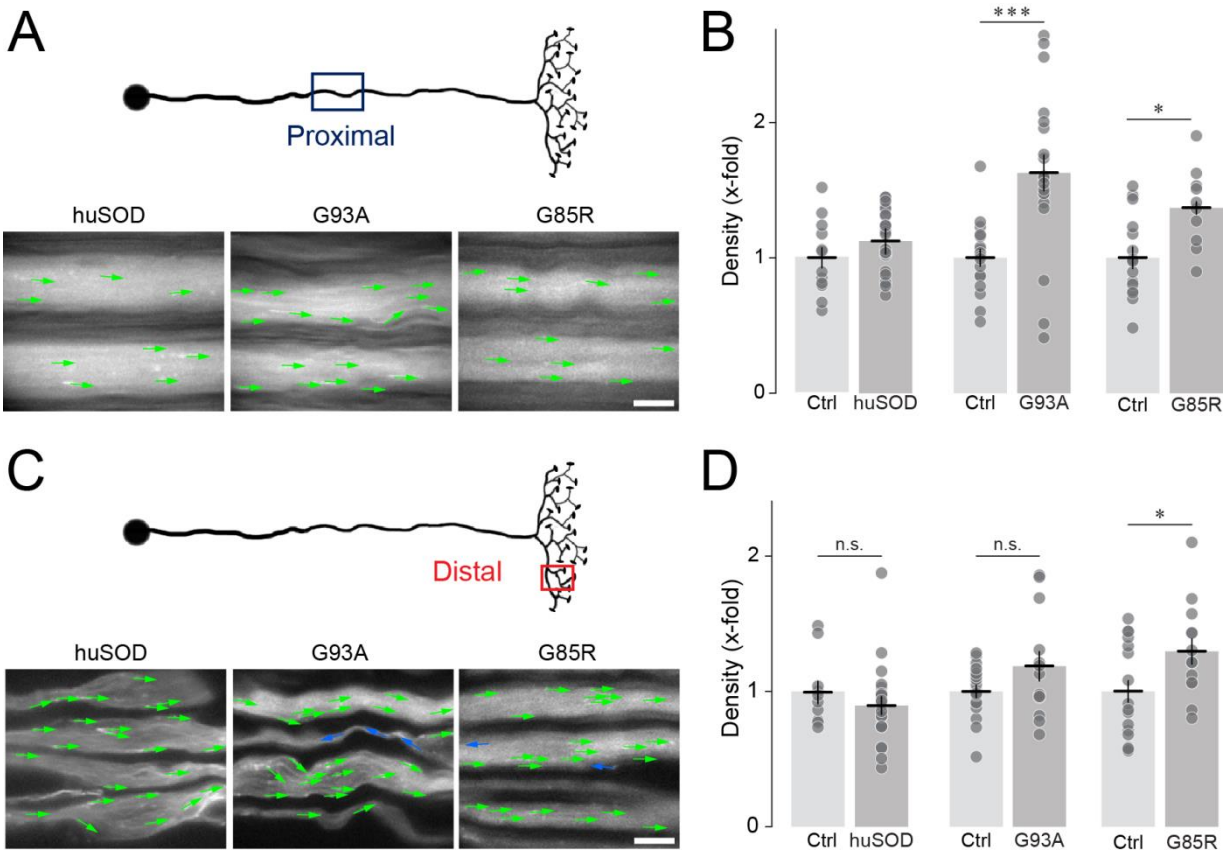

Fig. 3.22 Microtubule dynamics in mouse models of amyotrophic lateral sclerosis (ALS)

(**A, B**) Microtubule dynamics are significantly increased in proximal parts of motor axons of two models of familial ALS, but not in control mice that overexpress a non-mutated form of human SOD1 (**C**, **D**) In contrast, distal parts of motor axons show a less significant (G85R) or non-significant increase (G93A, huSOD) increase in comet density. (Ctrl: Respective wild-type litter-mates as controls; "huSOD", non-mutated form of SOD1, P120; "G93A": SOD1G93A mutation, P120; "G85R", SOD1G85R mutation, preterminal; n ≥ 10 neurites from ≥ 2 mice for each group). Scale bar in **A** and **C** 5 µm. ***, P<0.001; * P < 0.05; n.s. = non-significant. Modified from Kleele et al., 2014.

Overall, our new imaging approach has proven to be a powerful tool to study the status of the microtubule cytoskeleton under pathological conditions. My experiments revealed that an

increase in microtubule dynamics is not only a tag of destabilized or diseased axons, but potentially also a sign of axon remodeling.

3.4.2.2. Animal model of multiple sclerosis

Multiple sclerosis is an inflammatory disease characterized by a progressive axon degeneration and neurological disability (Nikic et al., 2011, Trapp & Nave 2008). Experiments performed by Catherine Sorbara (AG Kerschensteiner, LMU Munich) revealed that axonal transport is impaired in animals with acute experimental autoimmune encephalomyelitis (EAE) - a commonly used animal model of multiple sclerosis (Sorbara et al., 2014). In collaboration with Derron Bishop (Indiana School of Medicine, Muncie, USA), electron microscopy was performed on axons of control mice and of mice that were induced with EAE (two days after onset of disease). At stage 0, axons of EAE mice (normal appearing axon within an inflammatory lesion) microtubules are only slightly disorganized compared to control axons (**Fig. 3.23 A** and **B**). At stage 1 (swollen axon within an inflammatory lesion) however, there was a profound disorganization of microtubules (**Fig. 3.23. C**). Using the two-photon *in vivo* imaging assay in spinal cord axons of *Thy1*:EB3-YFP transgenic mice that I have developed, this study could show that microtubule dynamics are not significantly altered in stage 0 axons in an inflammatory lesion of EAE mice. In stage 1 within an inflammatory lesion axons in contrast microtubules are disorganized and hyper-dynamic (**Fig. 3.23 D-G**). The destabilization of the microtubule cytoskeleton however occurs mainly after axonal transport deficits set in. This observation makes it unlikely that alterations of the microtubules are the cause of transport impairments in EAE axons. Destabilized microtubules therefore might more be linked to the structural axon damage.

In summary these experiments show that the approach that I have developed is widely applicable also for other disease models.

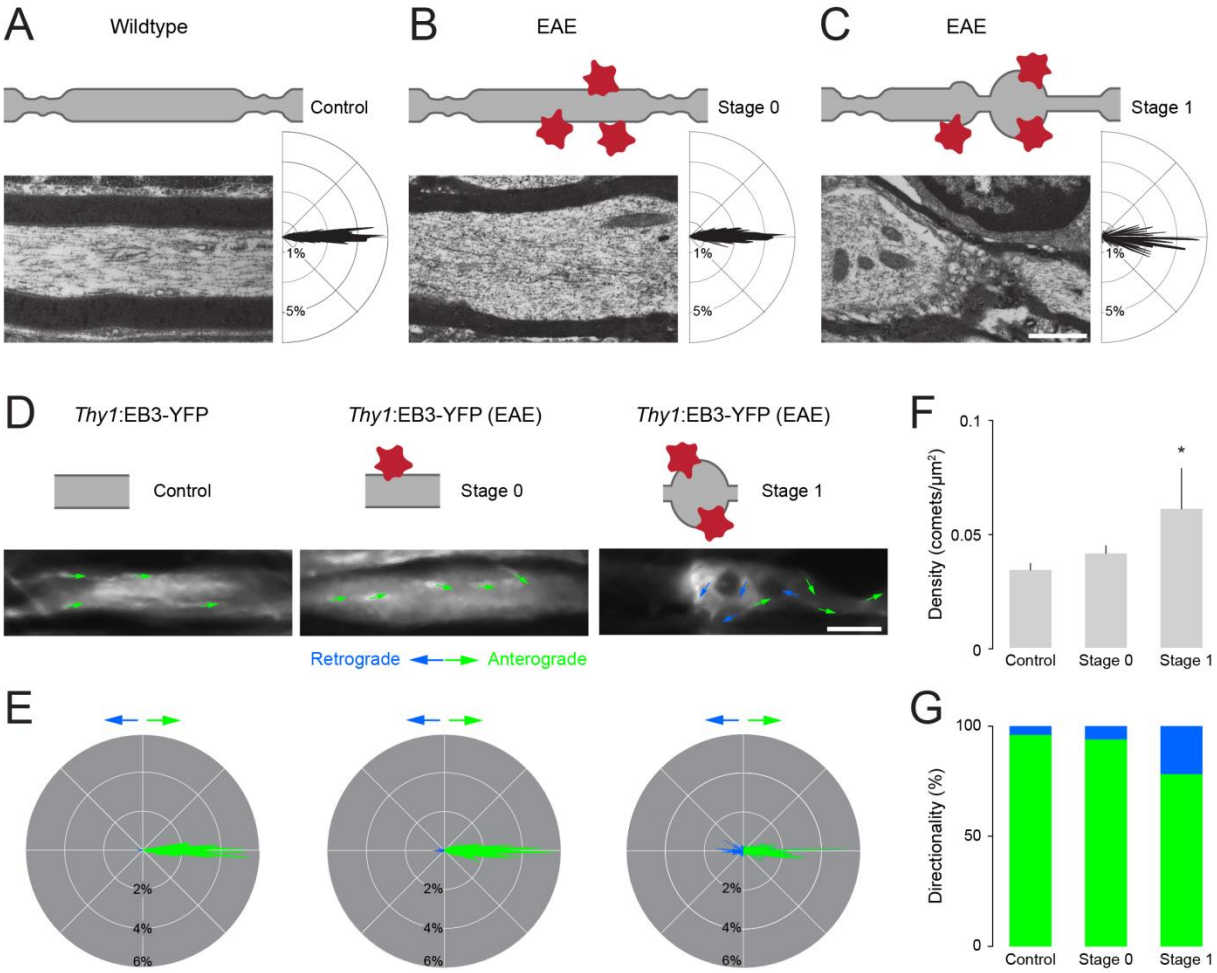

Fig. 3.23 Alterations of the microtubule cytoskeleton in an animal model of multiple sclerosis (MS)

(**A-C**) Ultrastructural analysis of axons from the lumbar spinal cord of (**A**) a wildtype mouse (control) and axons within an inflammatory lesion of a mouse two days after onset of EAE (**B**) with normal morphology (stage 0) or (**C**) with swollen morphology (stage 1). Polar plots illustrate the orientation of microtubules in relation to the axon axis (n = 22-65 axons from 3 mice per group). (**D**) *In vivo* two-photon microscopy of control axons from *Thy1*:EB3-YFP transgenic mice as well as stage 0 and stage 1 axons of *Thy1*:EB3-YFP transgenic mice two days after onset of EAE (represented as in previous figures). (**E-G**) Corresponding quantification of microtubule dynamics in control, stage 0 and stage 1 axons showing (**E**) directionality in relation to the neurite axis represented in a polar plot (**F**) comet density and (**G**) orientation (n ≥ 12 neurites from ≥ 4 mice for each group). * $P < 0.05$. Data obtained by Catherine Sorbara (LMU Munich) and Derron Bishop (Indiana School of Medicine, Muncie, USA). Modified from Sorbara et al., 2014.

3.5. Microtubule dynamics during developmental synapse elimination

It has been shown previously in non-vertebrate model system (Awasaki et al., 2006, Watts et al., 2004) and in fixed tissue (Bishop et al., 2004), that alterations in the microtubule cytoskeleton also occur during developmental pruning. After the initial establishment of a

neuronal network, many synaptic connections in the central and peripheral nervous are remodeled to ultimately result in a precisely wired neuronal network (Lichtman and Coleman 2000). In many cases such remodeling involves the resolution of transient synaptic connections, a phenomenon called synapse elimination. Synapse elimination is a widespread phenomenon in higher vertebrates, which often involves selective dismantling of individual axon branches. Over decades, the neuromuscular junction and its transition from innervation by multiple to a single motor axon has proven to be an excellent model system for studying synapse elimination. During embryonic development motor neurons establish connections with a large number of muscle cells. But during the first two weeks of postnatal life the removal of axonal branches leaves each muscle fiber with only one innervating axon (Lichtman & Colman 2000). The elimination of axonal inputs is driven by a competition between co-innervating inputs and neural activity seems to have an important influence (Holtmaat & Svoboda 2009). Despite a comprehensive understanding of the underlying developmental principles, the cellular and molecular mechanisms which are involved in axonal withdrawal are mostly unknown. Previous studies in our lab have shown that axonal transport of different cargos - for example mitochondria or peroxisomes- is shut down in axon branches that are dismantled or have formed a retraction bulb. We therefore wondered, whether the lack of transport in axon branches that are going to be dismantled is due to a break-down of the microtubule cytoskeleton. As microtubules are forming the tracks for fast axonal transport, their destabilization would automatically lead to a disruption of cargo supply. To test this, I used postnatal *Thy*1:EB3-YFP transgenic mice to image microtubule dynamics in developing motor axons. In general, density of dynamic microtubules in axon branches of young mice is higher than in motor axons of adult mice (**Fig. 3.24**). This might reflect the fact that such immature branches are still more plastic and less stable than mature axons.

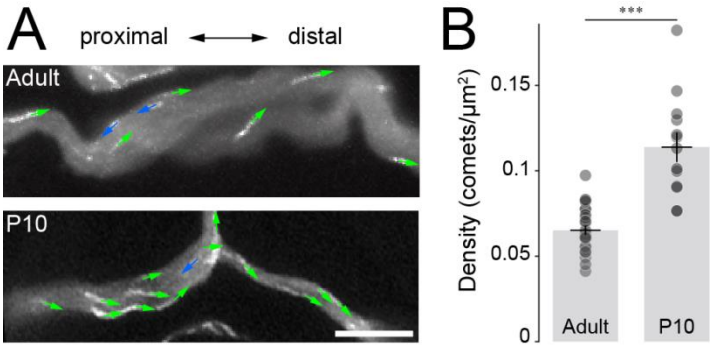

Fig. 3.24 Microtubule dynamics in young and adult motor axons

(**A**) Comet density in motor axons of adult (top) and P10 (below) *Thy1*:EB3-YFP mice (represented as previously). (**B**) Quantification of comet density in distal branches of adult and young axons (n ≥ 10 axons from ≥ 6 mice for each group). Scale bar in **A** 5 µm

3.5.1. Microtubule dynamics in competing axon branches

To test, if a change in the microtubule cytoskeleton can be assayed during synapse elimination using *Thy1*:EB3-YFP mice, I measured the density of dynamic microtubules in axons branches that are still involved in competition and in axons that already resolved competition during the first two post-natal weeks. Unfortunately the triangularis sterni explant cannot kept alive long enough to pursue the final outcome of competition between two co-innervating inputs, hence a more indirect measure of outcome has to be employed. Indeed, already based on morphology a dismantling axon branch that is losing competition for a postsynaptic target can be identified, because such axon branches become atrophic before they form a retraction bulb. (**Fig. 3.25 A**). To define the time window at which synapse elimination is taking place in the triangularis sterni muscle, we (these experiments were performed in close collaboration with Monika Brill, a post-doc in the lab) quantified the number of retraction bulbs, multiply-innervated and singly-innervated synapses at different early postnatal ages (**Fig. 3.25 B**). Based on these results the subsequent experiments were performed between postnatal day (P) 6 and P11. To study the status of the microtubule cytoskeleton at different stages of competition, I measured microtubule dynamics in presynaptic axon segments of retraction bulbs, doubly-innervated and singly-innervated synapses (**Fig. 3.25 C**). Doubly innervated synapses were grouped into winning inputs

("strong", i.e. non-atrophic branch) and losing inputs ("weak", i.e. atrophic branch) at asymmetric innervated muscle fibers and symmetrically innervated inputs (where the two inputs do not yet differ in morphology). Quantification of the comet density in these different groups revealed that microtubule dynamics are indeed increased in atrophic axon branches and retraction bulbs.

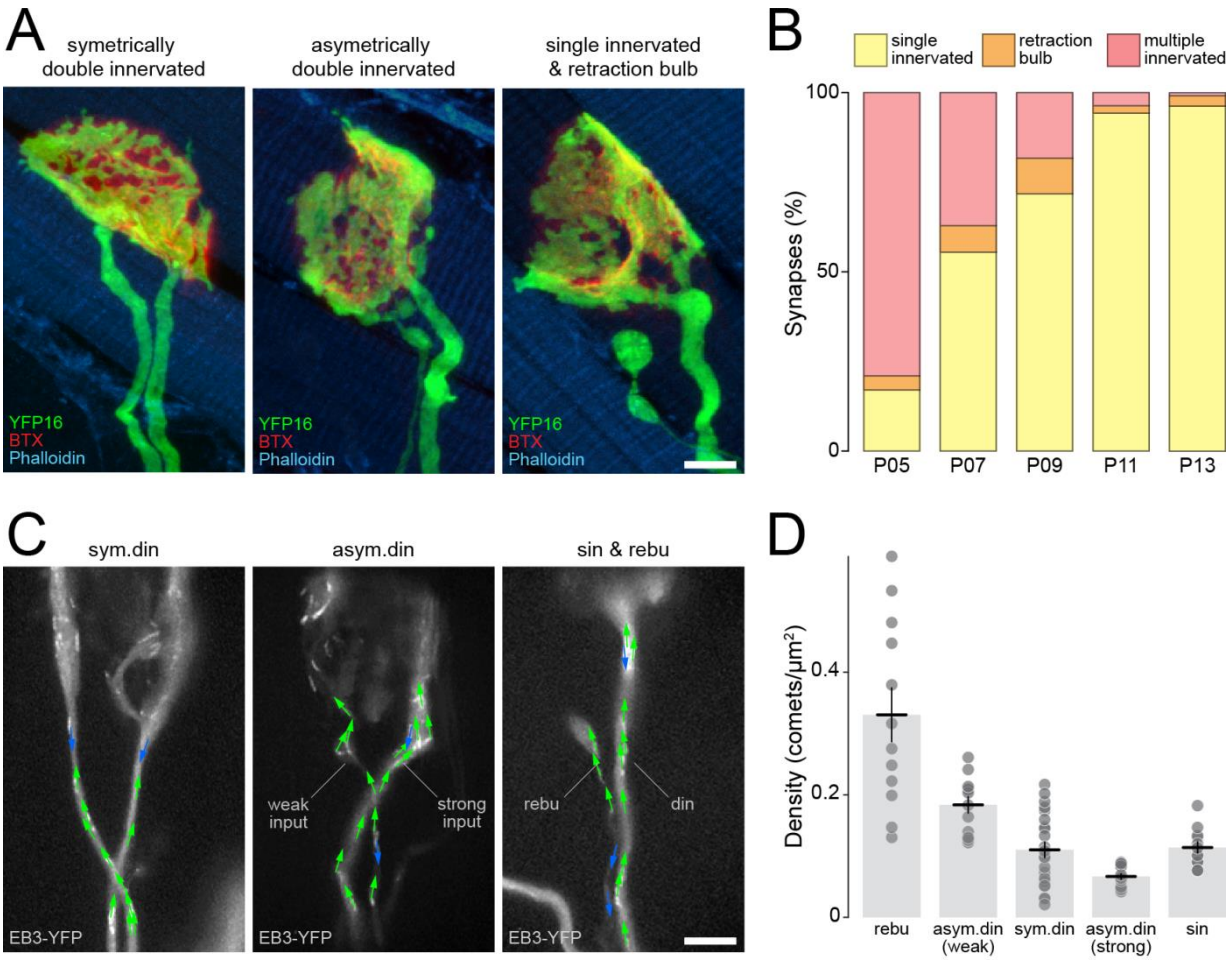

Fig. 3.25 Changes in morphology and microtubule dynamics in competing axon branches during developmental synapse elimination

(A) Confocal images of neuromuscular junctions (NMJs) during developmental synapse elimination in triangularis sterni muscles of *Thy1*:YFP16 transgenic mice at postnatal day 9 (postsynaptic receptors labeled with fluorescently-tagged bungarotoxin, **red;** muscle fibers labeled with phalloidin, **cyan**). (**B**) Percentage of NMJs in the triangularis explant that are multiply-innervated, singly-innervated or a retraction bulb. Quantification was performed in *Thy1*:YFP16 transgenic animals at different ages from P5-P13 (n ≥ 223 from 3 mice for each group). (**C**) Time-lapse series of microtubule dynamics in symmetrically double innervated NMJs ("sym.din"), asymmetrically double innervated NMJs ("asym.din"), singly innervated NMJs ("sin") and retraction bulbs ("rebu") of postnatal *Thy1*:EB3-YFP transgenic mice (represented as previously) The quantification was performed on the entire arbor that is in focus. (**D**) Corresponding quantification of microtubule dynamics in these different groups (n ≥ 12 motor axons from ≥ 4 mice for each group). Scale bar in **A** and **C** 5 µm.

From these recordings, the question arises whether changes in microtubule dynamics in a dismantling axon branch first occur at the distal part of the input and subsequently extend retrograde, or if these changes affect the entire branch synchronously. To test this, I measured microtubule dynamics in retraction bulbs at the most distal part and at the proximal part close to the last branch point (**Fig. 3.26**). Quantification of comet density revealed that there was no significant difference between the proximal and distal part. This suggests that the destabilization of the microtubule cytoskeleton affects the entire arbor to the same degree.

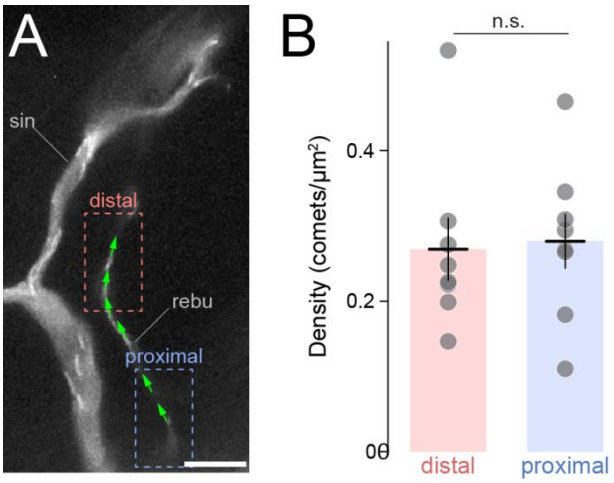

Fig. 3.26 Microtubule density at distal and proximal parts of a retraction bulb

(A) Comet density in the distal (pink box) and proximal (blue box) part of a retraction bulb ("rebu") that most likely previously innervated the same synapse as the single innervating branch ("sin") on the left (comets represented as previously). **(B)** Quantification of comet density shows no significant difference between the two compartments. n = 8 axons from 4 mice. Scale bar in **A** is 5 µm.

A destabilization of the microtubule cytoskeleton along the entire axon branch that gets dismantled might be the reason for the drop in axonal transport that was observed in these branches (*Brill, Kleele et al in preparation.*). To directly test if reduced axonal transport correlates to destabilization of the microtubule cytoskeleton, *Thy*1:EB3-YFP transgenic mice were crossed with *Thy1*:Mito-CFP mice (*Thy1*:CFP-CoxVIII, Mito K; (Misgeld et al., 2007)) to imaged microtubule dynamics and mitochondrial transport simultaneously in double innervated axon branches (**Fig. 3.27**). Double innervated inputs were again classified based on their morphology into symmetrically innervating branches and "weak" or "strong" inputs at skewed synapses. Correlation of mitochondrial transport and microtubule dynamics in co-innervating inputs shows that weaker axon branches have increases microtubule dynamics accompanied by a decrease in net axonal transport (anterograde minus retrograde

mitochondrial flux). The correlation of the two phenomena supports the hypothesis that a degradation of the cytoskeleton is responsible for the drop in axonal transport in weaker axon branches.

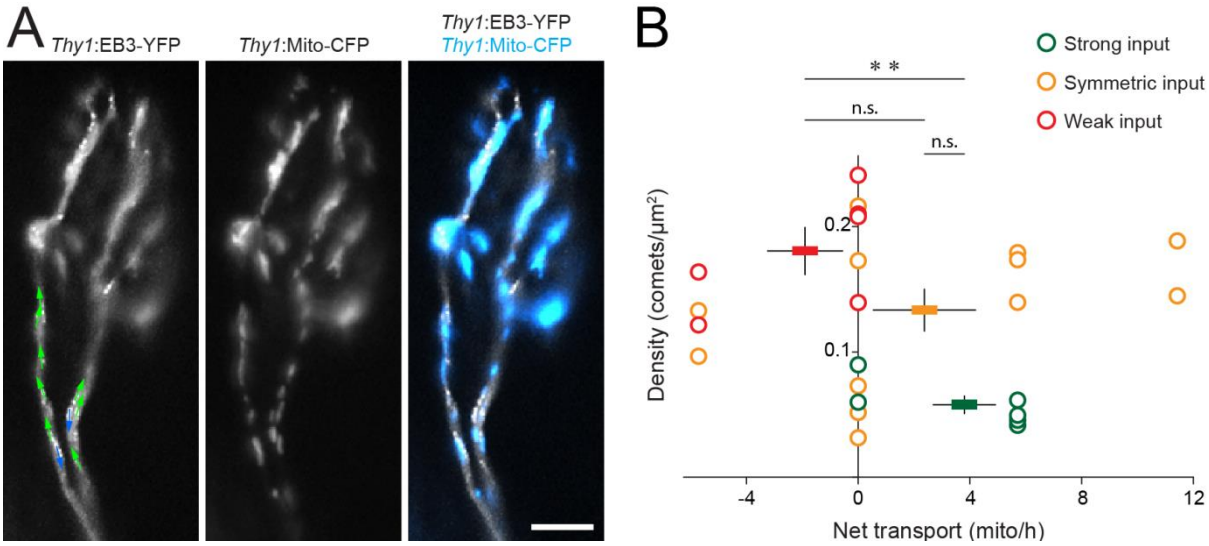

Fig. 3.27 Correlation of microtubule dynamics and mitochondrial transport

(A) Neuromuscular junction of a triangularis explant (10 frames of a time-lapse) from *Thy1*:EB3-YFP mice crossed to *Thy1*:Mito-CFP mice (left panel: EB3-YFP channel with microtubule dynamics represented as previously; middle: mitochondria labeled in CFP, right: merged image). (**B**) Correlation of net mitochondrial transport and comet density in individual strong (green circles), symmetric (orange circles) and weak (red circles) inputs. Average values for each group is presented as rectangle symbol in the corresponding color. n ≥ 6 axons from 3 mice for each group. Scale bar in **A** 5 µm. **, P<0.01; n.s. = non-significant.

Though dismantling axon branches that will lose competition for a postsynaptic target can be identified morphologically, it would be important to correlate changes in microtubule dynamics with the strength of a synaptic input even before morphological changes occur. This is especially important, as microtubule dynamics in symmetrically double innervated inputs show a large spread in microtubule dynamics (**Fig. 3.25 D**), indicating that intracellular changes occur before morphological differences can be recognized. A convenient method to estimate synaptic strength of each input is to define the synaptic territory that each input covers at the postsynaptic target (Turney & Lichtman 2012). For this, transgenic mice are used that have cytoplasmic fluorescent labeling. To measure the territory of one input, the

other axonal input is bleached by a confocal laser and a confocal stack that now shows only the territory of the other input can be acquired. As fluorescent cytoplasmic proteins diffuse back into the bleached arbor, this procedure can be repeated for the other input.

To correlate territory with microtubule dynamics, I crossed *Thy1*:EB3-YFP transgenic mice with *Thy1*:CFP5 transgenic animals, which express a cyan fluorescent protein in the cytoplasm. Microtubule density can now be directly linked to synaptic territory by time-lapse imaging of EB3 dynamics in co-innervating axon branches and subsequent definition of the synaptic territory by sequential photo-bleaching (**Fig. 3.28**). These measurements also allow in retrospect to estimate the synaptic territory of inputs that were grouped based on their morphology. Symmetric innervated inputs usually have a territory from 20-80 %, winning inputs from 80-100 % and losing inputs from 1-20 %. Quantification of comet density in competing axon branches revealed that microtubules are more dynamic in axon branches with less territory (**Fig. 3.28 C** and **D**). Density of comets is significantly increased in axonal inputs that have less than 40% synaptic territory and reach a >3-fold increase in retraction bulbs. In contrast, inputs that have a larger synaptic territory show a lower density of dynamic microtubules.

This suggests that the microtubule cytoskeleton is destabilized in weaker axon branches which are subsequently dismantled. These results are in line with previous experiments that implicated up-regulation of microtubule dynamics as an indicator of axon destabilization after injury or in disease (see **Chapter 3.4**).

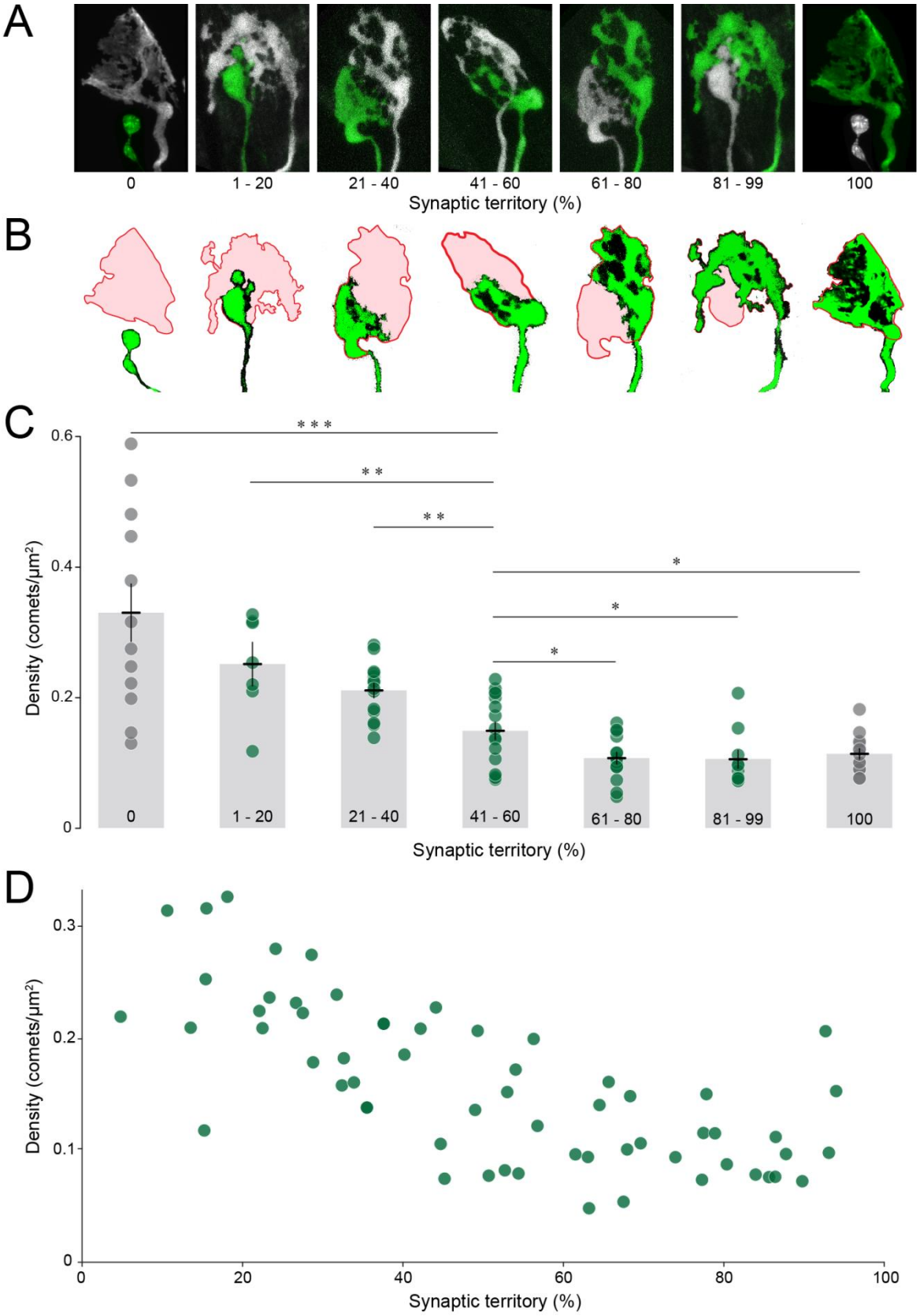

Fig. 3.28 Correlation of microtubule dynamics and synaptic territory during synapse elimination

(A) Confocal images of neuromuscular junctions (NMJs) from triangularis explants of postnatal *Thy1*:CFP5 transgenic animals were two inputs at a double innervated NMJ were consecutively bleached to define the territory of each input. Image shows overlay of two confocal images were one input is bleached respectively. Synaptic territory is indicated for the input pseudo-colored in green.

(**B**) Schematic representation of **A** which shows the synaptic territory that is covered by one of the two inputs. (**C**) Quantification of microtubule dynamics during neuromuscular synapse elimination in young *Thy1*:EB3-YFP mice crossed to *Thy1*:CFP5 mice. Axon branches are grouped according to the synaptic territory that they cover. (**D**) Un-binned correlation of EB3 comet density and synaptic territory for double innervated synapses. n ≥ 7 axons from ≥ 3 mice for each group. ***, P<0.001; **, P<0.01; * P < 0.05

3.5.2. Tubulin levels in competing axon branches

However, it is hard to prove with our assay that the increase in microtubule dynamics that I found can be interpreted as a breakdown of the microtubule cytoskeleton, because imaging EB3-YFP only allows quantifying the number of the microtubule plus tips, but not how this relates to a change in the mass of the microtubule population. To address this point, I performed immuno-staining for βIII-tubulin (which is a neuron-specific isoform) on fixed triangularis sterni muscles of *Thy1*:YFP16 (or *Thy1*:EB3-YFP x *Thy1*:CFP5) animals, where I determined the synaptic territory before fixation (**Fig. 3.29 A**). The expression of a cytoplasmic fluorescent protein was used not only for sequential bleaching, but also as a way to normalize for local variations in cytoplasmic volume or density. In this way the amount of total microtubules can be compared in different branches, were synaptic territory (and in some cases EB3 density) were quantified before. Indeed, volume-normalized levels of β-tubulin were high in single innervating branches or branches that cover a large synaptic territory. In contrast, inputs with a small territory have less β-tubulin and retraction bulbs have very low levels of β-tubulin (**Fig. 3.29 B**). This indicates that a high density of dynamics microtubule is associated with a low level of β-tubulin and therefore a degradation of the microtubule cytoskeleton. This became even clearer after fixing samples, where I previously imaged microtubule dynamics and determined the synaptic territory (**Fig. 3.29 C** and **D**).

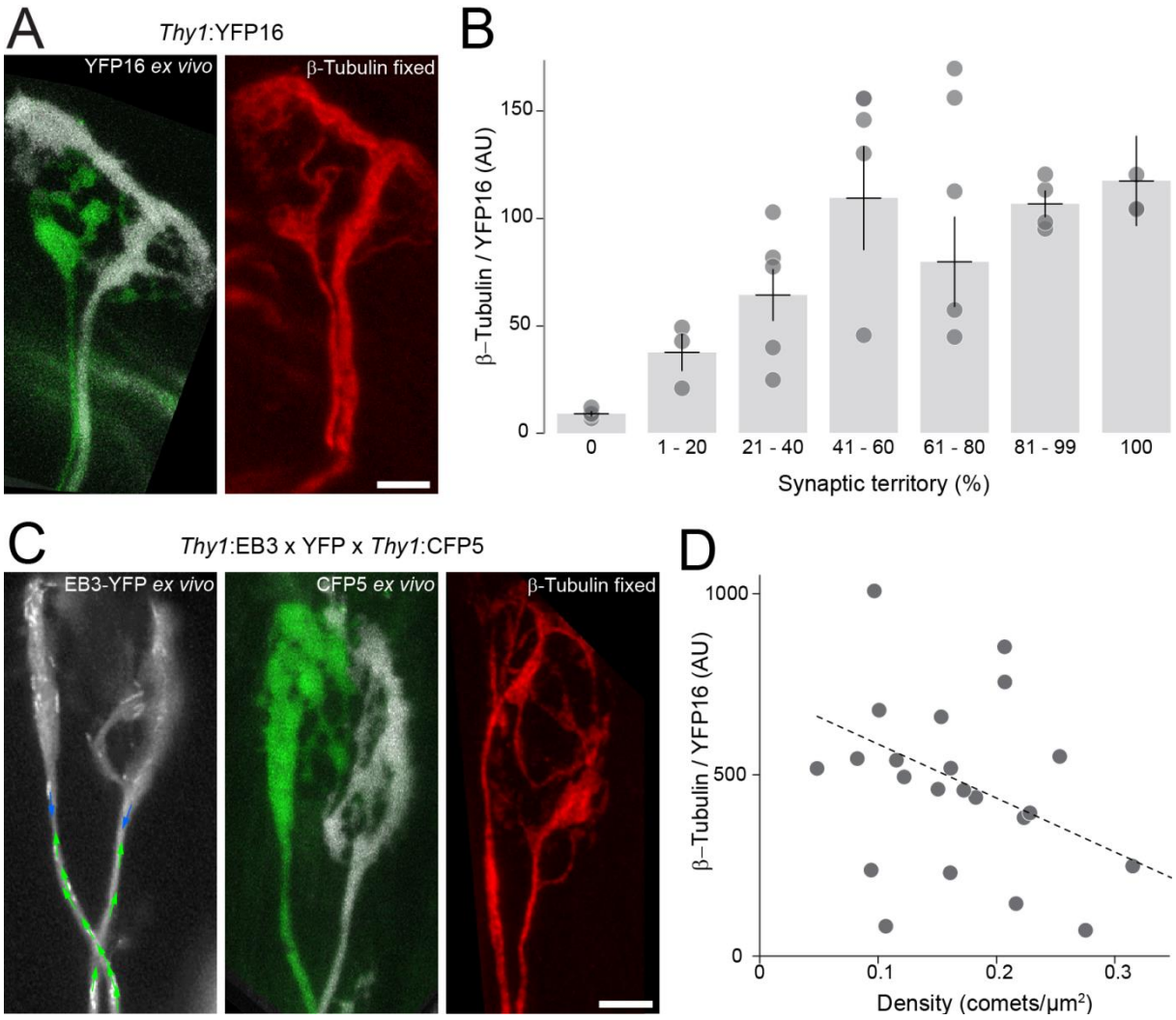

Fig. 3.29 Correlation of β-tubulin and synaptic territory or dynamic microtubules

(**A**) Confocal images of a double innervated neuromuscular junction (NMJs) from triangularis explants of a postnatal *Thy1*:YFP16 mouse were two inputs were consecutively bleached (left, pseudo-colored) and following fixation and staining with β-tubulin III antibody (right). (**B**) Quantification of β-tubulin intensity of individual inputs grouped according to their synaptic territory. (**C**) A double innervated NMJ of *Thy1*:EB3-YFP animals crossed to *Thy1*:CFP5 mice. Left panel shows a time-lapse sequence of EB3-YFP imaging (quantification performed on the entire arbor shown in the panel and represented as previously), middle panel is a confocal reconstruction of the two consecutively bleached inputs and the right panel shows the same NMJ after fixation and staining with βIII-tubulin. (**D**) Density of EB3 comets plotted against the intensity of βIII-tubulin for individual axon branches (n ≥ 7 axons from ≥ 3 mice). Scale bar in **A** and **C** 5 µm.

Taken together the results suggest that a destabilization and degradation of the microtubule cytoskeleton is a cellular phenomenon that occurs early in dismantling axons branches, even before they show morphological changes. The question whether this alteration is cause or consequence of axon branch degeneration is of course hard to address. However, one way to test which influence the stability of the microtubule cytoskeleton has on developmental

pruning is to treat postnatal mice with microtubule modifying drugs and investigate the outcome on synapse elimination.

3.5.3. Delay of synapse elimination after Epothilone B treatment

To test whether the degradation of the microtubule cytoskeleton promotes axon branch dismantling during neuromuscular synapse elimination, we hypothesized that a stabilization of microtubules should be able to prevent or delay synapse elimination if a causal relationship exists. To address this, we injected Epothilone B (a more microtubule-stabilizing drug that is more bioavailable in the nervous system than paclitaxel, (Stanton et al., 2011) into mice at P05 and the number of multiply-innervated synapses was counted on different days after injection (**Fig. 3.30 A**; dataset from Monika Brill). Indeed, especially on P9 and 11 Epothilone-injected mice show a larger percentage of poly-innervated synapses, compared to control animals that were injected with the carrier, polyethylene glycol (PEG), only. To directly analyze the effect of Epothilone B on microtubule dynamics, *Thy1*:EB3-YFP transgenic mice were also injected with Epothilone and PEG as a control at P05, and microtubule dynamics was measured at P06 (Fig. **3.30 B**). Epothilone B injected animals, but not PEG injected mice, show a decrease in comet density compared to non-injected animals. This suggests that low doses of Epothilone B can stabilize the microtubule cytoskeleton and delay axon branch removal. However, as the effect of Epothilone treatment on synapse elimination is relatively mild, the question arose whether a genetic approach would be more efficient and specific to prove that microtubule destabilization is a critical step in axon degeneration during developmental pruning. Moreover, identifying gene products involved in selective microtubule destabilization in dismantling branches would open the door for a molecular analysis of the underlying signaling cascades. Currently we are investigating mice

that lack microtubule-modifying gene products; however, due to the complex breeding schemes involved, so far no definitive results are available (Brill, Kleele *ongoing work*).

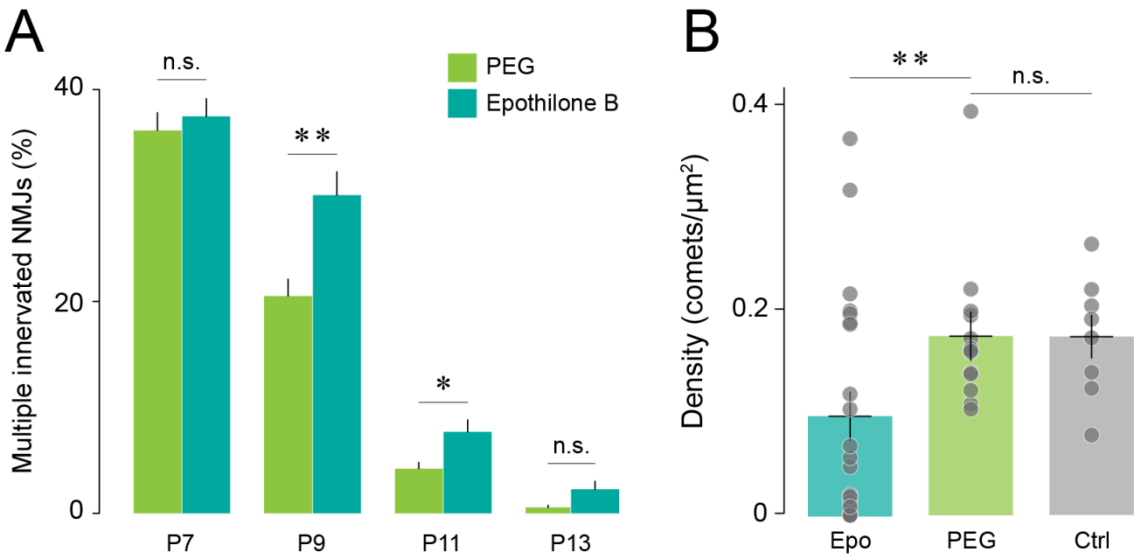

Fig. 3.30 Epothilone B treatment stabilizes microtubule dynamics and delays synapse elimination

(**A**) *Thy1*:YFP16 transgenic mice at that were injected at postnatal day 5 show a higher number of multi innervated synapses when they were injected with 2.6 µM Epothilone B compared to control mice which were injected with PEG only (n ≥ 4 axons from ≥ 3 mice). (**B**) Epothilone injection at P05 also leads to a decrease in comet density 24 hours later, while PEG alone has no effect compared to non-injected animals (n ≥ 8 axons from ≥ 3 mice). **, P<0.01; * P < 0.05; n.s. = non-significant

4. DISCUSSION

The microtubule cytoskeleton and its dynamic properties have long been of interest in cell biology and recently became also an important topic in the context of translational research. Especially neurons seem to be sensitive to changes in microtubule dynamics. Accordingly alterations of the microtubule cytoskeleton have been shown to be unifying themes in neuropathology. Even though the principal structure and behavior of microtubules are well known from studies *in vitro* (Baas et al., 1988, Perez et al., 1999, Stepanova et al., 2003) and in invertebrate organisms (Erez et al., 2007, Stone et al., 2008), only little is known about microtubule dynamics in higher organisms. This is to a large degree due to a lack of *in vivo* imaging methods that can visualize neural microtubule dynamics in a complex mammalian tissue context. I have now devised such an assay, which I believe will be useful to learn more about microtubule behavior not only in mature neurons *in situ* but also during development or plasticity. Moreover, it will also provide a tool study alterations of the microtubule cytoskeleton in the context of neuropathology and provide a read-out for therapeutic studies aimed at stabilizing microtubules. The assay that I established during my PhD thesis is based on new transgenic mice that can be used for *in vivo* imaging of microtubule dynamics and polarization in different compartments of mammalian neurons in the peripheral and central nervous system. For many of these compartments my colleagues and I also established suitable imaging modalities, so that my work provides a comprehensive resource to investigate the status of the microtubule cytoskeleton in the developing, mature and diseased nervous system. I found that an increase in microtubule dynamics is a common early sign of axon destabilization after injury and in neurodegenerative disease. Furthermore, microtubule densities are also increased during regeneration and neurite remodeling. This leads to the conclusion that an up-regulation of microtubule dynamics might be a general indicator for axonal plasticity in health and disease.

4.1. Imaging microtubule dynamics *ex vivo* and *in vivo* in mammalian neurons

The knowledge of subcellular processes that underlie dynamic behaviors of cells has for a long time been vague. The discovery of green fluorescent protein in jellyfish (Shimomura 2009), which lead to the development of fluorescently tagged proteins, and advances in imaging techniques have provided the means to address previously unresolved questions. Using these techniques *in vitro* allowed observing cells in real-time and provided important insights into subcellular dynamics. However, *in vitro* studies lack interactions at a systemic level and typically use immature cells, so that it is not always clear to what degree such findings can be transferred to higher vertebrates and the mature organism *in vivo*. Especially in neurons, which form a complex interaction network amongst themselves and with surrounding glia cells, it might be critical to observe events in the context of an intact tissue (Lichtman & Fraser 2001). *In vivo* imaging of subcellular structures and molecules has proven to be a powerful approach to increase knowledge about complex cellular processes in the nervous system. An increasing number of techniques have become available to study cell biological properties in neurons and to observe subcellular structures, for example mitochondria (Breckwoldt et al., 2014, Misgeld et al., 2007), synaptic vesicles (Umemori et al., 2004) or intracellular calcium (Chen et al., 2012b). However, a tool to visualize the neuronal cytoskeleton is still missing, although microtubule rearrangements critically influence the behavior of other cellular structures and are often affected in pathology.

4.1.1. EB3-YFP as a tool to visualize dynamic microtubules

Fluorescently tagged end-binding proteins have been used in the past to visualize microtubule dynamics, but so far they have only been applied *in vitro* (Baas et al., 1988, Perez et al., 1999, Stepanova et al., 2003) and in non-mammalian model organisms (Erez et al., 2007, Norden et al., 2009, Stone et al., 2008). The aim of this PhD thesis was therefore to

establish a new imaging approach that allows investigating microtubule rearrangements in a wide range of neurites under physiological conditions, after injury and during chronic neurodegeneration. Using a genetic approach based on stable and well-characterized transgenic mouse lines overcomes many limitations that afflict alternative approaches. For example application of fluorescently-conjugated tubulin subunits that is successfully used in cell culture to visualize microtubules, is nearly impossible in intact *in vivo* preparations. But also compared to the obvious alternative to make transgenic mice that express fluorescently tagged tubulin, there were reasons why we believe that using +TIP labels for visualizing microtubule dynamics is advantageous. First, introducing a protein domain of substantial size (such as an XFP) into a rather rigid macromolecular structure (such as a microtubule) harbors the risk of toxicity (Komarova et al., 2005). Indeed, in the past this approach has resulted in mice that were not suitable for *in vivo* imaging (Abe et al., 2011). Therefore we assumed that toxicity might be reduced, if fluorescently-tagged microtubule associated proteins (MAPs) were used to visualize microtubule dynamics. However, using MAPs that decorate the lengths of microtubules, such as tau or EMTB (Eom et al., 2011), might be problematic, because overexpression of such MAPs has profound biological effects, which is known for example for tau in the context of Alzheimer's disease (Medina & Avila 2014). Also my own attempts of making an EMTB-CFP transgenic mouse failed, because overexpression of EMTB-CFP in HEK cells and in zebrafish seemed to be toxic (*data not shown*). Additionally limitations in resolution with conventional light microscopy would prohibit identification of individual microtubules in setting with dense labeling of filaments, which can also be seen in immuno-stainings against neuronal tubulin (see **Fig. 3.4**, **Fig. 3.29**). Thus we concluded, also based on previous use in both in neuronal (Stepanova et al., 2003) and glia cells (Eom et al., 2011) that fluorescently-tagged +TIPs provide a more attractive and direct way to visualize microtubule dynamics. Amongst the +TIPs that could be used, the members of the EB family (EB1 and EB3) have been most popular for this purpose, and EB3 especially has been shown to lack

major toxic effects and to provide effective labeling in previous zebrafish work (Norden et al., 2009). Therefore we decided to use EB3 tagged with yellow fluorescent protein to visualize microtubule dynamics in intact mammalian neurons. To this end we generated transgenic mice that express EB3-YFP under the control of *Thy1* regulatory elements (Feng et al., 2000).

4.1.2. Exclusion of toxicity

Still, before our assay can be transferred to new applications, some considerations need to be kept in mind: First, our approach is based on transgenic animals that overexpress a biologically active fusion protein, which could act as gain-of function or dominant negative interference. Despite these concerns, we believe that this is not a major problem in low expressing *Thy1*:EB3-YFP mouse lines. This conviction is based on at least four independent lines of argument: (1) +TIP-based assays for microtubule dynamics have been used successfully and without reported toxicity in cell culture of mammalian (Stepanova et al., 2003) and non-mammalian species (Erez et al., 2007), as well as *in vivo* in flies (Stone et al., 2008) and in zebrafish (Norden et al., 2009). (2) The transgenic strains used for experiments have a relatively low level of overexpression revealed by single cell PCR (**Fig. 3.7**). Also EB3-YFP staining is restricted to microtubule tips and shows the typical comet like pattern (**Fig. 3.1**). In contrast, high-expressing lines showed a static labeling of the entire microtubule lattice. Axons in these high-expressing mice at more advanced ages showed axonal spheroids. However, similar alterations have even been described for YFP overexpression alone (Bridge et al., 2009), leaving the notion undecided, whether it is overexpression of EB3 or rather of YFP that mediates the described pathology. (3) We did so far not detect any sign of pathology. Transgenic animals show normal behavior, breeding and life span. Moreover, a broad range of investigations on motor neuronal health and function (see **Fig. 3.3**, **Fig. 3.6**) as well as axonal ultrastructure (see **Fig. 3.5**) failed to reveal any abnormalities. (4) Furthermore,

for those parameters of microtubule behavior that can be compared, our assay is in accordance with previous approaches (e.g. comet-like vs. filamentous distribution; coincidence of transgene- and transfection-based labeling *in vitro*; microtubule orientation (Baas et al., 1988, Stepanova et al., 2003). These findings suggest that at least major toxic effects can be excluded and that our assay is at least not worse than the substantial body of cell biological and neurobiological work on microtubule dynamics, which is to a large degree based on EB-fusions.

In addition to general toxicity, specific effects of EB3 overexpression also have to be considered. EB3 interacts with a number of other plus-end binding proteins, such as CLIPs (Duellberg et al., 2014, Komarova et al., 2009) and overexpression of EB3-YFP could interfere with these interactions. However the endogenous EB3 is still present, so if anything, only a partial loss of function would be expected. Also control experiments for at least for one other +TIP protein (EB1) localization in EB3-YFP transgenic and wild-type neurons did not show any difference in protein localization (see **Fig. 3.8**). This is also in line with previously published data that show *in vitro* that EB3 overexpression only interferes with other +TIPs at high levels of overexpression that coincide with loss of a comet-like staining pattern (Komarova et al., 2005).

4.1.3. Challenges and limitations of imaging microtubule dynamics

During my PhD thesis I have imaged microtubule dynamics in various compartments *in vivo* and *ex vivo* (see **Fig. 3.9 - 3.14**). During these experiments it became apparent that imaging EB3-YFP comets in a complex tissue environment can be challenging so that interpretation of the resulting parameters deserves careful consideration. Imaging comets is significantly more challenging than imaging other subcellular structures of similar length, such as mitochondria (Misgeld et al., 2007). Two reasons might account for this: First, in

width the structured imaged has a size approximately an order of magnitude below the diffraction limit (microtubule diameter is 25 nm). Thus EB3 comets probably contain a much lower number of fluorophores than, for example, a matrix-labeled mitochondrion. Second, the affinity and specificity of EB3-YFP microtubule binding is limited, which is why transgenically expressed EB3-YFP also accumulates in the cytoplasm and along the microtubule shaft. This means that when expression levels are increased, comet labeling initially still becomes brighter, but beyond a certain level of expression the signal-to-background ratio actually decreases as label starts to accumulate in the cytoplasm or along the microtubule shaft. Indeed, this is what we seem to observe in the high-expressing line (J030, see **Fig. 3.1**). In this sense, +TIP imaging has an intrinsic limitation in "signal-to-background ratio". This limitation particularly affects scanning imaging modalities, where the signal-to-noise ratio is limited by low photon counts per pixel (Lichtman & Conchello 2005). Hence, especially CNS *in vivo* imaging of microtubule dynamics proved more difficult than previous subcellular imaging, because it requires two-photon scanning microscopy to overcome scattering. To successfully image comets in this setting requires a careful design of excitation and emission optics of the two-photon system. In contrast, imaging comets in peripheral axons derived from *Thy1*:EB3-YFP mice is fairly straight-forward, because wide-field microscopy can be used, which collects many more photons per pixel than a scanning microscope. Due to the same signal-to-background limitations, automated analysis of labeled +TIP, which was successfully applied *in vitro* (Applegate et al., 2011), could not be used for tracking comets in our experiments. However, the fact that detector design in scanning microscopy is improving and now already allows EB3 imaging in spinal cord (see **Fig. 3.13**) and cortex (see **Fig. 3.14**), suggests that our assay will become widely applicable not only in the PNS, but also in the CNS. And while above mentioned considerations are important to keep in mind for future applications, the assay described here adds microtubule remodeling to

the growing list of cell biological properties of neurons that can be measured *in vivo* in the mammalian nervous system during development, homeostasis and disease.

4.1.4. Quantification and interpretation of changes in microtubule dynamics

Recordings of the transgenic fusion protein EB3-YFP revealed the tips of microtubules as dynamic pattern of "comet-like" structures against a faint background of cytoplasmic labeling. However, the question arose, which quantification of these recordings is sufficient to make a statement about the status of the microtubule cytoskeleton while being sensitive enough to detect changes in microtubule dynamics. It turned out that determining the density of EB3 comets provides a direct measure of the local dynamics of the microtubule cytoskeleton. At first glance, a measurement of comet density as volumetric density in neurite seems to be the right choice. However, in practical terms it turned out that a two-dimensional analysis, where comet density is normalized to the area of the neurite is a more precise expression, although it assumes a standard thickness of the detection volume. The reason for this is that, due to the low signal-to-background ratio of the EB3-YFP signal, imaging modalities had to be chosen, which have a rather poor z-resolution (wide-field imaging or scanning microscopy with an open pinhole). For example for two-photon imaging, which is probably the most suitable imaging technique in an *in vivo* context, at λex = 800 nm and a 1.0 NA objective that I typically use the estimated z-resolution based on Rayleigh would be:

$$d_z = 1.4 * n_{water} * \lambda_{ex} / NA_2 = 1.5\ \mu m$$

As proximal motor axons typically have a diameter of ~ 6 μm (5.8 ± 0.1 μm; 43 axons) and even distal axons have a diameter of ~ 4 μm (4.2 ±0.2 μm; 43 axons) an volumetric estimate introduces a considerable uncertainty. Instead, I measured EB3 comet density by placing a single focal plane into the center of the axon. With the assumption that the measured axons in

my samples typically extend significantly beyond the depth-of-field of imaging, we measure a "standard volume", which is related to the measured area by a stable depth – the value is reported as an area density, as I could not precisely determine the sampled depth. One prediction of this assumption is that comet density expressed per area is not correlated with axon thickness Indeed when I plotted comet density versus axon diameter for different neurites I could not detect any correlation (**Fig. 4.1 A**). Also the average comet density would be expected to be rather constant across the diameter of the axons that I usually measured, compared to axons that are thinner than the depth-of-field, where the curvature of a cylinder would lead to a lower apparent density towards the periphery. This was confirmed by comparing comet density in the central and peripheral parts of axons (**Fig. 4.1 B**).

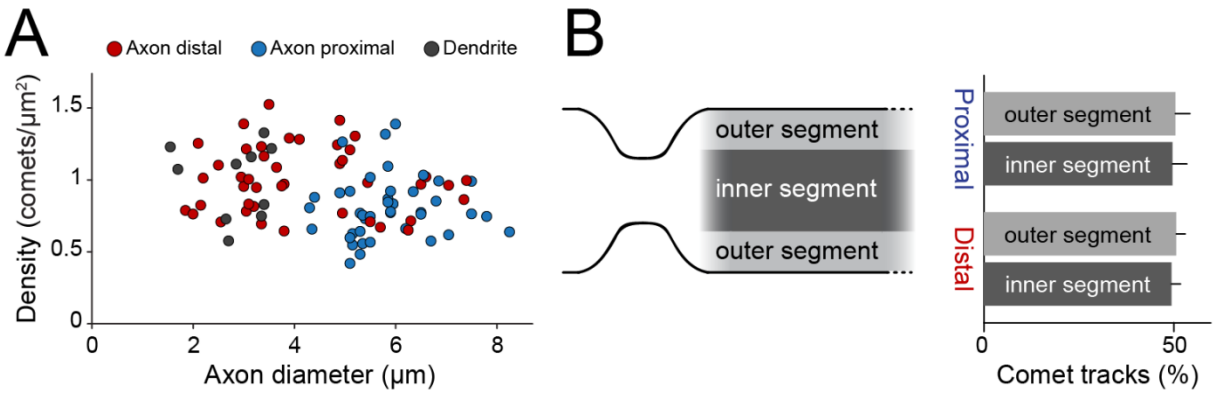

Fig. 4.1 Comet density in relation to axon diameter and position within the axon

(**A**) Plotting axon diameter against comet density in distal and proximal motor axon segments of a triangularis explant, as well as in Purkinje cell dendrites revealed that there is no detectable correlation between diameter of the axon and comet density when two-dimensional analysis was used. (**B**) Density of microtubules is not different in central ("inner segment") and peripheral ("outer segment") parts of the axon cylinder both in distal and proximal motor axon segments, when assuming a standard volume for EB3 measurements.

But one instance where microtubule dynamics were measured in axons with less than 1.5 µm diameter was in retraction bulbs during developmental synapse elimination. But given the fact that with a volumetric normalization based on a cylindrical geometry of the axon

$$V = d^2 * \pi * h / 4$$

(V= Volume; d = diameter of axon; h = length of axon segment)

one would calculate a higher difference in comet densities compared to thicker axons than in a 2-D normalization. This means that my results would, if at all, even underestimate the increase in microtubule dynamics that we see in retraction bulbs. Moreover, volumetric imaging would make a sufficient temporal sampling difficult, as several images have to be required per sampling time-point, which in turn adds tracking errors. Also thin cortical dendrites that I measured through the cranial window might have a diameter below the depth-of-field measured. But for the chronic imaging of cortical dendrites, this error should not affect the comparability of two values over time as such dendrites are known not to undergo major morphological changes in adult animals over one week.

Finally, beside the appropriate technical approach of quantification, one should also keep in mind that – while EB3-YFP marks a well-defined structure in cell biological terms and provides a rather immediate read-out of microtubule dynamics – relating this to the overall stability of the microtubule cytoskeleton is not trivial. An increase in comet density alone does not directly predict whether the microtubule cytoskeleton undergoes an expansion or contraction, because dynamic microtubules would be expected to be more abundant in both settings. However, both expansion and breakdown of the microtubule cytoskeleton are linked to early steps of neurite loss and outgrowth, so that our assay provides a possibility to identify sites of imminent neuronal remodeling. In addition, this limitation can be overcome, by comparing EB3 measurements with immunostaining-based assessments of microtubules. For this, immunostaining against neuronal tubulin has proven to be a sufficient way to distinguish between net expansion and breakdown of the microtubule cytoskeleton as it allows determining the overall amount of microtubules. For example, in developmental settings my own experiments show that combining EB3-imaging with tubulin staining can disambiguate situations where high comet densities indicate sites of microtubule degradation rather than expansion (see **Fig. 3.29**). Moreover, the hypothesis, that an increase of microtubule dynamics

is linked to an overall degradation of the microtubule cytoskeleton in retracting axons, is further supported by electron microscopy studies, which show a breakdown of microtubules in dismantling axon branches (Bishop et al., 2004). Previous ultra-structural analyses have also shown a net depolymerization of microtubules after sciatic nerve axotomy (Park et al., 2013), where I also observed an increase in microtubule dynamics.

4.2. Microtubule dynamics in different compartments of the nervous system

While – as detailed above – there might be some challenges and limitations to EB3 imaging, in my hands this new assay has still proven valuable in better understanding microtubule behavior in a variety of neurites of the peripheral and central nervous system *in vivo* and *ex vivo*. Overall the results show that the basic properties of axonal microtubules in neurons are almost identical in the mature PNS and CNS (see **Table 3.2**). Moreover, chronic imaging of microtubule dynamics *in vivo* in individual cortical neurites revealed that parameters of microtubule dynamics are stable over days. Also, comparing the basic microtubule parameters measured with my approach with data from previous *in vitro* and invertebrate systems indicates that principal microtubule properties, such as orientation or length, are evolutionary conserved. Nevertheless, I also found some parameters of microtubule dynamics to differ significantly from cell culture and invertebrate work. For instance the speed of microtubules is two-fold higher in cell culture and in flies, compared to what I have measured. Also my results show fundamental differences between vertebrate and invertebrate species in terms of cytoskeletal structure, for example in dendrites, where a minus-end out orientation was reported (Stone et al., 2008), while we find the mixed orientation anticipated from *in vitro* studies in vertebrate neurons. Taken together, our approach for the first time allows directly measuring basic properties of microtubules (degree of dynamic instability, orientation, density of microtubules) in different compartments of the

peripheral and central nervous system. There are currently no other practical assays to visualize microtubule dynamics in the mammalian nervous system, although a number of highly visible studies (Barten et al., 2012, d'Ydewalle et al., 2011, Erturk et al., 2007, Fanara et al., 2007) implicate destabilized microtubules in disease and attempt partial stabilization as a means of therapeutic intervention. However, all these studies are lacking a direct assay to directly confirm the proclaimed action at the target site, which stresses the need for a reliable vertebrate *in vivo* assay.

4.3. Microtubule dynamics under pathological conditions

Our approach, when applied to physiological situations in the peripheral and central nervous system did often confirm predictions derived from *in vitro*, non-mammalian and static systems. Other experiments, especially in the context of pathology revealed previously unknown aspects of microtubule dynamics. *Thy1*:EB3-YFP mice have proven to be a powerful tool to monitor the status of the microtubule cytoskeleton during acute or chronic injury in models of trauma and ALS. Various previous studies have shown that alterations of the microtubule cytoskeleton often occurs early after injury or during neurodegenerative disease, even before neurons show morphological changes, and that these alterations often lead to other malfunctions in the cell. Therefore our assay provides a useful tool to study changes in microtubule dynamics in a host of injury or disease models.

4.3.1. Microtubule dynamics after acute injury

The results I obtained show that microtubule dynamics are increased immediately after axon injury, which is first locally restricted but after a few hours, increased microtubule dynamics can be observed along the entire proximal axon stump. Furthermore a global

increase in axons can also be observed during regeneration and axon outgrowth, suggesting that an increase in microtubule dynamics is not only a sign of axonal stress, but also linked to neurite remodeling. Thus, an increase in microtubule dynamics can likely be caused by different signaling cascades, depending on the cellular context in which they occur. Previous studies revealed that Ca^{2+} can modulate the interaction of microtubules with +TIPs and other regulatory proteins (Kapur et al., 2012). Therefore the immediate and locally restricted increase of comet density after acute injury (see **Fig. 3.18**) could be caused by an increase in intracellular calcium, which has been shown to occur immediately after laser transection in peripheral and spinal cord axons and spans approximately the length where I observed increased comet densities (Breckwoldt et al., 2014). The increase in microtubule dynamics in the distal arbor of an injured axon is more likely part of the Wallerian degeneration program, as it occurs only around 6 hours after injury before Wallerian degeneration sets in and is abolished in ΔNLS transgenic mice (see **Fig. 3.19**). At last, also uninjured axons, which receive a growth stimulus, and regenerating axons *per se* have a significant increase in comet density (see **Fig. 3.19**, **Fig. 3.20**), suggesting that increased microtubule dynamics are not only triggered by pathological alterations, but are also necessary for neuronal remodeling and plasticity. Furthermore, my experiments have shown that despite some of the phenomena have also been reported in invertebrate injury models (Stone et al., 2010), in many respects, mechanisms of degeneration and regenerations differ substantially between invertebrate and mammalian neurons (El Bejjani & Hammarlund 2012, Tanaka & Ferretti 2009). Although an up-regulation of dynamic microtubules after injury has been described in flies, severing of an axon in those experiments lead to an increase in microtubule dynamics in the cell body and was also reported to only occur in some cases immediately after cut (Chen et al., 2012a). An immediate increase in dynamic microtubules that is initially locally restricted, as I observed, was not described in the fly study. Several studies in different invertebrate models also show that microtubule polarity is reversed in injured and regenerating axons (Erez et al., 2007,

Stone et al., 2010, Stone et al., 2012) which in Aplysia leads to the formation of so called "traps" (Erez et al., 2007). Based on these studies, scientists in the field have claimed that such change in microtubule polarity seems to be required for regeneration of the axon stumps. Even though this might be true for non-mammalian model, my results have revealed that axons in mammals do not change their polarity after injury but nevertheless regenerate successfully. As this exemplifies, one should be cautious when transferring insights obtained in from invertebrate model systems to mammalian organisms. Our assay now allows directly corroborating such predictions in the mammalian nervous system.

4.3.2. Application of microtubule modifying drugs

As detailed above, as a structure of pathomechanistic importance in many neurological conditions, microtubules are a promising target for potential therapies. Microtubule stabilizing drugs are actually already in clinical use, as they are applied as cytostatic agents for cancer treatment (Jordan & Wilson 2004). However, a major disadvantage of these drugs is that at cytostatic levels they lead to neurotoxicity with severe side effects (Stanton et al., 2011). In contrast, low doses of microtubule stabilizing drugs have been found to increase axon stability after neurotrauma. Therefore moderate microtubule stabilization was suggested as a therapeutic approach to prevent axon loss, promote regeneration or block neurodegeneration (d'Ydewalle et al., 2011, Fanara et al., 2007, Hellal et al., 2011) and even went into a clinical trial for Alzheimer's disease (Perry et al., 2010).

Altogether, it appears critical to define accurate dosing to achieve moderate stabilization. My results suggest that our assay could serve as an *in vivo* read-out for dose-finding experiments. Furthermore, the effects of a pharmacological treatment can now be directly tested in different models of neuronal injury or disease. Our experiments revealed a fairly steep dose-response curve for Paclitaxel (see **Fig. 3.15**) predicting a rather small therapeutic window. Indeed,

when paclitaxel was applied in different doses before axon severing, only the concentration that was within the concentration window of partial stabilization was capable of stabilizing axons. Lower doses had no effect on axon fragmentation, whereas higher concentrations even lead to an increase in fragmentation (see **Fig. 3.16**).

4.3.3. Microtubule dynamics in neurodegenerative disease

The drastic changes in microtubule dynamics that I found after acute axon injury raised the question whether similar changes occur in neurodegenerative diseases. Several studies have shown that a destabilization of the microtubule cytoskeleton is associated with a number of neurodegenerative diseases, such as Alzheimer's dementia (Perry et al., 2010), Chacot-Marie-Tooth disease (d'Ydewalle et al., 2011) or amyotrophic lateral sclerosis (Fanara et al., 2007). Nevertheless, these studies are mainly based on post-hoc immuno-stainings of posttranslational tubulin modifications which only indirectly relate to microtubule dynamics. Indeed, the lack of an *in vivo* model has been explicitly recognized as a drawback in prior studies of the role of microtubule dynamics in neurodegenerative disease (Fanara et al., 2007). Our assay now allowed investigating changes of microtubule dynamics in an animal model of amyotrophic lateral sclerosis. Comet density was significantly increased in motor axons of mice that express a mutated form of SOD (hence modeling a form of familial ALS), but not in mice that overexpress non-mutated human SOD (see **Fig. 3.22**). Intriguing is that microtubule dynamics are already increased in axons that still have a normal morphological appearance. This suggests that an altered microtubule cytoskeleton is a rather early event in this disease model and that stabilization of microtubules could indeed be an interesting therapeutic strategy to preserve axons from degeneration or at least delay the disease process. Moreover, unpublished date in our lab revealed, that microtubule dynamics are also increased in an

animal model of multiple sclerosis (see **Fig. 3.23**). Microtubule destabilization could be found in spinal axons of EAE at late stages of axon damage within an inflammatory lesion.

These findings show that our new assay is valuable to explore the role of microtubule remodeling in a broad range of mouse models of neurological diseases and test potential therapeutic strategies.

4.4. Microtubule dynamics during development

While the first project of my PhD thesis was focused on the role of microtubule dynamics under physiological and pathological conditions in the mature nervous system (Kleele et al., 2014), the second project that I have been working on focusses on the role of microtubule dynamics during development (Brill, Kleele et al., *in preparation*). My results have demonstrated that axon branches which undergo developmental pruning also show an increase in microtubule dynamics (see **Fig. 3.25 - 3.28**). Correlated tubulin staining links this phenomenon to an overall degradation of the microtubule cytoskeleton (see **Fig. 3.29**). It is important to stress the fact that the up-regulation of microtubule dynamics occur before any definitive morphological signs of pruning (such as branch atrophy or retraction bulb formation) can be observed. Compared to previous studies, these finding might for the first time allow predicting the outcome of synapse elimination at an early stage of competition. However, due to technical limitations it is not yet possible to combine measuring microtubule dynamics with following subsequent synapse elimination to corroborate which axon branch eventually survives. However, the delay in synapse elimination that we found after stabilization of the cytoskeleton with Epothilone B (see **Fig. 3.30**) suggests that microtubule remodeling contributes to synapse elimination and might be critical players during axon branch dismantling. Moreover, the rearrangements in the cytoskeleton that I have found during development and in pathological conditions resemble each other and can be delayed by

similar approaches. This indicates that the neuromuscular junction and its transition from multiple to single innervation is not only an interesting model system to study nervous system development, but could also deepen our understanding of the cellular mechanisms that lead to axon degeneration in disease and after injury.

4.5. Further possible applications

The new imaging assay that I have established has proven to be a powerful tool to image microtubule dynamics *in vivo* and allows monitoring the status of the microtubule cytoskeleton in acute and chronic models of axonal injury. *Thy1*:EB3-YFP transgenic mice can now of course be used to study cytoskeletal rearrangements in a broad range of other mouse models of neurodegenerative diseases. Moreover, this approach provides a direct read-out of the effect of microtubule-modifying drugs, which opens up the possibility of performing a large number of new experiments related to controlled microtubule stabilization, for example after spinal trauma. Given that microtubule dynamics have also been shown to regulate spine dynamics (Jaworski et al., 2009), the assay could also be used to study remodeling neurite segments *in vivo* and to investigate the role of cytoskeletal rearrangements during memory formation and learning. Chronic imaging of microtubule dynamics in the cortex *in vivo* could allow investigating pathological alterations in the brain, for examples change in microtubule dynamics in mouse models of Alzheimer mice before and during plaque formation. Finally, imaging microtubule dynamics during spontaneous remodeling processes, such as those found in developing motor axons in development, could provide a deeper insight into the cellular mechanisms that underlie neuronal plasticity.

4.6. General conclusions

The aim of this study was to establish a novel imaging method, based on transgenic mice, that allows to image microtubule dynamics *in vivo* in neurons. Microtubules are known to play fundamental roles in maintaining proper neuronal function and polarity - and are often affected in neurodegenerative processes. Our approach now allows assaying microtubule dynamics and polarization in different compartments of the nervous system and can be applied to a range of physiological and pathological situations. Previous studies were mainly based on *in vitro* and invertebrate model systems or rather used histological *post mortem* analysis. Some of my experiments could confirm predictions derived from such studies. At the same time, other experiments that I performed revealed previously unknown aspects of microtubule dynamics, for example during acute or chronic axon injury in models of trauma and ALS. I found an increase in dynamic microtubules after injury, in neurodegenerative disease and during neurite remodeling, before axons showed morphological indications of degeneration or re-growth. Moreover, increased microtubule dynamics appear to serve as an early indicator of axon destabilization, as it equally precedes degenerative destruction (e.g. in Wallerian degeneration or in ALS models), as well as denervation-induced outgrowth. As I could also observe an increase in microtubule dynamics in intact neurons that received a growth stimulus by nearby denervation of targets, it appears likely that cytoskeletal rearrangements are also critical during neuronal plasticity. This leads to the conclusion that increased microtubule dynamics might serve as an early indicator of neurite remodeling in health and disease.

5. PUBLICATIONS

Kleele T, Marinkovic P, Williams PR, Stern S, Weigand EE, Engerer P, Naumann R, Hartmann J, Karl RM, Bradke F, Bishop D, Herms J, Konnerth A, Kerschensteiner M, Godinho L and Misgeld T, 2014. **An assay to image neuronal microtubule dynamics in mice**. *Nature communications* 5: 4827

Sorbara C, Wagner NE, Ladwig A, Nikic I, Merkler D, Kleele T, Marinkovic P, Naumann R, Godhino L, Bareyre FM, Bishop D, Misgeld T and Kerschensteiner M. **Pervasive axonal transport deficits in multiple sclerosis models**. *Nature Neuroscience under revision*

Brill M*, Kleele T*, Wang M, Reuter M, Bishop D, Misgeld T. **Cellular mechanisms of developmental synapse elimination.** (*equally contributed) *In preparation*

6. REFERENCES

Abe T, Kiyonari H, Shioi G, Inoue K, Nakao K, et al.,. 2011. Establishment of conditional reporter mouse lines at ROSA26 locus for live cell imaging. *Genesis* 49: 579-90

Ahmad FJ, Yu W, McNally FJ, Baas PW. 1999. An essential role for katanin in severing microtubules in the neuron. *The Journal of cell biology* 145: 305-15

Akhmanova A, Hoogenraad CC. 2005. Microtubule plus-end-tracking proteins: mechanisms and functions. *Current opinion in cell biology* 17: 47-54

Akhmanova A, Hoogenraad CC, Drabek K, Stepanova T, Dortland B, et al.,. 2001. Clasps are CLIP-115 and -170 associating proteins involved in the regional regulation of microtubule dynamics in motile fibroblasts. *Cell* 104: 923-35

Akhmanova A, Steinmetz MO. 2008. Tracking the ends: a dynamic protein network controls the fate of microtubule tips. *Nature reviews. Molecular cell biology* 9: 309-22

Akhmanova A, Steinmetz MO. 2010. Microtubule +TIPs at a glance. *Journal of cell science* 123: 3415-9

Akhmanova A, Steinmetz MO. 2011. Microtubule end binding: EBs sense the guanine nucleotide state. *Current biology : CB* 21: R283-5

Angaut-Petit D, Faille L. 1987. Inability of regenerating mouse motor axons to innervate a denervated target. *Neuroscience letters* 75: 163-8

Applegate KT, Besson S, Matov A, Bagonis MH, Jaqaman K, Danuser G. 2011. plusTipTracker: Quantitative image analysis software for the measurement of microtubule dynamics. *Journal of structural biology* 176: 168-84

Audebert S, Desbruyeres E, Gruszczynski C, Koulakoff A, Gros F, et al.,. 1993. Reversible polyglutamylation of alpha- and beta-tubulin and microtubule dynamics in mouse brain neurons. *Molecular biology of the cell* 4: 615-26

Awasaki T, Tatsumi R, Takahashi K, Arai K, Nakanishi Y, et al.,. 2006. Essential role of the apoptotic cell engulfment genes draper and ced-6 in programmed axon pruning during Drosophila metamorphosis. *Neuron* 50: 855-67

Baas PW, Ahmad FJ. 2013. Beyond taxol: microtubule-based treatment of disease and injury of the nervous system. *Brain : a journal of neurology* 136: 2937-51

Baas PW, Deitch JS, Black MM, Banker GA. 1988. Polarity orientation of microtubules in hippocampal neurons: uniformity in the axon and nonuniformity in the dendrite. *Proceedings of the National Academy of Sciences of the United States of America* 85: 8335-9

Baas PW, Qiang L. 2005. Neuronal microtubules: when the MAP is the roadblock. *Trends in cell biology* 15: 183-7

Baas PW, Vidya Nadar C, Myers KA. 2006. Axonal transport of microtubules: the long and short of it. *Traffic* 7: 490-8

Balice-Gordon RJ, Lichtman JW. 1994. Long-term synapse loss induced by focal blockade of postsynaptic receptors. *Nature* 372: 519-24

Ballatore C, Aspland SE, Castillo R, Desharnais J, Eustaquio T, et al.,. 2005. A facile route to paclitaxel C-10 carbamates. *Bioorganic & medicinal chemistry letters* 15: 2477-80

Barten DM, Fanara P, Andorfer C, Hoque N, Wong PY, et al.,. 2012. Hyperdynamic microtubules, cognitive deficits, and pathology are improved in tau transgenic mice with low doses of the microtubule-stabilizing agent BMS-241027. *The Journal of neuroscience : the official journal of the Society for Neuroscience* 32: 7137-45

Beirowski B, Babetto E, Gilley J, Mazzola F, Conforti L, et al.,. 2009. Non-nuclear Wld(S) determines its neuroprotective efficacy for axons and synapses in vivo. *The Journal of neuroscience : the official journal of the Society for Neuroscience* 29: 653-68

Belmont LD, Mitchison TJ. 1996. Identification of a protein that interacts with tubulin dimers and increases the catastrophe rate of microtubules. *Cell* 84: 623-31

Billuart P, Winter CG, Maresh A, Zhao X, Luo L. 2001. Regulating axon branch stability: the role of p190 RhoGAP in repressing a retraction signaling pathway. *Cell* 107: 195-207

Bishop D, Nikic I, Brinkoetter M, Knecht S, Potz S, et al.,. 2011. Near-infrared branding efficiently correlates light and electron microscopy. *Nature methods* 8: 568-70

Bishop DL, Misgeld T, Walsh MK, Gan WB, Lichtman JW. 2004. Axon branch removal at developing synapses by axosome shedding. *Neuron* 44: 651-61

Bjelic S, De Groot CO, Scharer MA, Jaussi R, Bargsten K, et al.,. 2012. Interaction of mammalian end binding proteins with CAP-Gly domains of CLIP-170 and p150(glued). *Journal of structural biology* 177: 160-7

Bollag DM, McQueney PA, Zhu J, Hensens O, Koupal L, et al.,. 1995. Epothilones, a new class of microtubule-stabilizing agents with a taxol-like mechanism of action. *Cancer research* 55: 2325-33

Bonnet C, Boucher D, Lazereg S, Pedrotti B, Islam K, et al.,. 2001. Differential binding regulation of microtubule-associated proteins MAP1A, MAP1B, and MAP2 by tubulin polyglutamylation. *The Journal of biological chemistry* 276: 12839-48

Breckwoldt MO, Pfister FM, Bradley PM, Marinkovic P, Williams PR, et al.,. 2014. Multiparametric optical analysis of mitochondrial redox signals during neuronal physiology and pathology in vivo. *Nature medicine* 20: 555-60

Bridge KE, Berg N, Adalbert R, Babetto E, Dias T, et al.,. 2009. Late onset distal axonal swelling in YFP-H transgenic mice. *Neurobiology of aging* 30: 309-21

Brinkley W. 1997. Microtubules: a brief historical perspective. *Journal of structural biology* 118: 84-6

Brunden KR, Trojanowski JQ, Smith AB, 3rd, Lee VM, Ballatore C. 2014. Microtubule-stabilizing agents as potential therapeutics for neurodegenerative disease. *Bioorg Med Chem* 22: 5040-49

Brunden KR, Yao Y, Potuzak JS, Ferrer NI, Ballatore C, et al.,. 2011. The characterization of microtubule-stabilizing drugs as possible therapeutic agents for Alzheimer's disease and related tauopathies. *Pharmacological research : the official journal of the Italian Pharmacological Society* 63: 341-51

Buffelli M, Burgess RW, Feng G, Lobe CG, Lichtman JW, Sanes JR. 2003. Genetic evidence that relative synaptic efficacy biases the outcome of synaptic competition. *Nature* 424: 430-4

Burton PR. 1988. Dendrites of mitral cell neurons contain microtubules of opposite polarity. *Brain research* 473: 107-15

Burton PR, Paige JL. 1981. Polarity of axoplasmic microtubules in the olfactory nerve of the frog. *Proceedings of the National Academy of Sciences of the United States of America* 78: 3269-73

Cairns NJ, Lee VM, Trojanowski JQ. 2004. The cytoskeleton in neurodegenerative diseases. *The Journal of pathology* 204: 438-49

Caroni P. 1997. Overexpression of growth-associated proteins in the neurons of adult transgenic mice. *Journal of neuroscience methods* 71: 3-9

Cartelli D, Casagrande F, Busceti CL, Bucci D, Molinaro G, et al.,. 2013. Microtubule alterations occur early in experimental parkinsonism and the microtubule stabilizer epothilone D is neuroprotective. *Sci Rep* 3: 1837

Caviston JP, Holzbaur EL. 2006. Microtubule motors at the intersection of trafficking and transport. *Trends in cell biology* 16: 530-7

Chen L, Stone MC, Tao J, Rolls MM. 2012a. Axon injury and stress trigger a microtubule-based neuroprotective pathway. *Proceedings of the National Academy of Sciences of the United States of America* 109: 11842-7

Cho Y, Cavalli V. 2012. HDAC5 is a novel injury-regulated tubulin deacetylase controlling axon regeneration. The EMBO journal 31: 3063-78

Chen Q, Cichon J, Wang W, Qiu L, Lee SJ, et al.,. 2012b. Imaging neural activity using *Thy1*-GCaMP transgenic mice. *Neuron* 76: 297-308

Chevalier-Larsen E, Holzbaur EL. 2006. Axonal transport and neurodegenerative disease. *Biochimica et biophysica acta* 1762: 1094-108

Cho Y, Sloutsky R, Naegle KM, Cavalli V. 2013. Injury-induced HDAC5 nuclear export is essential for axon regeneration. *Cell* 155: 894-908

Coleman MP, Freeman MR. 2010. Wallerian degeneration, wld(s), and nmnat. *Annual review of neuroscience* 33: 245-67

Conde C, Caceres A. 2009. Microtubule assembly, organization and dynamics in axons and dendrites. *Nature reviews. Neuroscience* 10: 319-32

Coupe P, Munz M, Manjon JV, Ruthazer ES, Collins DL. 2012. A CANDLE for a deeper in vivo insight. *Medical image analysis* 16: 849-64

d'Ydewalle C, Krishnan J, Chiheb DM, Van Damme P, Irobi J, et al.,. 2011. HDAC6 inhibitors reverse axonal loss in a mouse model of mutant HSPB1-induced Charcot-Marie-Tooth disease. *Nature medicine* 17: 968-74

Dallavalle S, Pisano C, Zunino F. 2012. Development and therapeutic impact of HDAC6-selective inhibitors. Biochemical pharmacology 84: 756-65

Das V, Miller JH. 2012. Microtubule stabilization by peloruside A and paclitaxel rescues degenerating neurons from okadaic acid-induced tau phosphorylation. The European journal of neuroscience 35: 1705-17

Davalos D, Lee JK, Smith WB, Brinkman B, Ellisman MH, et al.,. 2008. Stable in vivo imaging of densely populated glia, axons and blood vessels in the mouse spinal cord using two-photon microscopy. *Journal of neuroscience methods* 169: 1-7

de Forges H, Bouissou A, Perez F. 2012. Interplay between microtubule dynamics and intracellular organization. *The international journal of biochemistry & cell biology* 44: 266-74

Dent EW, Gertler FB. 2003. Cytoskeletal dynamics and transport in growth cone motility and axon guidance. *Neuron* 40: 209-27

Desai A, Mitchison TJ. 1997. Microtubule polymerization dynamics. *Annual review of cell and developmental biology* 13: 83-117

Downing KH, Nogales E. 1998a. Tubulin and microtubule structure. *Current opinion in cell biology* 10: 16-22

Downing KH, Nogales E. 1998b. Tubulin structure: insights into microtubule properties and functions. *Current opinion in structural biology* 8: 785-91

Draberova E, Vinopal S, Morfini G, Liu PS, Sladkova V, et al.,. 2011. Microtubule-severing ATPase spastin in glioblastoma: increased expression in human glioblastoma cell lines and inverse roles in cell motility and proliferation. *Journal of neuropathology and experimental neurology* 70: 811-26

Duellberg C, Trokter M, Jha R, Sen I, Steinmetz MO, Surrey T. 2014. Reconstitution of a hierarchical +TIP interaction network controlling microtubule end tracking of dynein. *Nature cell biology* 16: 804-11

Durand GM, Marandi N, Herberger SD, Blum R, Konnerth A. 2006. Quantitative single-cell RT-PCR and Ca2+ imaging in brain slices. *Pflugers Archiv : European journal of physiology* 451: 716-26

Edelstein A, Amodaj N, Hoover K, Vale R, Stuurman N. 2010. Computer control of microscopes using microManager. *Current protocols in molecular biology / edited by Frederick M. Ausubel ... [et al.,.]* Chapter 14: Unit14 20

El Bejjani R, Hammarlund M. 2012. Neural regeneration in Caenorhabditis elegans. *Annual review of genetics* 46: 499-513

Enes J, Langwieser N, Ruschel J, Carballosa-Gonzalez MM, Klug A, et al.,. 2010a. Electrical activity suppresses axon growth through Ca(v)1.2 channels in adult primary sensory neurons. *Current biology : CB* 20: 1154-64

Eom TY, Stanco A, Weimer J, Stabingas K, Sibrack E, et al.,. 2011. Direct visualization of microtubules using a genetic tool to analyse radial progenitor-astrocyte continuum in brain. *Nature communications* 2: 446

Erck C, Peris L, Andrieux A, Meissirel C, Gruber AD, et al.,. 2005. A vital role of tubulin-tyrosine-ligase for neuronal organization. *Proceedings of the National Academy of Sciences of the United States of America* 102: 7853-8

Erez H, Malkinson G, Prager-Khoutorsky M, De Zeeuw CI, Hoogenraad CC, Spira ME. 2007. Formation of microtubule-based traps controls the sorting and concentration of vesicles to restricted sites of regenerating neurons after axotomy. *The Journal of cell biology* 176: 497-507

Erturk A, Hellal F, Enes J, Bradke F. 2007. Disorganized microtubules underlie the formation of retraction bulbs and the failure of axonal regeneration. *The Journal of neuroscience : the official journal of the Society for Neuroscience* 27: 9169-80

Evans KJ, Gomes ER, Reisenweber SM, Gundersen GG, Lauring BP. 2005. Linking axonal degeneration to microtubule remodeling by Spastin-mediated microtubule severing. *The Journal of cell biology* 168: 599-606

Falnikar A, Tole S, Baas PW. 2011. Kinesin-5, a mitotic microtubule-associated motor protein, modulates neuronal migration. *Molecular biology of the cell* 22: 1561-74

Fanara P, Banerjee J, Hueck RV, Harper MR, Awada M, et al.,. 2007. Stabilization of hyperdynamic microtubules is neuroprotective in amyotrophic lateral sclerosis. *The Journal of biological chemistry* 282: 23465-72

Fassier C, Tarrade A, Peris L, Courageot S, Mailly P, et al.,. 2013. Microtubule-targeting drugs rescue axonal swellings in cortical neurons from spastin knockout mice. *Disease models & mechanisms* 6: 72-83

Fiorillo C, Moro F, Yi J, Weil S, Brisca G, et al.,. 2014. Novel dynein DYNC1H1 neck and motor domain mutations link distal spinal muscular atrophy and abnormal cortical development. *Human mutation* 35: 298-302

Fawcett DW, Porter KR. 1954. A study of the fine structure of ciliated epithelia. *Journal of morphology* 94

Feng G, Mellor RH, Bernstein M, Keller-Peck C, Nguyen QT, et al.,. 2000. Imaging neuronal subsets in transgenic mice expressing multiple spectral variants of GFP. *Neuron* 28: 41-51

Franker MA, Hoogenraad CC. 2013. Microtubule-based transport - basic mechanisms, traffic rules and role in neurological pathogenesis. *Journal of cell science* 126: 2319-29

Fuhrmann M, Mitteregger G, Kretzschmar H, Herms J. 2007. Dendritic pathology in prion disease starts at the synaptic spine. *The Journal of neuroscience : the official journal of the Society for Neuroscience* 27: 6224-33

Fukushima N, Furuta D, Hidaka Y, Moriyama R, Tsujiuchi T. 2009. Post-translational modifications of tubulin in the nervous system. *Journal of neurochemistry* 109: 683-93

Galbraith JA, Terasaki M. 2003. Controlled damage in thick specimens by multiphoton excitation. *Molecular biology of the cell* 14: 1808-17

Galjart N. 2010. Plus-end-tracking proteins and their interactions at microtubule ends. *Current biology : CB* 20: R528-37

Gardiner J, Barton D, Marc J, Overall R. 2007. Potential role of tubulin acetylation and microtubule-based protein trafficking in familial dysautonomia. *Traffic* 8: 1145-9

Gardner MK, Zanic M, Howard J. 2013. Microtubule catastrophe and rescue. Current opinion in cell biology 25: 14-22

Gennerich A, Vale RD. 2009. Walking the walk: how kinesin and dynein coordinate their steps. *Current opinion in cell biology* 21: 59-67

Goellner B, Aberle H. 2012. The synaptic cytoskeleton in development and disease. *Developmental neurobiology* 72: 111-25

Gordon-Weeks PR, Fournier AE. 2014. Neuronal cytoskeleton in synaptic plasticity and regeneration. *Journal of neurochemistry* 129: 206-12

Gornstein E, Schwarz TL. 2014. The paradox of paclitaxel neurotoxicity: Mechanisms and unanswered questions. *Neuropharmacology* 76 Pt A: 175-83

Gouveia SM, Akhmanova A. 2010. Cell and molecular biology of microtubule plus end tracking proteins: end binding proteins and their partners. *International review of cell and molecular biology* 285: 1-74

Gumy LF, Chew DJ, Tortosa E, Katrukha EA, Kapitein LC, et al.,. 2013. The kinesin-2 family member KIF3C regulates microtubule dynamics and is required for axon growth and regeneration. *The Journal of neuroscience : the official journal of the Society for Neuroscience* 33: 11329-45

Hammond JW, Cai D, Verhey KJ. 2008. Tubulin modifications and their cellular functions. *Current opinion in cell biology* 20: 71-6

Hartmann J, Blum R, Kovalchuk Y, Adelsberger H, Kuner R, et al.,. 2004. Distinct roles of Galpha(q) and Galpha11 for Purkinje cell signaling and motor behavior. *The Journal of neuroscience : the official journal of the Society for Neuroscience* 24: 5119-30

Hayashi I, Ikura M. 2003. Crystal structure of the amino-terminal microtubule-binding domain of end-binding protein 1 (EB1). *The Journal of biological chemistry* 278: 36430-4

Hazan J, Fonknechten N, Mavel D, Paternotte C, Samson D, et al.,. 1999. Spastin, a new AAA protein, is altered in the most frequent form of autosomal dominant spastic paraplegia. *Nature genetics* 23: 296-303

Heidemann SR, McIntosh JR. 1980. Visualization of the structural polarity of microtubules. *Nature* 286: 517-9

Hellal F, Hurtado A, Ruschel J, Flynn KC, Laskowski CJ, et al.,. 2011. Microtubule stabilization reduces scarring and causes axon regeneration after spinal cord injury. *Science* 331: 928-31

Hempen B, Brion JP. 1996. Reduction of acetylated alpha-tubulin immunoreactivity in neurofibrillary tangle-bearing neurons in Alzheimer's disease. *Journal of neuropathology and experimental neurology* 55: 964-72

Hendricks AG, Perlson E, Ross JL, Schroeder HW, 3rd, Tokito M, Holzbaur EL. 2010. Motor coordination via a tug-of-war mechanism drives bidirectional vesicle transport. *Current biology : CB* 20: 697-702

Hirokawa N. 1998. Kinesin and dynein superfamily proteins and the mechanism of organelle transport. *Science* 279: 519-26

Hirokawa N. 2011. From electron microscopy to molecular cell biology, molecular genetics and structural biology: intracellular transport and kinesin superfamily proteins, KIFs: genes, structure, dynamics and functions. *Journal of electron microscopy* 60 Suppl 1: S63-92

Hirokawa N, Niwa S, Tanaka Y. 2010. Molecular motors in neurons: transport mechanisms and roles in brain function, development, and disease. *Neuron* 68: 610-38

Holtmaat A, Bonhoeffer T, Chow DK, Chuckowree J, De Paola V, et al.,. 2009. Long-term, high-resolution imaging in the mouse neocortex through a chronic cranial window. *Nature protocols* 4: 1128-44

Holtmaat A, Svoboda K. 2009. Experience-dependent structural synaptic plasticity in the mammalian brain. *Nature reviews. Neuroscience* 10: 647-58

Hoogenraad CC, Akhmanova A, Grosveld F, De Zeeuw CI, Galjart N. 2000. Functional analysis of CLIP-115 and its binding to microtubules. *Journal of cell science* 113 (Pt 12): 2285-97

Hubbert C, Guardiola A, Shao R, Kawaguchi Y, Ito A, et al.,. 2002. HDAC6 is a microtubule-associated deacetylase. *Nature* 417: 455-8

Huzil JT, Chik JK, Slysz GW, Freedman H, Tuszynski J, et al.,. 2008. A unique mode of microtubule stabilization induced by peloruside A. *Journal of molecular biology* 378: 1016-30

Ikegami K, Setou M. 2010. Unique post-translational modifications in specialized microtubule architecture. *Cell structure and function* 35: 15-22

Inoué D, Dan K. 1951. Birefringence in edosperm mitosis. *Journal of Morphology* 89: 16

Jaglin XH, Chelly J. 2009. Tubulin-related cortical dysgeneses: microtubule dysfunction underlying neuronal migration defects. *Trends in genetics : TIG* 25: 555-66

Janke C, Bulinski JC. 2011. Post-translational regulation of the microtubule cytoskeleton: mechanisms and functions. *Nature reviews. Molecular cell biology* 12: 773-86

Janke C, Kneussel M. 2010. Tubulin post-translational modifications: encoding functions on the neuronal microtubule cytoskeleton. *Trends in neurosciences* 33: 362-72

Janke C, Rogowski K, Wloga D, Regnard C, Kajava AV, et al.,. 2005. Tubulin polyglutamylase enzymes are members of the TTL domain protein family. *Science* 308: 1758-62

Jaworski J, Hoogenraad CC, Akhmanova A. 2008. Microtubule plus-end tracking proteins in differentiated mammalian cells. *The international journal of biochemistry & cell biology* 40: 619-37

Jaworski J, Kapitein LC, Gouveia SM, Dortland BR, Wulf PS, et al.,. 2009. Dynamic microtubules regulate dendritic spine morphology and synaptic plasticity. *Neuron* 61: 85-100

Jordan MA, Wilson L. 2004. Microtubules as a target for anticancer drugs. *Nature reviews. Cancer* 4: 253-65

Eric R. Kandel JHS, Thomas M. Jessell. 2000. *Principles of Neural Science*. McGraw-Hill Medical.

Kapitein LC, Hoogenraad CC. 2011. Which way to go? Cytoskeletal organization and polarized transport in neurons. *Molecular and cellular neurosciences* 46: 9-20

Kapur M, Wang W, Maloney MT, Millan I, Lundin VF, et al.,. 2012. Calcium tips the balance: a microtubule plus end to lattice binding switch operates in the carboxyl terminus of BPAG1n4. *EMBO reports* 13: 1021-9

Karabay A, Yu W, Solowska JM, Baird DH, Baas PW. 2004. Axonal growth is sensitive to the levels of katanin, a protein that severs microtubules. *The Journal of neuroscience : the official journal of the Society for Neuroscience* 24: 5778-88

Kato S. 2008. Amyotrophic lateral sclerosis models and human neuropathology: similarities and differences. *Acta neuropathologica* 115: 97-114

Kazantsev AG, Thompson LM. 2008. Therapeutic application of histone deacetylase inhibitors for central nervous system disorders. *Nature reviews. Drug discovery* 7: 854-68

Kerschensteiner M, Reuter MS, Lichtman JW, Misgeld T. 2008. Ex vivo imaging of motor axon dynamics in murine triangularis sterni explants. *Nature protocols* 3: 1645-53

Kerschensteiner M, Schwab ME, Lichtman JW, Misgeld T. 2005. In vivo imaging of axonal degeneration and regeneration in the injured spinal cord. *Nature medicine* 11: 572-7

Khawaja S, Gundersen GG, Bulinski JC. 1988. Enhanced stability of microtubules enriched in detyrosinated tubulin is not a direct function of detyrosination level. *The Journal of cell biology* 106: 141-9

Kleele T, Marinkovic P, Williams PR, Stern S, Weigand EE, et al.,. 2014. An assay to image neuronal microtubule dynamics in mice. *Nature communications* 5: 4827

Knoferle J, Koch JC, Ostendorf T, Michel U, Planchamp V, et al.,. 2010. Mechanisms of acute axonal degeneration in the optic nerve in vivo. *Proceedings of the National Academy of Sciences of the United States of America* 107: 6064-9

Kolman A. 2004. Epothilone D (Kosan/Roche). *Current opinion in investigational drugs* 5: 657-67

Komarova Y, De Groot CO, Grigoriev I, Gouveia SM, Munteanu EL, et al.,. 2009. Mammalian end binding proteins control persistent microtubule growth. *The Journal of cell biology* 184: 691-706

Komarova Y, Lansbergen G, Galjart N, Grosveld F, Borisy GG, Akhmanova A. 2005. EB1 and EB3 control CLIP dissociation from the ends of growing microtubules. *Molecular biology of the cell* 16: 5334-45

Komarova YA, Akhmanova AS, Kojima S, Galjart N, Borisy GG. 2002. Cytoplasmic linker proteins promote microtubule rescue in vivo. *The Journal of cell biology* 159: 589-99

Kuijpers M, Hoogenraad CC. 2011. Centrosomes, microtubules and neuronal development. *Molecular and cellular neurosciences* 48: 349-58

Lacroix B, van Dijk J, Gold ND, Guizetti J, Aldrian-Herrada G, et al.,. 2010. Tubulin polyglutamylation stimulates spastin-mediated microtubule severing. *The Journal of cell biology* 189: 945-54

Lee HH, Jan LY, Jan YN. 2009. Drosophila IKK-related kinase Ik2 and Katanin p60-like 1 regulate dendrite pruning of sensory neuron during metamorphosis. *Proceedings of the National Academy of Sciences of the United States of America* 106: 6363-8

Lee VM, Goedert M, Trojanowski JQ. 2001. Neurodegenerative tauopathies. *Annual review of neuroscience* 24: 1121-59

Li H, Li SH, Johnston H, Shelbourne PF, Li XJ. 2000. Amino-terminal fragments of mutant huntingtin show selective accumulation in striatal neurons and synaptic toxicity. *Nature genetics* 25: 385-9

Li R, Gundersen GG. 2008. Beyond polymer polarity: how the cytoskeleton builds a polarized cell. *Nature reviews. Molecular cell biology* 9: 860-73

Liao G, Gundersen GG. 1998. Kinesin is a candidate for cross-bridging microtubules and intermediate filaments. Selective binding of kinesin to detyrosinated tubulin and vimentin. *The Journal of biological chemistry* 273: 9797-803

Lichtman JW, Colman H. 2000. Synapse elimination and indelible memory. *Neuron* 25: 269-78

Lichtman JW, Conchello JA. 2005. Fluorescence microscopy. *Nature methods* 2: 910-9

Lichtman JW, Fraser SE. 2001. The neuronal naturalist: watching neurons in their native habitat. *Nature neuroscience* 4 Suppl: 1215-20

Lipka J, Kuijpers M, Jaworski J, Hoogenraad CC. 2013. Mutations in cytoplasmic dynein and its regulators cause malformations of cortical development and neurodegenerative diseases. *Biochemical Society transactions* 41: 1605-12

Lopez-Munoz F, Boya J, Alamo C. 2006. Neuron theory, the cornerstone of neuroscience, on the centenary of the Nobel Prize award to Santiago Ramon y Cajal. *Brain research bulletin* 70: 391-405

Luo L, O'Leary DD. 2005. Axon retraction and degeneration in development and disease. *Annu Rev Neurosci* 28: 127-56

Mandelkow EM, Mandelkow E, Milligan RA. 1991. Microtubule dynamics and microtubule caps: a time-resolved cryo-electron microscopy study. *The Journal of cell biology* 114: 977-91

Manton I, Clarke R. 1952. An electron microscopy study of the spermatozoid of sphagnum. *Journal of experimental botany* 3: 21

Maor-Nof M, Yaron A. 2013. Neurite pruning and neuronal cell death: spatial regulation of shared destruction programs. *Current opinion in neurobiology* 23: 990-6

Marinkovic P, Godinho L, Misgeld T. 2011. Generation and Screening of Mice with Transgenic Neuronal Labeling Controlled by *Thy-1* Regulatory Elements. *Imaging in Neuroscience: A Laboratory Manual*: Capter 22

Marinkovic P, Reuter MS, Brill MS, Godinho L, Kerschensteiner M, Misgeld T. 2012. Axonal transport deficits and degeneration can evolve independently in mouse models of amyotrophic lateral sclerosis. *Proceedings of the National Academy of Sciences of the United States of America* 109: 4296-301

Mattson MP. 1999. Establishment and plasticity of neuronal polarity. *Journal of neuroscience research* 57: 577-89

McIntosh JR. 1974. An introduction to microtubules. *Journal of supramolecular structure* 2: 385-92

McMurray CT. 2000. Neurodegeneration: diseases of the cytoskeleton? *Cell death and differentiation* 7: 861-5

McNally FJ, Vale RD. 1993. Identification of katanin, an ATPase that severs and disassembles stable microtubules. *Cell* 75: 419-29

Medina M, Avila J. 2014. New perspectives on the role of tau in Alzheimer's disease. Implications for therapy. *Biochemical pharmacology* 88: 540-7

Mimori-Kiyosue Y, Shiina N, Tsukita S. 2000. The dynamic behavior of the APC-binding protein EB1 on the distal ends of microtubules. *Current biology : CB* 10: 865-8

Misgeld T, Kerschensteiner M, Bareyre FM, Burgess RW, Lichtman JW. 2007. Imaging axonal transport of mitochondria in vivo. *Nature methods* 4: 559-61

Mitchison T, Kirschner M. 1984. Dynamic instability of microtubule growth. *Nature* 312: 237-42

Monnerie H, Tang-Schomer MD, Iwata A, Smith DH, Kim HA, Le Roux PD. 2010. Dendritic alterations after dynamic axonal stretch injury in vitro. *Experimental neurology* 224: 415-23

Moon HM, Wynshaw-Boris A. 2013. Cytoskeleton in action: lissencephaly, a neuronal migration disorder. *Wiley interdisciplinary reviews. Developmental biology* 2: 229-45

Mullins FH, Hargreaves AJ, Li JY, Dahlstrom A, McLean WG. 1994. Tyrosination state of alpha-tubulin in regenerating peripheral nerve. *Journal of neurochemistry* 62: 227-34

Myers KA, He Y, Hasaka TP, Baas PW. 2006. Microtubule transport in the axon: Re-thinking a potential role for the actin cytoskeleton. *The Neuroscientist : a review journal bringing neurobiology, neurology and psychiatry* 12: 107-18

Neukirchen D, Bradke F. 2011. Neuronal polarization and the cytoskeleton. *Seminars in cell & developmental biology* 22: 825-33

Neukomm LJ, Freeman MR. 2014. Diverse cellular and molecular modes of axon degeneration. *Trends in cell biology* 24: 515-23

Nguyen QT, Sanes JR, Lichtman JW. 2002. Pre-existing pathways promote precise projection patterns. *Nature neuroscience* 5: 861-7

Nikic I, Merkler D, Sorbara C, Brinkoetter M, Kreutzfeldt M, et al.,. 2011. A reversible form of axon damage in experimental autoimmune encephalomyelitis and multiple sclerosis. *Nature medicine* 17: 495-9

Niwa S, Takahashi H, Hirokawa N. 2013. beta-Tubulin mutations that cause severe neuropathies disrupt axonal transport. *The EMBO journal* 32: 1352-64

Noda Y, Niwa S, Homma N, Fukuda H, Imajo-Ohmi S, Hirokawa N. 2012. Phosphatidylinositol 4-phosphate 5-kinase alpha (PIPKalpha) regulates neuronal microtubule depolymerase kinesin, KIF2A and suppresses elongation of axon branches. *Proceedings of the National Academy of Sciences of the United States of America* 109: 1725-30

Nogales E. 2000. Structural insights into microtubule function. *Annual review of biochemistry* 69: 277-302

Norden C, Young S, Link BA, Harris WA. 2009. Actomyosin is the main driver of interkinetic nuclear migration in the retina. *Cell* 138: 1195-208

O'Brien RJ, Wong PC. 2011. Amyloid precursor protein processing and Alzheimer's disease. *Annual review of neuroscience* 34: 185-204

Palazzo A, Ackerman B, Gundersen GG. 2003. Cell biology: Tubulin acetylation and cell motility. *Nature* 421: 230

Park JY, Jang SY, Shin YK, Koh H, Suh DJ, et al.,. 2013. Mitochondrial swelling and microtubule depolymerization are associated with energy depletion in axon degeneration. *Neuroscience* 238: 258-69

Perez F, Diamantopoulos GS, Stalder R, Kreis TE. 1999. CLIP-170 highlights growing microtubule ends in vivo. *Cell* 96: 517-27

Peris L, Wagenbach M, Lafanechere L, Brocard J, Moore AT, et al.,. 2009. Motor-dependent microtubule disassembly driven by tubulin tyrosination. *The Journal of cell biology* 185: 1159-66

Pilling AD, Horiuchi D, Lively CM, Saxton WM. 2006. Kinesin-1 and Dynein are the primary motors for fast transport of mitochondria in Drosophila motor axons. *Molecular biology of the cell* 17: 2057-68

Poirier K, Saillour Y, Bahi-Buisson N, Jaglin XH, Fallet-Bianco C, et al.,. 2010. Mutations in the neuronal ss-tubulin subunit TUBB3 result in malformation of cortical development and neuronal migration defects. *Human molecular genetics* 19: 4462-73

Prota AE, Bargsten K, Zurwerra D, Field JJ, Diaz JF, et al.,. 2013. Molecular mechanism of action of microtubule-stabilizing anticancer agents. *Science* 339: 587-90

Ramón y Cajal S. 1999. *Advice for a young investigator*. Cambridge, Mass: MIT Press. xx, 150 p. pp.

Reed NA, Cai D, Blasius TL, Jih GT, Meyhofer E, et al.,. 2006. Microtubule acetylation promotes kinesin-1 binding and transport. *Current biology : CB* 16: 2166-72

Reddy PH, Mao P, Manczak M. 2009. Mitochondrial structural and functional dynamics in Huntington's disease. *Brain research reviews* 61: 33-48

Reichenbach H, Hofle G. 2008. Discovery and development of the epothilones : a novel class of antineoplastic drugs. *Drugs in R&D* 9: 1-10

Reid E, Kloos M, Ashley-Koch A, Hughes L, Bevan S, et al.,. 2002. A kinesin heavy chain (KIF5A) mutation in hereditary spastic paraplegia (SPG10). *American journal of human genetics* 71: 1189-94

Ringholz GM, Appel SH, Bradshaw M, Cooke NA, Mosnik DM, Schulz PE. 2005. Prevalence and patterns of cognitive impairment in sporadic ALS. *Neurology* 65: 586-90

Rivieccio MA, Brochier C, Willis DE, Walker BA, D'Annibale MA, et al. 2009. HDAC6 is a target for protection and regeneration following injury in the nervous system. Proceedings of the National Academy of Sciences of the United States of America 106: 19599-604

Roll-Mecak A, McNally FJ. 2010. Microtubule-severing enzymes. *Current opinion in cell biology* 22: 96-103

Rolls MM, Satoh D, Clyne PJ, Henner AL, Uemura T, Doe CQ. 2007. Polarity and intracellular compartmentalization of Drosophila neurons. *Neural development* 2: 7

Romanelli E, Sorbara CD, Nikic I, Dagkalis A, Misgeld T, Kerschensteiner M. 2013. Cellular, subcellular and functional in vivo labeling of the spinal cord using vital dyes. *Nature protocols* 8: 481-90

Sabry JH, O'Connor TP, Evans L, Toroian-Raymond A, Kirschner M, Bentley D. 1991. Microtubule behavior during guidance of pioneer neuron growth cones in situ. The Journal of cell biology 115: 381-95

Salinas S, Carazo-Salas RE, Proukakis C, Schiavo G, Warner TT. 2007. Spastin and microtubules: Functions in health and disease. *Journal of neuroscience research* 85: 2778-82

Sammak PJ, Borisy GG. 1988. Direct observation of microtubule dynamics in living cells. *Nature* 332: 724-6

Samson F, Donoso JA, Heller-Bettinger I, Watson D, Himes RH. 1979. Nocodazole action on tubulin assembly, axonal ultrastructure and fast axoplasmic transport. *The Journal of pharmacology and experimental therapeutics* 208: 411-7

Schiff PB, Horwitz SB. 1980. Taxol stabilizes microtubules in mouse fibroblast cells. *Proceedings of the National Academy of Sciences of the United States of America* 77: 1561-5

Schmidt WJ. 1939. Doppelbrechung der Kernspindel und Zugfasertheorie der Chromosomenbewegung. *Chromosoma* 1: 12

Schmitt FO. 1968. Fibrous proteins--neuronal organelles. *Proceedings of the National Academy of Sciences of the United States of America* 60: 1092-101

Schulze E, Kirschner M. 1988. New features of microtubule behaviour observed in vivo. *Nature* 334: 356-9

Schuyler SC, Pellman D. 2001. Microtubule "plus-end-tracking proteins": The end is just the beginning. *Cell* 105: 421-4

Sengottuvel V, Leibinger M, Pfreimer M, Andreadaki A, Fischer D. 2011. Taxol facilitates axon regeneration in the mature CNS. *The Journal of neuroscience : the official journal of the Society for Neuroscience* 31: 2688-99

Sharp DJ, Ross JL. 2012. Microtubule-severing enzymes at the cutting edge. *Journal of cell science* 125: 2561-9

Shimomura O. 2009. Discovery of green fluorescent protein (GFP) (Nobel Lecture). *Angewandte Chemie* 48: 5590-602

Simon JR, Salmon ED. 1990. The structure of microtubule ends during the elongation and shortening phases of dynamic instability examined by negative-stain electron microscopy. *Journal of cell science* 96 (Pt 4): 571-82

Song Y, Brady ST. 2014. Stabilization of neuronal connections and the axonal cytoskeleton. *Bioarchitecture* 4: 22-4

Sorbara CD, Wagner NE, Ladwig A, Nikic I, Merkler D, Kleele T., et al. 2014. Pervasive Axonal Transport Deficits in Multiple Sclerosis Models. *Neuron*

Spalding KL, Bhardwaj RD, Buchholz BA, Druid H, Frisen J. 2005. Retrospective birth dating of cells in humans. *Cell* 122: 133-43

Stanton RA, Gernert KM, Nettles JH, Aneja R. 2011. Drugs that target dynamic microtubules: a new molecular perspective. *Medicinal research reviews* 31: 443-81

Stepanova T, Slemmer J, Hoogenraad CC, Lansbergen G, Dortland B, et al.,. 2003. Visualization of microtubule growth in cultured neurons via the use of EB3-GFP (end-binding protein 3-green fluorescent protein). *The Journal of neuroscience : the official journal of the Society for Neuroscience* 23: 2655-64

Stiess M, Bradke F. 2011. Neuronal polarization: the cytoskeleton leads the way. *Developmental neurobiology* 71: 430-44

Stokin GB, Lillo C, Falzone TL, Brusch RG, Rockenstein E, et al.,. 2005. Axonopathy and transport deficits early in the pathogenesis of Alzheimer's disease. *Science* 307: 1282-8

Stone MC, Nguyen MM, Tao J, Allender DL, Rolls MM. 2010. Global up-regulation of microtubule dynamics and polarity reversal during regeneration of an axon from a dendrite. *Molecular biology of the cell* 21: 767-77

Stone MC, Rao K, Gheres KW, Kim S, Tao J, et al.,. 2012. Normal spastin gene dosage is specifically required for axon regeneration. *Cell reports* 2: 1340-50

Stone MC, Roegiers F, Rolls MM. 2008. Microtubules have opposite orientation in axons and dendrites of Drosophila neurons. *Molecular biology of the cell* 19: 4122-9

Su GH, Sohn TA, Ryu B, Kern SE. 2000. A novel histone deacetylase inhibitor identified by high-throughput transcriptional screening of a compound library. *Cancer research* 60: 3137-42

Su LK, Qi Y. 2001. Characterization of human MAPRE genes and their proteins. *Genomics* 71: 142-9

Tahirovic S, Bradke F. 2009. Neuronal polarity. *Cold Spring Harbor perspectives in biology* 1: a001644

Tanaka EM, Ferretti P. 2009. Considering the evolution of regeneration in the central nervous system. *Nature reviews. Neuroscience* 10: 713-23

Tang-Schomer MD, Johnson VE, Baas PW, Stewart W, Smith DH. 2012. Partial interruption of axonal transport due to microtubule breakage accounts for the formation of periodic varicosities after traumatic axonal injury. *Experimental neurology* 233: 364-72

Tang-Schomer MD, Patel AR, Baas PW, Smith DH. 2010. Mechanical breaking of microtubules in axons during dynamic stretch injury underlies delayed elasticity, microtubule disassembly, and axon degeneration. *FASEB journal : official publication of the Federation of American Societies for Experimental Biology* 24: 1401-10

Thevenaz P, Ruttimann UE, Unser M. 1998. A pyramid approach to subpixel registration based on intensity. *IEEE transactions on image processing : a publication of the IEEE Signal Processing Society* 7: 27-41

Tischfield MA, Baris HN, Wu C, Rudolph G, Van Maldergem L, et al.,. 2010. Human TUBB3 mutations perturb microtubule dynamics, kinesin interactions, and axon guidance. *Cell* 140: 74-87

Trapp BD, Nave KA. 2008. Multiple sclerosis: an immune or neurodegenerative disorder? *Annual review of neuroscience* 31: 247-69

Trushina E, Dyer RB, Badger JD, 2nd, Ure D, Eide L, et al.,. 2004. Mutant huntingtin impairs axonal trafficking in mammalian neurons in vivo and in vitro. *Molecular and cellular biology* 24: 8195-209

Turney SG, Lichtman JW. 2012. Reversing the outcome of synapse elimination at developing neuromuscular junctions in vivo: evidence for synaptic competition and its mechanism. *PLoS biology* 10: e1001352

Umemori H, Linhoff MW, Ornitz DM, Sanes JR. 2004. FGF22 and its close relatives are presynaptic organizing molecules in the mammalian brain. *Cell* 118: 257-70

van Dijk J, Rogowski K, Miro J, Lacroix B, Edde B, Janke C. 2007. A targeted multienzyme mechanism for selective microtubule polyglutamylation. *Molecular cell* 26: 437-48

Verbrugge S, Kapitein LC, Peterman EJ. 2007. Kinesin moving through the spotlight: single-motor fluorescence microscopy with submillisecond time resolution. *Biophysical journal* 92: 2536-45

Verhey KJ, Gaertig J. 2007. The tubulin code. *Cell cycle* 6: 2152-60

Wade RH. 2009. On and around microtubules: an overview. *Molecular biotechnology* 43: 177-91

Walker RA, O'Brien ET, Pryer NK, Soboeiro MF, Voter WA, et al.,. 1988. Dynamic instability of individual microtubules analyzed by video light microscopy: rate constants and transition frequencies. *The Journal of cell biology* 107: 1437-48

Wani MC, Taylor HL, Wall ME, Coggon P, McPhail AT. 1971. Plant antitumor agents. VI. The isolation and structure of taxol, a novel antileukemic and antitumor agent from Taxus brevifolia. *Journal of the American Chemical Society* 93: 2325-7

Watts RJ, Schuldiner O, Perrino J, Larsen C, Luo L. 2004. Glia engulf degenerating axons during developmental axon pruning. *Current biology : CB* 14: 678-84

Welte MA. 2004. Bidirectional transport along microtubules. *Current biology : CB* 14: R525-37

West LM, Northcote PT, Battershill CN. 2000a. Peloruside A: a potent cytotoxic macrolide isolated from the new zealand marine sponge Mycale sp. The Journal of organic chemistry 65: 445-9

Westermann S, Weber K. 2003. Post-translational modifications regulate microtubule function. *Nature reviews. Molecular cell biology* 4: 938-47

Witte H, Neukirchen D, Bradke F. 2008. Microtubule stabilization specifies initial neuronal polarization. *The Journal of cell biology* 180: 619-32

Wittmann T, Waterman-Storer CM. 2001. Cell motility: can Rho GTPases and microtubules point the way? *Journal of cell science* 114: 3795-803

Wuerker RB, Palay SL. 1969. Neurofilaments and microtubules in anterior horn cells of the rat. *Tissue & cell* 1: 387-402

Yang Y, Mahaffey CL, Berube N, Frankel WN. 2006. Interaction between fidgetin and protein kinase A-anchoring protein AKAP95 is critical for palatogenesis in the mouse. *The Journal of biological chemistry* 281: 22352-9

Yau KW, van Beuningen SF, Cunha-Ferreira I, Cloin BM, van Battum EY, et al.,. 2014. Microtubule minus-end binding protein CAMSAP2 controls axon specification and dendrite development. *Neuron* 82: 1058-73

Yu W, Qiang L, Solowska JM, Karabay A, Korulu S, Baas PW. 2008. The microtubule-severing proteins spastin and katanin participate differently in the formation of axonal branches. *Molecular biology of the cell* 19: 1485-98

Zhai Q, Wang J, Kim A, Liu Q, Watts R, et al.,. 2003. Involvement of the ubiquitin-proteasome system in the early stages of wallerian degeneration. *Neuron* 39: 217-25

Zhang B, Carroll J, Trojanowski JQ, Yao Y, Iba M, et al.,. 2012. The microtubule-stabilizing agent, epothilone D, reduces axonal dysfunction, neurotoxicity, cognitive deficits, and Alzheimer-like pathology in an interventional study with aged tau transgenic mice. *The Journal of neuroscience : the official journal of the Society for Neuroscience* 32: 3601-11

Zhang B, Maiti A, Shively S, Lakhani F, McDonald-Jones G, et al.,. 2005. Microtubule-binding drugs offset tau sequestration by stabilizing microtubules and reversing fast axonal transport deficits in a tauopathy model. *Proceedings of the National Academy of Sciences of the United States of America* 102: 227-31

Zhang J, Dong XP. 2012. Dysfunction of microtubule-associated proteins of MAP2/tau family in Prion disease. *Prion* 6: 334-8

Zhao C, Takita J, Tanaka Y, Setou M, Nakagawa T, et al.,. 2001. Charcot-Marie-Tooth disease type 2A caused by mutation in a microtubule motor KIF1Bbeta. *Cell* 105: 587-97